Energy Conversion and its Control by Synchronization of Pendulum

Yuichi Yokoi

Abstract

Human society is built on electric power transmission technology and information communication technology. These technologies are based on synchronization. Synchronization is a universal phenomenon in physical, chemical, biological, and engineering systems. The regulation of rhythms in synchronization has attracted much attention from researchers. Then, the information communication technology develops with many applications of signal synchronization. The power or energy aspect has been already realized as power network, but the energy aspect of synchronization is not completed in spite of the rich possibilities of engineering applications.

In the thesis, we establish a flow of research on the energy aspect of synchronization from the basic analysis to the application of energy conversion. The target application is energy scavenging by a synchronized motion of the parametric pendulum. The parametric pendulum inherently converts the external vibration to its motion in the rotational direction, which accompanies energy. The typical periodic motions of the parametric pendulum are libration and rotation. These synchronized motions give a significant viewpoint to the energy aspect of synchronization. In order to understand the energy conversion by synchronization and apply it to the energy scavenging, we analyze the energy conversion in frequency entrainment for each motion. The periodic librations derive from exciting static states. On the other hand, the periodic rotations appear at high energy states in the periodic state space. The onset of the periodic rotations depends on the initial state of the pendulum. We propose a control method for starting a periodic rotation of the parametric pendulum based on synchronization as an application of phase regulation by energy conversion.

The former part of the thesis is devoted to investigation into energy conversion in frequency entrainment of libration and rotation. At the entrained states, response curves are obtained numerically and theoretically for energy supplied to the system and characteristics of the entrained motion. Comparison of both the motions indicates that the entrained rotations can convert a larger amount of energy than the entrained librations. In the transient regime, the regulation of phase in the frequency entrainment is analyzed in terms of energy exchange. The notion of phase is the heart in the theory of synchronization. We can find a relationship between the phase regulation and the energy conversion only for rotation. Therefore, energy conversion is associated with amplitude for libration and with phase for rotation.

In the latter part, a control method is proposed for starting a periodic rotation of the parametric pendulum. We construct the control with delay based on the possibility

to regulate the phase of rotation by exchanging energy which is obtained in the former part. The performance of the proposed control is examined numerically. In addition, the feasibility is verified experimentally by using a vertically excited mechanical pendulum. Bifurcation phenomenon with respect to the delay is observed to clarify the tolerance of the control with mistuned delay. We advocate that window in the domain of delay exhibits qualitatively similar structure to synchronization region. This result implies that the proposed control with delay induces synchronization in the controlled system.

Acknowledgements

I would like to express my foremost and sincere gratitude to my supervisor, Professor Takashi Hikihara for his continuous encouragement, patient guidance and valuable suggestions to accomplish this research.

I would like to appreciate Assistant Professor Yoshihiko Susuki for his insightful suggestions and encouragement. He introduced me to differential equations and nonlinear dynamics. I would also like to appreciate Professor Marian Wiercigroch of Aberdeen University for his collaboration and fruitful advice. He provided me with opportunities to work on mechanical pendulum and to stay in Aberdeen as a visiting scholar.

I would like to thank Professor Minoru Suzuki and Professor Hiroshi Yamakawa for their valuable suggestions and for serving on my dissertation committee. Professor Suzuki provided me with a physical point of view to research. Professor Yamakawa discussed nonlinear dynamics and control of mechanical systems with me.

I thank the numerous faculty and students in the Graduate School of Engineering, Kyoto University. In particular, I would like to thank Professor Shinji Doi for his valuable discussion and Assistant Professor Toru Matsushima for his support and encouragement. I would like to thank all the members of Professor Hikihara's research groups including the past members. I would like to appreciate Professor Tsuyoshi Funaki, Osaka University, for his helpful comments and discussions. I am very grateful to Assistant Professor Nobuo Satoh for his helpful comments and advices in experiments. I would like to appreciate Assistant Professor Kohei Yamasue, Tohoku University, for his precious comments on the time-delayed feedback control. I would like to appreciate Assistant Professor Masayuki Kimura, The University of Shiga Prefecture, for valuable discussions and helpful comments regarding experiments in this research. In particular, I would like to appreciate Ms. Keiko Saito, Ms. Tomoko Oono, Ms. Ryoko Deguchi, Dr. Ryo Takahashi, Dr. Minghua Li, Dr. Phankong Nathabhat, Mr. Suketu Naik, Mr. Tsuguhiro Takuno, Mr. Masataka Minami, Mr. Jimin Oh, Mr. Takuro Oku, and Mr. Atsushi Yao for their supports to research environment, encouragement, and valuable discussions.

I am also very grateful to the support of the Ministry of Education, Culture, Sports, Science and Technology in Japan, the Global COE program.

Finally, I would like to thank my parents, Kenji and Eiko Yokoi, for their continual support and encouragement.

Contents

List of Acronyms and Symbols

Acronyms

A/D   Analog-to-Digital
D/A   Digital-to-Analog
DC   Direct Current

Symbols

A	Excitation amplitude
a_R	Amplitude of fundamental oscillatory component of rotation
B	Excitation amplitude
b_L	Amplitude of libration
c	Damping coefficient
e_L, e_P, e_R	Excitation
K	Control gain
k	Damping coefficient
l	Rotation number
N	Constant torque
n	Periodic number
p	Excitation amplitude
r	Rotation number
S_L, S_R	Stored energy
T_L, T_P, T_R	Excitation period
t	Time
t_0	Beginning time
u	Variable or control input
v	Variable
W_L^*, W_R^*	Supplied energy
y	Variable

β	Damping parameter
γ	Damping parameter
δ_{R}	Phase deviation of fundamental oscillatory component of rotation
Θ	Angular displacement
θ	Angular displacement
$\theta_{\mathrm{L}}, \theta_{\mathrm{R}}$	Phase for frequency entrainment
μ	Damping parameter
ν	Excitation frequency
τ	Delay time
υ	Angular velocity
ϕ	Variable
ϕ_{L}	Phase of libration
ψ_{R0}	Phase difference of fundamental oscillatory component of rotation
Ω	Excitation frequency
ω	Excitation frequency
${}^{n}\mathsf{S}^{r}_{(i)}$	i-th completely stable orbit or fixed point in which a pendulum rotates r times during n periods
$\langle \cdot \rangle$	Time average

Chapter 1

Introduction

Human society is supported by electric power transmission technology and information communication technology. Synchronization of electric generators underlies the power transmission. The information communication technology is also based on signal synchronization. Synchronization is a universal phenomenon in physical, chemical, biological, and engineering systems. A lot of researchers have shown interest in analysis of the phenomenon, in particular the regulation of rhythms. Then, the information communication technology develops with many applications of signal synchronization. The power or energy aspect of synchronization has been already achieved in power network, but the energy aspect of synchronization is not completed in spite of the rich possibilities of engineering applications.

1.1   Energy aspect of synchronization

Synchronization takes on two different aspects: regulating rhythm and exchanging energy between oscillators. The regulation of rhythms of oscillators can be visibly confirmed as cycle or frequency. This aspect has attracted a lot of interest from researchers [1, 2]. The notion of phase was introduced for understanding the regulation of rhythms in synchronization [3–8]. Based on the notion, a state of an oscillator is assigned to a value of the phase. As a result, theoretical investigations have been carried out into transient regimes of synchronization phenomena and synchronized states in complicated systems such as interacting many oscillators [7–11]. The other aspect as the exchange of energy underlies the occurrence of synchronization. The phenomenon is induced and sustained by the interaction of oscillators. The interaction accompanies the exchange of energy between the oscillators. Thus, the underlying energy exchange is necessary for the phenomenon. As an engineering application of the energy aspect, we can mention synchronization of generators in electrical power systems [12–16]. The synchronizing generators exchange energy with keeping a common frequency, which enables the transmission and distribution of electrical energy. The energy aspect of synchronization is not an additional effect but an essential factor in the application.

    Several groups of researchers have focused on the energy aspect of synchronization.

Cartwright examined the time average of energy stored in the van der Pol oscillator for various steady states and showed that the entrained state appears at higher energy than the drift and asynchronous states [17]. Kuramitsu *et al.*, by using the Brayton-Moser formulation [18] of nonlinear electrical circuits, defined the averaged potential as the time average of power dissipated from a coupled system of self-oscillatory circuits such as the van der Pol oscillators [19–21]. They showed that the frequency entrainment develops in the direction that the averaged potential decreases. Sarasola *et al.* evaluated synchronization in coupled chaotic systems by using the notion of energy stored in and dissipated from the systems [22–24]. Paley *et al.* employed the time derivative of kinetic energy to control collective motions of phase oscillators [25].

Takagi referred to difference between oscillators and rotators from the energy aspect of synchronization [12], where we use *oscillators* as librating objects in comparison with rotating objects denoted by *rotators*. Blekhman indicated a different point in the energy aspect [1]: "The most substantial difference is that usually only clocks with sufficiently close partial frequencies can self-synchronize, while in the case of rotating rotors the effect can occur also at very different partial angular velocities. This is partially related to another practical and important difference: In the case of the self-synchronization of oscillating objects, like pendulum clocks, much less power can be transmitted between the objects than in the case of rotors (vibro-exciters)." These statements imply that the energy aspect of synchronization is possibly understood from the type of oscillation.

The different types of oscillations can be interpreted as topologically different kinds of periodic orbits in nonlinear dynamics. Pikovsky *et al.* recognized that synchronization of rotators is different from the phenomenon of oscillators, in the sense that a single rotator is not a self-sustained system. The oscillation of librating object is called *libration*, and the oscillation of rotator is *rotation* [26]. These oscillations can be observed as the typical oscillations of a pendulum.

1.2   Energy scavenging by parametric pendulum

The parametrically excited pendulum exhibits a variety of behaviors such as a static state at the downward position, periodic librations and rotations, and chaos [27–40]. The parametric pendulum inherently converts the external vibration to its motion in the rotational direction [41]. Since the motion in the rotational direction can be associated with the operation of a generator, it is expected that energy is derived from external sources by using a motion of the parametric pendulum. The process leads to *energy harvesting* or *energy scavenging*. The periodic motions are regarded as favorable motions of the parametric pendulum in terms of steady operation in the applications. The periodic rotations were numerically investigated with respect to the stability and the existence domain in the excitation parameter space [32, 34, 35]. Theoretical studies were performed for the periodic librations and rotations [38, 39].

As a vertical vibration in nature, we focus on the heave motion of sea wave. Fig. 1.1 shows a conceptual diagram of energy scavenging from the heave motion of sea wave
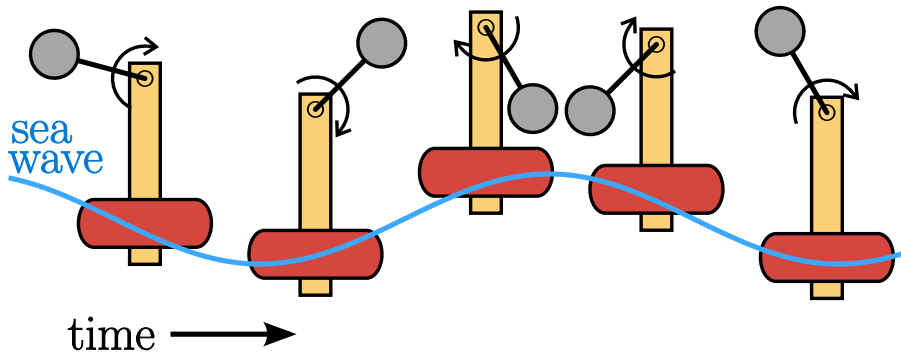
Figure 1.1: Conceptual diagram of energy extraction from the heave motion of sea wave by the parametric pendulum.

by the parametric pendulum. Ocean energy has huge potential from a global point of view, but lags behind solar and wind energy in the practical application [42]. Recently ocean wave has attracted attentions as a renewable energy source in particular in Europe [43–46]. Over the past 30 years, surface winds which are useful for wind power generation have declined in several areas of the northern hemisphere [47]. This report implies that external sources for energy scavenging should be diversified, and possibly promotes the development of ocean energy extraction.

Energy conversion of the parametric pendulum is achieved through its motion in the rotational direction. In particular the periodic librations and rotations are closely related with resonant and synchronized states. For each type of the periodic motions, understanding the mechanism of the energy conversion gives a guideline for the practical and efficient aspect of energy scavenging by the parametric pendulum.

1.3   Control based on synchronization

The mechanism of synchronization is applicable to control for the onset of target motions. Forced synchronization occurs in an oscillator with an external input. In other words, the application of an external input to an oscillator induces the synchronization.

This effect of synchronization has been shed light on by Pecora and Carroll as complete synchronization of chaotic oscillators [48,49]. In the regime of complete synchronization, identical or non-identical chaotic oscillators exhibit almost same behavior through the strong coupling. Even though one of the chaotic oscillators is replaced by the corresponding chaotic signal generator, the complete synchronization is still kept. The chaotic system consisting of the other oscillators is controlled by regulating the state of the chaotic signal generator. The controlled state of the chaotic system is not restricted to chaotic oscillation. Ott, Grebogi, and Yorke introduced the concept of controlling chaos to stabilize an unstable periodic orbit embedded in a chaotic attractor [50]. Pyragas extended the target from discrete systems to continuous systems

and proposed the external force control as a method for controlling chaos [51]. The external force control can be regarded as a control method by using a signal generator. Furthermore, he proposed the delayed feedback control in which the signal is generated by a delayed state of the system [51]. A lot of experimental applications of the control have been carried out with the benefit of the property to require no exact mathematical model of the system [52–55]. The control method nulls the control input after stabilizing an unstable periodic orbit. The delayed feedback control can be regarded as a control method which synchronizes the current state and the time delayed one [53,56].

The control based on synchronization can be easily extended to control for stable periodic rotations. The chaos control operates due to the properties of chaos such as the topological transitivity and the sensitive dependence on small perturbation [57,58]. It is obvious that these properties are not observed in periodic rotations. However, the periodic structure of the state space which generates rotation can replace the topological transitivity. Since the desired motion is a stable periodic rotation, the sensitive dependence is not required. Thus the chaos control can operate for periodic rotations without the above chaotic properties. The onset of the periodic rotations of the parametric pendulum, which we introduced in the previous section, depends on the initial state [35]. The control based on synchronization must be applicable to the periodic rotations. In particular, the delayed feedback control is suited for starting the energy scavenging by the parametric pendulum. After the onset of a periodic motion, the control satisfies the null control input desirable from the viewpoint of energy scavenging. The parametric excitation or external vibration of nature cannot be measured exactly and fixed, and the damping effect in mechanical systems is so complicated that the exact model is not available [59,60]. However, the delayed feedback control can realize the target motion without the exact model.

1.4   Purpose and organization

The purpose of the thesis is to understand and apply the conversion of energy by synchronization. As an application of the energy conversion, we introduce energy scavenging by a resonant or synchronized motion of the parametrically excited pendulum. In order to understand the energy conversion at synchronized states, a fundamental synchronization, namely frequency entrainment, is analyzed in terms of energy. The obtained perceptions of energy conversion at the entrained states indicate that the periodic rotations are suitable for the energy scavenging by the parametric pendulum. The relationship between the phase regulation and the energy conversion is applied to control for starting a periodic rotation.

Chapter 2 describes the theory of synchronization for a pendulum. First, we review the notion of phase which plays a central role in the theory of synchronization. Then, the notion of energy conversion in synchronization is introduced. A value of energy stored in a pendulum can be assigned with a closed orbit. Energy possibly becomes a more general notion than amplitude. In addition, we give a self-sustained oscillator and

a rotator defined in the state space of a pendulum which are analyzed in the following chapters. The steady oscillations are interpreted as the limit cycles which are distinguishable according to the topological property. Finally, the parametric pendulum is introduced as a energy conversion device for energy scavenging.

Chapter 3 is devoted to analysis of frequency entrainment of libration in the van der Pol oscillator. We investigate the entrained states and the transient regime for the frequency entrainment. For the entrained states, an averaged equation is derived to give a theoretical approach. Energy conversion is studied by using response curves which are shown numerically and theoretically. The obtained theoretical expression characterizes the energy conversion at the entrained states. For the transient regime, a phase equation is derived which describes the dynamics of phase for the entrainment of libration. Analyzing energy stored in the system with the phase dynamics shows that energy is converted regardless of the phase dynamics in the transient regime. The results and the approaches in this chapter can be confirmed in terms of the validity and the generality by comparing with reported results. This is significant for analysis of frequency entrainment of rotation in the next chapter.

In chapter 4, we analyze frequency entrainment of rotation in the phase-locked system by using the same approaches as chapter 3. Phase for the frequency entrainment of rotation is identified through response characteristics and an expression of the limit cycle. A phase equation is derived as the same form as the phase equation for libration. The energy conversion at the entrained states is understood by using response curves. In the transient regime, we associate energy stored in the system with the phase dynamics. In the end of this chapter, difference is discussed between the frequency entrainment of libration and rotation. The difference is clarified mainly from the viewpoint of energy. The result indicates advantages of rotation over libration for energy conversion. In addition, the relationship between the phase regulation and the energy conversion leads to the concept of control for starting a periodic rotation by exchanging energy.

In chapter 5, we propose a control method for starting a periodic rotation of the parametric pendulum. The discussion in chapter 4 implies that rotation is more efficient than libration for energy conversion of the parametric pendulum. On the basis of the results in the previous research, we reveal a problem related with the onset of the periodic rotations for energy scavenging. The onset of the periodic rotations depends on the initial state of the pendulum. A start control is designed based on the relationship between the phase regulation and the energy conversion. The remaining of this chapter numerically establishes the performance of the start control with respect to the domain of attraction and the bifurcation diagram.

Chapter 6 verifies the feasibility of the start control from the experimental approach. The parametric pendulum is realized by exciting the mechanical pendulum vertically. First, the experimental setup and the system parameters are described. We adjust suitable excitation parameters which induce the target periodic rotation. Then, the control scheme is implemented in the experimental setup. The experiments elucidate the performance of the control method depending on the control parameters.

In particular, we focus on the bifurcation phenomenon with respect to the delay time. The phenomenon is explained in comparison with synchronization region. Finally, we demonstrate the energy scavenging by a periodic rotation of the mechanical pendulum.

In chapter 7, the conclusions of this study are summarized. Some proposals for the future work is also presented.

Chapter 2

Pendulum and its Synchronization

This chapter provides preliminaries about the dynamics of a pendulum and the synchronization. First, we summarize the notion of phase and energy in synchronization. Then, the cylindrical state space and two types of oscillations are explained. Synchronization phenomena occur for both oscillations. We give a dynamical system with each of the two types of limit cycles. Finally, it is shown that the parametric pendulum exhibits the two oscillations.

2.1 Phase for synchronization

Phase is an essential physical quantity in synchronization. We first define the notion of phase for a limit cycle in an n-dimensional autonomous system. Then, the equation which describes the dynamics of phase for synchronization is derived for an n-dimensional non-autonomous system.

2.1.1 Definition of phase

The notion of phase is defined according to $[2, 5, 6, 8]$. Consider an n-dimensional autonomous system given by

$$\frac{\mathrm{d}\boldsymbol{x}}{\mathrm{d}t} = \boldsymbol{f}(\boldsymbol{x}), \quad \boldsymbol{x} \in \mathbb{R}^n \tag{2.1}$$

with an asymptotically stable T_0-periodic limit cycle. In the state space, the limit cycle is represented by a closed orbit, depicted by C. The limit cycle possesses the following properties:

$$\frac{\mathrm{d}\boldsymbol{x}}{\mathrm{d}t} = \boldsymbol{f}(\boldsymbol{x}) \quad \text{and} \quad \boldsymbol{x}(t + T_0) = \boldsymbol{x}(t). \quad \boldsymbol{x} \in C \tag{2.2}$$

We focus on the vicinity of the closed orbit C corresponding to the limit cycle. Since C is assumed to be stable, each state point $\boldsymbol{x}$ in the vicinity of C approaches the closed orbit C as $t \to \infty$. In order to describe an expression for this asymptotically stable motion in the vicinity of C, we begin with the closed orbit C. A certain value of
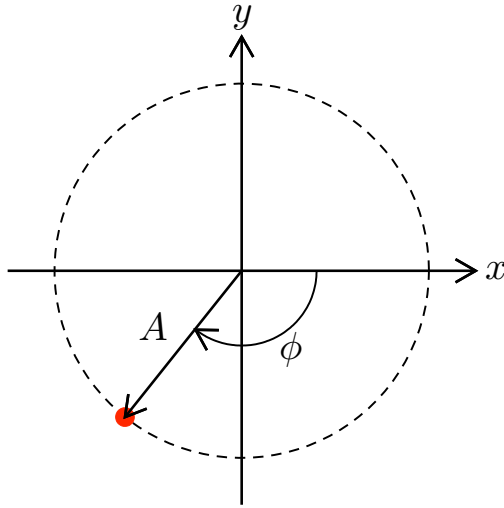
Figure 2.1: Limit cycle in a quasilinear oscillator described as $x(t) = A \cos \phi(t) = A \cos(\omega_0 t + \phi_0)$, where $y = dx/dt$.

a quantity ϕ is assigned with each point $\boldsymbol{x}$ on C so that ϕ increases at constant speed with development of the motion. This assignment is formulated as

$$\frac{d\phi(\boldsymbol{x})}{dt} = \omega_0, \quad \boldsymbol{x} \in C \tag{2.3}$$

where ω_0 is the constant increase of ϕ. The quantity ϕ may be called *phase* defined on the closed orbit C. The value of phase is identified at an integer multiple of the period T_0. For the definition of phase, we can give a simple example in which the system (2.1) corresponds to a 2-dimensional quasilinear oscillator in Fig. 2.1. The stable limit cycle of the oscillator can be described as the sinusoidal function $x(t) = A \cos(\omega_0 t + \phi_0)$. Here ω_0 denotes the angular frequency and ϕ_0 the initial phase. The oscillation is identified by the amplitude A and the phase $\phi(t) = \omega_0 t + \phi_0$. The phase $\phi(t)$ of the oscillation increases without bound. However the cosine is a periodic function, that is, $\cos(\phi + 2\pi) = \cos \phi$. Thus two phases that differ from 2π degenerate to a physical state.

The definition of the phase ϕ is extended to each $\boldsymbol{x}$ in the vicinity of the closed orbit C. Fig. 2.2 illustrates a circular tube which corresponds to the vicinity of C. The phase ϕ is associated with each state point $\boldsymbol{x}$ inside the tube. The tubular region containing all neighborhoods of C is depicted by G in Fig. 2.2. This region G is defined as a subset in the domain of attraction for C. We track two points $\boldsymbol{x}_C$ and $\boldsymbol{x}_G$. The point $\boldsymbol{x}_C$ lies on the closed orbit C and the other point $\boldsymbol{x}_G$ exists in G except C. The definition of the phase ϕ can be applied to $\boldsymbol{x}_C$. Now let the two points $\boldsymbol{x}_C$ and $\boldsymbol{x}_G$ start to move simultaneously. Then $\boldsymbol{x}_G$ approaches to the closed orbit C. This suggests that the phase $\phi(\boldsymbol{x}_G)$ is assigned to $\boldsymbol{x}_G$. As $t \to \infty$, the two points move on C at a finite distance from each other. By using the notion of phase, this situation is formulated as $\phi(\boldsymbol{x}_C) - \phi(\boldsymbol{x}_G) = $ const. In particular, infinitely small distance between the two points
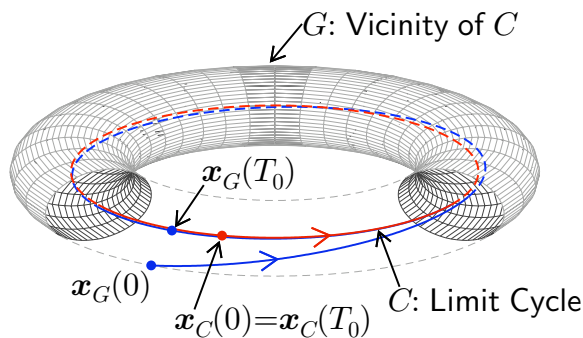
Figure 2.2: Circular tube G corresponding to the vicinity of the limit cycle orbit C.

corresponds to $\phi(\boldsymbol{x}_C) = \phi(\boldsymbol{x}_G)$. Since $\boldsymbol{x}_G$ is an arbitrary point in G, the consistent phase shows that a certain value of the phase ϕ can be assigned with each point $\boldsymbol{x}$ in G. Therefore, the tubular region G is completely filled with a one-parameter family of hypersurfaces which consist of the state points associated with the same phase. The $(n-1)$-dimensional hypersurfaces, denoted by $I(\phi)$, form so-called isochrons [4, 6] if they are extended to the entire state space. From the definition of phase in G, all the points on a common isochron remain on another common isochron after any interval. The phase for a state point changes as the same rate as the phase of the other points on the common isochron. Thus,

$$\frac{\mathrm{d}\phi(\boldsymbol{x}_G)}{\mathrm{d}t} = \frac{\mathrm{d}\phi(\boldsymbol{x}_C)}{\mathrm{d}t} = \frac{\mathrm{d}\phi(\boldsymbol{x})}{\mathrm{d}t} = \omega_0. \quad \boldsymbol{x} \in G \tag{2.4}$$

Eq. (2.4) can be transformed as

$$\frac{\mathrm{d}\phi(\boldsymbol{x})}{\mathrm{d}t} = \frac{\partial \phi}{\partial \boldsymbol{x}} \cdot \frac{\mathrm{d}\boldsymbol{x}}{\mathrm{d}t} = \frac{\partial \phi}{\partial \boldsymbol{x}} \cdot \boldsymbol{f}(\boldsymbol{x}) = \omega_0. \quad \boldsymbol{x} \in G \tag{2.5}$$

2.1.2 Phase equation

In addition to the notion of phase, we review the phase equation [2, 3, 7, 8, 61] which describes the dynamics of phase for synchronization. We have already derived the phase equation for the system (2.1). That is, Eq. (2.3) or Eq. (2.4). However, these equations do not give any information. The reason is that the phase equation is expected to describe the dynamics of phase for an oscillator influenced by another oscillator. From the reason, a phase equation should be derived for a perturbation of the system (2.1).

Consider an n-dimensional non-autonomous system as the perturbed system (2.1)

$$\frac{\mathrm{d}\boldsymbol{x}}{\mathrm{d}t} = \boldsymbol{f}(\boldsymbol{x}) + \epsilon \boldsymbol{p}(t, \boldsymbol{x}), \tag{2.6}$$

where ϵ is the small parameter and $\boldsymbol{p}$ represents the perturbation which depends on the time t and the state $\boldsymbol{x}$. A T-periodic solution is assumed to exist as the perturbation of the limit cycle. The perturbation theory allows us to identify the limit cycle and

9

the periodic orbit. Then, the definition of phase is expanded to the system (2.6). As a result, in the perturbation of the domain G, denoted by G',

$$\frac{\mathrm{d}\phi(\boldsymbol{x})}{\mathrm{d}t} = \frac{\partial\phi}{\partial\boldsymbol{x}} \cdot \frac{\mathrm{d}\boldsymbol{x}}{\mathrm{d}t} = \frac{\partial\phi}{\partial\boldsymbol{x}} \cdot \boldsymbol{f}(\boldsymbol{x}) + \frac{\partial\phi}{\partial\boldsymbol{x}} \cdot \epsilon\boldsymbol{p}(t,\boldsymbol{x}) = \omega_0 + \epsilon\frac{\partial\phi}{\partial\boldsymbol{x}} \cdot \boldsymbol{p}(t,\boldsymbol{x}). \quad \boldsymbol{x} \in G' \quad (2.7)$$

Now the state point $\boldsymbol{x}$ is represented by the corresponding phase $\phi(\boldsymbol{x})$. The last term $\epsilon\partial\phi/\partial\boldsymbol{x} \cdot \boldsymbol{p}(t,\boldsymbol{x})$ can be described as the function, denoted by $\varPhi$, of the time t and the phase ϕ as follows:

$$\frac{\mathrm{d}\phi}{\mathrm{d}t} = \omega_0 + \varPhi(t,\phi). \tag{2.8}$$

This equation is the phase equation which we now consider.

In order to make it easy to analyze the phase equation, the equation is generally transformed into the averaged form by applying the averaging method [62]. By using the transformation $\phi(\boldsymbol{x}(t)) = \omega t + \psi(t)$ with $\omega = 2\pi/T$ and the averaging method, the phase equation is given by

$$\frac{\mathrm{d}\psi}{\mathrm{d}t} = \omega_0 - \omega + \varPsi(\psi), \tag{2.9}$$

where the function $\varPsi$ is the time average of $\varPhi$.

2.2   Energy conversion in synchronization

In this section, we construct the notion of energy conversion for dynamical systems in which synchronization appears. Energy as a conserved quantity can be associated with a closed orbit.

Consider the dynamical system (2.6). We assume that the vector field $\boldsymbol{f}$ can be decomposed into the sum of vector fields $\boldsymbol{f}_{\mathrm{c}}$ and $\epsilon\boldsymbol{f}_{\mathrm{d}}$, where ϵ is the small parameter. The vector field $\boldsymbol{f}_{\mathrm{c}}$ corresponds to a conservative system, and $\epsilon\boldsymbol{f}_{\mathrm{d}}$ changes the conservative system to a system with limit cycle. That is,

$$\frac{\mathrm{d}\boldsymbol{x}}{\mathrm{d}t} = \boldsymbol{f}(\boldsymbol{x}) + \epsilon\boldsymbol{p}(t,\boldsymbol{x}) = \boldsymbol{f}_{\mathrm{c}}(\boldsymbol{x}) + \epsilon\boldsymbol{f}_{\mathrm{d}}(\boldsymbol{x}) + \epsilon\boldsymbol{p}(t,\boldsymbol{x}) = \boldsymbol{f}_{\mathrm{c}}(\boldsymbol{x}) + \epsilon\big\{\boldsymbol{f}_{\mathrm{d}}(\boldsymbol{x}) + \boldsymbol{p}(t,\boldsymbol{x})\big\}. \tag{2.10}$$

The conservative system $\mathrm{d}\boldsymbol{x}/\mathrm{d}t = \boldsymbol{f}_{\mathrm{c}}(\boldsymbol{x})$ has conserved quantities. One of them is energy, denoted by $S(\boldsymbol{x})$, stored in the system from a physical standpoint. The stored energy $S(\boldsymbol{x})$ possesses the following property:

$$\frac{\mathrm{d}S}{\mathrm{d}t} = \frac{\partial S}{\partial\boldsymbol{x}} \cdot \frac{\mathrm{d}\boldsymbol{x}}{\mathrm{d}t} = \frac{\partial S}{\partial\boldsymbol{x}} \cdot \boldsymbol{f}_{\mathrm{c}}(\boldsymbol{x}) = 0. \tag{2.11}$$

In the system (2.10), the stored energy $S(\boldsymbol{x})$ is not conserved. The time derivative of $S(\boldsymbol{x})$ is

$$\begin{aligned}
\frac{\mathrm{d}S}{\mathrm{d}t} &= \frac{\partial S}{\partial\boldsymbol{x}} \cdot \frac{\mathrm{d}\boldsymbol{x}}{\mathrm{d}t} \\
&= \frac{\partial S}{\partial\boldsymbol{x}} \cdot \boldsymbol{f}_{\mathrm{c}}(\boldsymbol{x}) + \frac{\partial S}{\partial\boldsymbol{x}} \cdot \epsilon\boldsymbol{f}_{\mathrm{d}}(\boldsymbol{x}) + \frac{\partial S}{\partial\boldsymbol{x}} \cdot \epsilon\boldsymbol{p}(t,\boldsymbol{x}) \\
&= \epsilon\frac{\partial S}{\partial\boldsymbol{x}} \cdot \boldsymbol{f}_{\mathrm{d}}(\boldsymbol{x}) + \epsilon\frac{\partial S}{\partial\boldsymbol{x}} \cdot \boldsymbol{p}(t,\boldsymbol{x}).
\end{aligned} \tag{2.12}$$

Eq. (2.12) reveals that the temporal change of the stored energy is determined by effect from the vector field $\boldsymbol{f}_{\mathrm{d}}$ which constructs the structure with a limit cycle and the perturbation $\boldsymbol{p}$ which induces synchronization. Now, for any motion of $\boldsymbol{x}$, integration of Eq. (2.12) in any interval $[t_1, t_2]$, where $t_1 < t_2$, gives

$$S(t_2) - S(t_1) = \int_{t_1}^{t_2} \epsilon \frac{\partial S}{\partial \boldsymbol{x}} \cdot \boldsymbol{f}_{\mathrm{d}}(\boldsymbol{x}) \, \mathrm{d}t + \int_{t_1}^{t_2} \epsilon \frac{\partial S}{\partial \boldsymbol{x}} \cdot \boldsymbol{p}(t, \boldsymbol{x}) \, \mathrm{d}t. \qquad (2.13)$$

Since the stored energy $S(\boldsymbol{x}(t))$ is a function of time t, we describe the stored energy as $S(t)$. Eq. (2.13) clarifies that the variation of the stored energy is equivalent to energy supplied and dissipated by the vector field $\boldsymbol{f}_{\mathrm{d}}$ and the perturbation $\boldsymbol{p}$. In this sense, we consider *energy conversion* in dynamical systems. This notion of energy conversion is not restricted to synchronization.

An additional advantage is described which appears with the introduction of energy. On the definition of phase, the addressed state space is restricted to the vicinity of a periodic orbit corresponding to a synchronous state. The definition of phase and the extension require the criterial periodic orbit. Eq. (2.10) implies that the periodic orbit can be expressed as a perturbation of a closed orbit in the conservative system. In the conservative system, each closed orbit is assigned a value of the stored energy. Thus the value of the stored energy can be associated with the synchronized state through the perturbation method. In the same way, the relationship can be extended to the neighborhoods of the periodic orbit. There is no closed orbit governed by the dynamics of the system in the vicinity of the periodic orbit. We can interpret transient motion of $\boldsymbol{x}$ in the vicinity as temporal change of the phase ϕ, the energy S, and the other conserved quantities. In particular, for a pendulum, a current state is identified by the phase ϕ and the stored energy S because the pendulum is a 2-dimensional system.

2.3   Two types of oscillations in cylindrical state space

The state space of a pendulum can be considered as the cylindrical phase space [26,63]. Throughout the thesis, we call it the cylindrical state space for avoiding confusion with phase for synchronization. In the cylindrical state space, there exist two types of periodic orbits. This section explains the cylindrical state space and the two types of periodic orbits. Frequency entrainment appears in the system with a limit cycle [2,64]. There are limit cycles which are the topologically same as the periodic orbits. In the following we introduce two dynamical systems for the entrainment phenomena of the oscillations, which are studied in Chapters 3 and 4, respectively.

2.3.1   Cylindrical state space

The dynamics of a pendulum can be described by using temporal change of the angular displacement and the velocity. At a moment t, the angular displacement and the
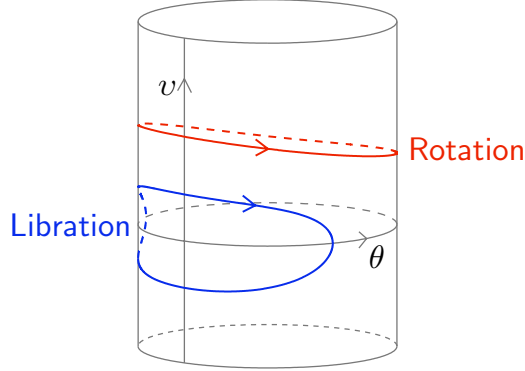
Figure 2.3: Cylindrical state space with two topologically different kinds of closed orbits: a libration and a rotation. The libration is topologically same as a closed orbit on the state plane. The rotation encircles the cylinder.

velocity are denoted by $\theta(t)$ and $\upsilon(t)$, respectively. Since the angular displacement θ has the periodicity of 2π, a motion of pendulum is associated with the corresponding trajectories on the (θ, υ)-state plane. The trajectories can be identified after the transformation $\theta(t) + 2\pi n \mapsto \theta(t)$ for the integer n. By identifying the planes divided at the interval 2π in the direction of θ, the periodical state space of the pendulum is uniquely determined. Fig. 2.3 shows the cylindrical state space [26, 63] which represents the state space of a pendulum. The cylinder well depicts the continuity of the uniquely determined state space in the direction of the angular displacement θ.

There are two topologically different kinds of closed orbits on the cylinder as shown in Fig. 2.3. One of them can exist on the state plane as shown in Fig. 2.4 and called a periodic orbit of the first kind [63] or a *libration* [26]. The periodic orbit satisfies the following property with the angular displacement θ of a pendulum:

$$\theta(t) = \theta(t - T), \tag{2.14}$$

where T denotes the period. The other periodic orbit encircles the cylinder as shown in Fig. 2.3 and called a periodic orbit of the second kind [63] or a *rotation* [26]. The periodic orbit satisfies the following property:

$$\theta(t) = \theta(t - T) + 2\pi r, \tag{2.15}$$

where r is the integer except zero. The rotation shown in Fig. 2.3 depicts the case of $r = 1$. These closed orbits correspond to periodic motions of a pendulum.

In the thesis, we consider synchronization phenomena in a pendulum. Frequency entrainment represents a synchronous motion of an oscillation described by the corresponding limit cycle. The synchronization occurs for each of the two typical motions of a pendulum [2]. We explain the limit cycles corresponding to libration and rotation in the following.
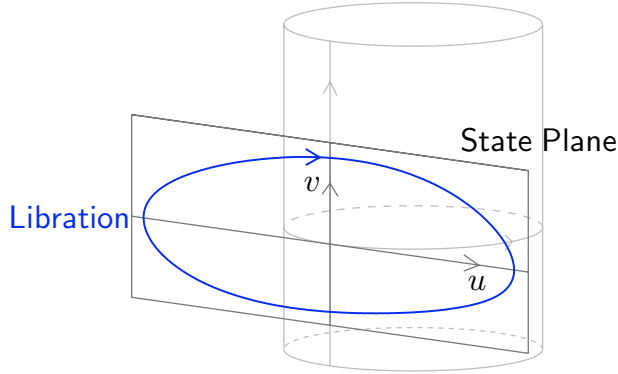
Figure 2.4: Librational limit cycle on the state plane of the van der Pol oscillator (2.16), where $v = \mathrm{d}u/\mathrm{d}t$. Libration existing on the cylindrical state space can exist on the state plane.

2.3.2 Libration

The limit cycle corresponding to libration has been known as a fundamental knowledge of the nonlinear dynamics [26,65]. In order to distinguish the limit cycle from the cycle corresponding to rotation, we call this type of cycle a librational limit cycle or a limit cycle of the first kind [63]. Now we can introduce the van der Pol oscillator [66] as the system with a librational limit cycle. In the forced van der Pol oscillator, frequency entrainment appears [17,64,66]. The dynamics of the forced van der Pol oscillator is described by the ordinary differential equation of u [64],

$$\frac{\mathrm{d}^2 u}{\mathrm{d}t^2} - \mu(1 + \beta u + \gamma u^2)\frac{\mathrm{d}u}{\mathrm{d}t} + u = B \sin \nu t, \tag{2.16}$$

where μ denotes the magnitude of the nonlinear damping, and β and γ are the parameters related to the characteristics of the damping. The term $B \sin \nu t =: e_{\mathrm{L}}(t)$ represents the periodic excitation. A librational limit cycle and the state plane of the van der Pol oscillator are shown in Fig. 2.4, where $v = \mathrm{d}u/\mathrm{d}t$.

We show a librational limit cycle and a periodic libration in the system (2.16). Fig. 2.5(a) shows a waveform and the closed orbit of the librational limit cycle at $\mu = 0.15$ and $\beta = \gamma = 4/3$ [64]. The limit cycle represents the self-sustained oscillation in the system (2.16). The angular frequency of the limit cycle is around 0.99. By applying the periodic excitation with $\nu = 0.99$ to the system (2.16), we can observe frequency entrainment of the librational limit cycle. The entrained state at $B = 0.05$ is represented by the periodic libration shown in Fig. 2.5(b).

2.3.3 Rotation

Next, we consider a rotational limit cycle. We introduce the phase-locked system with a rotational limit cycle. The phase-locked system represents [2, 26, 67] a single
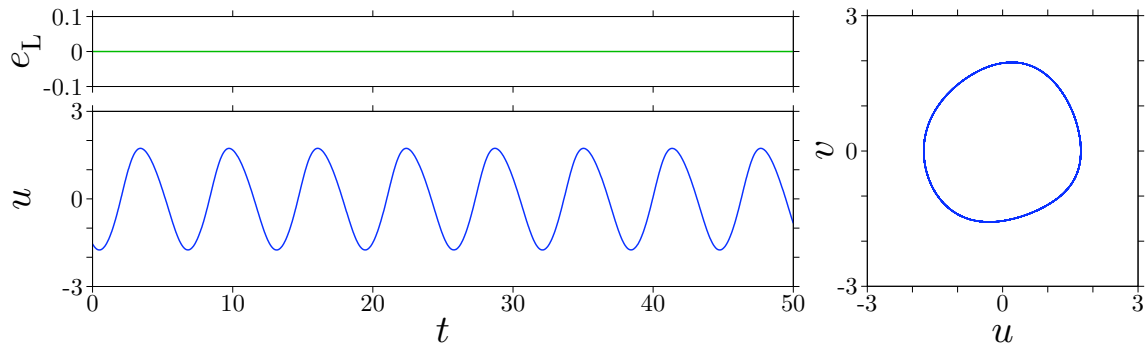
(a) Librational limit cycle.
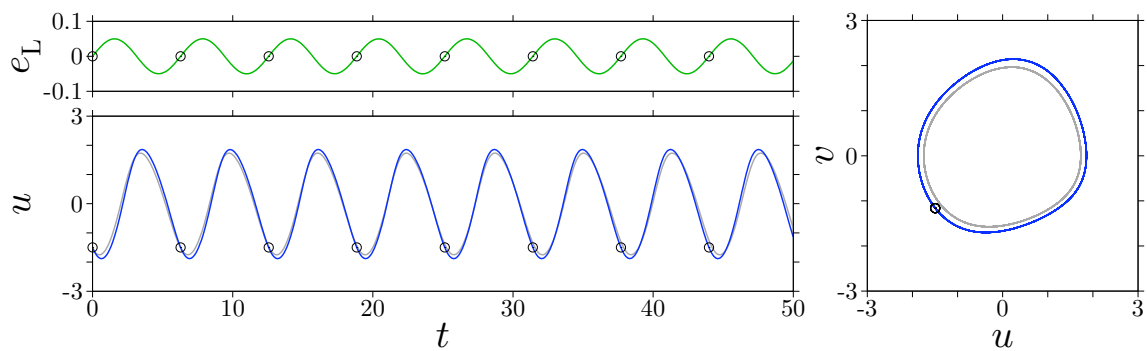
(b) Periodic libration.

Figure 2.5: Librational limit cycle and periodic libration in the system (2.16) at $\mu = 0.15$ and $\beta = \gamma = 4/3$. The periodic excitation $e_{\mathrm{L}}(t)$ is fixed at the amplitude $B = 0.05$ and the angular frequency $\nu = 0.99$ because the angular frequency of the limit cycle is around 0.99. The circles $\odot$ depicts the stroboscopic points of e_{L}. The gray lines in (b) corresponds to the lines in (a).
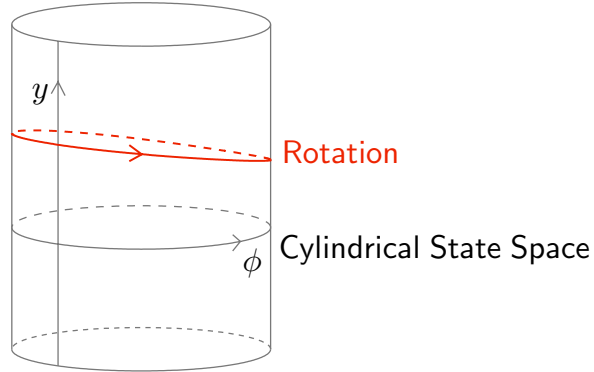
Figure 2.6: Rotational limit cycle in the cylindrical state space of the phase-locked system, where $y = \mathrm{d}\phi/\mathrm{d}t$.

mechanical pendulum [68], the Josephson junction circuit [69–72], the phase-locked loop circuit [73, 74], and a simple power system [13, 75]. In the phase-locked system, frequency entrainment appears [2, 74]. The dynamics of the phase-locked system is described by the ordinary differential equation of ϕ,

$$\frac{\mathrm{d}^2\phi}{\mathrm{d}t^2} + k\frac{\mathrm{d}\phi}{\mathrm{d}t} + \sin\phi = N + A\sin\Omega t, \qquad (2.17)$$

where k denotes the damping, N the constant force, and the term $A\sin\Omega t =: e_{\mathrm{R}}(t)$ the periodic excitation. A rotational limit cycle and the state space of the phase-locked system are shown in Fig. 2.6, where $y = \mathrm{d}\phi/\mathrm{d}t$.

Figure 2.7(a) shows temporal change and the closed orbit of the rotational limit cycle at $k = 0.1$ and $N = 0.2$. The values of parameters satisfy the condition which describes the existence of a stable rotational limit cycle [65]. The angular frequency of the limit cycle is around 1.93. The application of the periodic excitation with $\Omega = 1.93$ to the system (2.17) induces frequency entrainment of the rotational limit cycle. The entrained state at $A = 0.05$ is represented by the periodic rotation shown in Fig. 2.7(b).

2.4 Parametric pendulum

In the thesis, we introduce the parametric pendulum as application of energy conversion through synchronization. Periodic motions of the parametric pendulum can be regarded as conversion from the vertical vibration to its motion in the rotational direction. Because the converting motion is induced with energy, the energy conversion by the parametric pendulum is applicable to energy scavenging. First, the equation of motion is derived for the parametric pendulum. Then, libration and rotation of the parametric pendulum are briefly reviewed. In addition, we give another motivation to study the energy conversion of the parametric pendulum in the sense of synchronization.
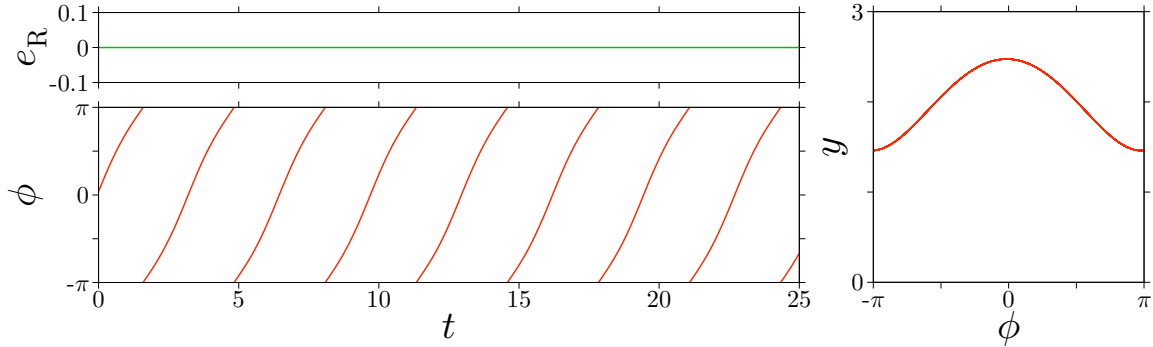
(a) Rotational limit cycle.
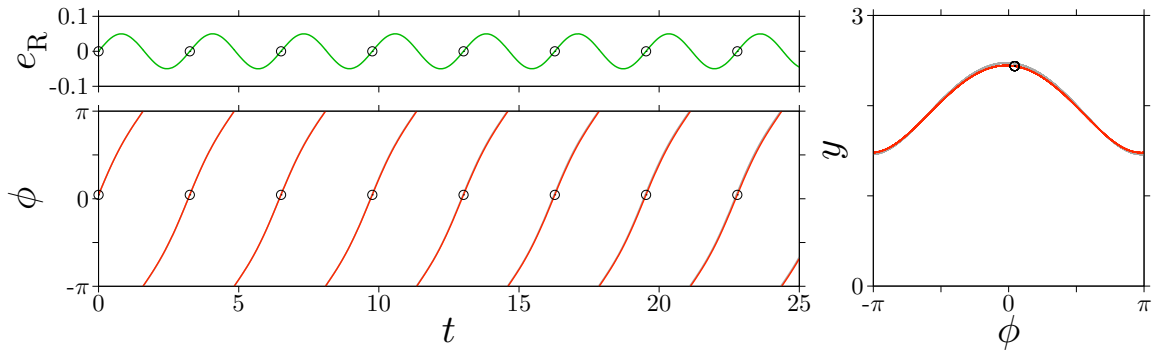
(b) Periodic rotation.

Figure 2.7: Rotational limit cycle and periodic rotation in the system (2.17) at $k = 0.1$ and $N = 0.2$. The periodic excitation $e_{\mathrm{R}}(t)$ is fixed at the amplitude $A = 0.05$ and the angular frequency $\Omega = 1.93$ because the angular frequency of the limit cycle is around 1.93. The circles $\odot$ depicts the stroboscopic points of e_{R}. The gray lines in (b) corresponds to the lines in (a).
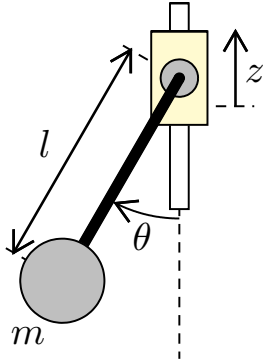
Figure 2.8: Model of a vertically excited pendulum.

2.4.1 Equation of motion

Figure 2.8 illustrates a vertically excited pendulum. The pendulum consists of a mass m and a support with length l. The angular displacement of the pendulum from the downward position is defined by θ. We assume that the viscous damping influences the motion of the pendulum, and the vertical displacement $z(t)$ of the pivot point is excited sinusoidally as $z(t) = A \cos \Omega t$. Here A is the amplitude and Ω is the angular frequency of the excitation. The motion of the vertically excited pendulum is described by the following ordinary differential equation:

$$ml^2 \frac{\mathrm{d}^2\theta}{\mathrm{d}t^2} + \gamma l \frac{\mathrm{d}\theta}{\mathrm{d}t} + ml \left(g - \frac{\mathrm{d}^2 z}{\mathrm{d}t^2} \right) \sin \theta = 0, \tag{2.18}$$

where γ is the damping coefficient and g represents the gravitational acceleration. By scaling time t by $\tau = \Omega_0 t$ with respect to the natural frequency $\Omega_0 = \sqrt{g/l}$, the equation of motion (2.18) is transformed into the following non-dimensional form:

$$\frac{\mathrm{d}^2\theta}{\mathrm{d}\tau^2} + c \frac{\mathrm{d}\theta}{\mathrm{d}\tau} + (1 + p \cos \omega\tau) \sin \theta = 0, \tag{2.19}$$

where the parameters are defined as follows: the damping $c := \gamma \Omega_0 / mg$, the excitation amplitude $p := \Omega^2 A / g$, and the excitation frequency $\omega = \Omega / \Omega_0$.

2.4.2 Steady motions

As typical motions, periodic librations and rotations of the parametric pendulum are reviewed. Fig. 2.9(a) shows a periodic libration. The period is twice the excitation period. Fig. 2.9(b) shows a periodic rotation which has the same period as the excitation. In the thesis, these periodic motions are associated with an entrained libration and rotation in the previous section. It is noted that these motions do not represent entrained oscillations because these motions are not induced from limit cycles. However,
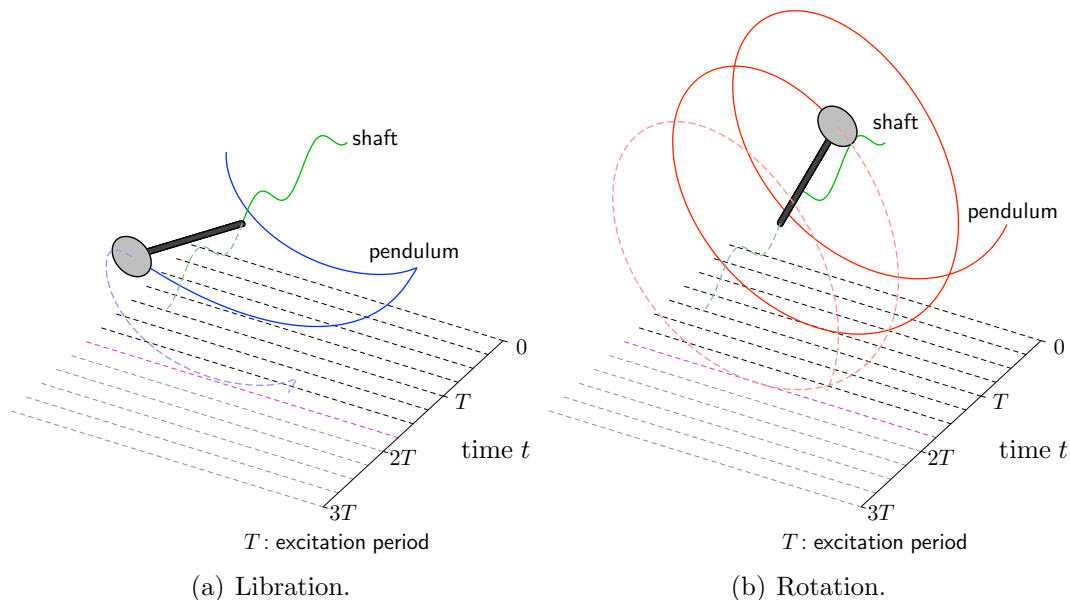
(a) Libration.

(b) Rotation.

Figure 2.9: Periodic motions of the parametric pendulum.

we mentioned that the notion of energy conversion is extended to any motions in the introduction. By using the perception about energy conversion in synchronization of libration and rotation, we understand the energy conversion by the periodic librations and rotations of the parametric pendulum.

2.4.3 Mutual synchronization in coupled pendulums

We introduce the parametric pendulum from another standpoint. The ordinary differential equation (2.19) for the parametric pendulum can describe the dynamics of coupled pendulums or rotators [68]. Periodic motions of the parametric pendulum correspond to synchronous motions of the coupled pendulums.

Let us begin with the equation of motion for coupled two damped driven pendulums [76, 77]

$$ml^2\frac{\mathrm{d}^2\theta_{1,2}}{\mathrm{d}t^2} + \gamma l\frac{\mathrm{d}\theta_{1,2}}{\mathrm{d}t} + mgl\sin\theta_{1,2} + K\sin\left(\theta_{1,2} - \theta_{2,1}\right) = N, \qquad (2.20)$$

where m and l is the mass and the length of the pendulums, and g is the gravitational acceleration. γ is the damping coefficient and N denotes the driving torque. The last term on the left-hand side represents the coupling which is originated from the Kuramoto model [76, 77]. For the angular displacements $\theta_{1,2}$, we introduce the sum and the difference coordinates:

$$\theta_+ = \frac{\theta_1 + \theta_2}{2} \quad \text{and} \quad \theta_- = \frac{\theta_1 - \theta_2}{2}. \qquad (2.21)$$

18

These coordinate transformations into the Eq. (2.20) leads to two differential equations. Here we focus on the coordinate θ_-. The obtained equation for θ_- is

$$ml^2 \frac{\mathrm{d}^2\theta_-}{\mathrm{d}t^2} + \gamma l \frac{\mathrm{d}\theta_-}{\mathrm{d}t} + mgl \cos\theta_+ \sin\theta_- + 2K \sin\theta_- = 0. \tag{2.22}$$

Furthermore we assume that the torque N is sufficiently large so that the angular velocity of the rotating pendulums are almost constant. The condition is described as

$$\theta_{1,2} \approx \Omega t + \phi_{1,2}, \tag{2.23}$$

where Ω denotes the angular velocity and $\phi_{1,2}$ is the initial angle of each pendulum. For $\theta := \theta_-$, non-dimensionalization with respect to the natural angular frequency, $\Omega_0 = \sqrt{2K/ml^2}$, transforms Eq. (2.22) into

$$\frac{\mathrm{d}^2\theta}{\mathrm{d}\tau^2} + c\frac{\mathrm{d}\theta}{\mathrm{d}\tau} + \left(1 + p\cos\omega\tau\right)\sin\theta = 0. \tag{2.24}$$

The parameters in Eq. (2.24) are defined as follows:

$$\tau := \Omega_0 t + \tau_0, \quad c := \frac{\gamma}{\sqrt{2mK}}, \quad p := \frac{mgl}{2K}, \quad \text{and} \quad \omega := \frac{2\Omega}{\Omega_0}, \tag{2.25}$$

where τ_0 is selected at $\tau_0 = (\phi_1 + \phi_2)\Omega_0/2\Omega$ to regulate the initial phase of the parametric excitation $p\cos\omega\tau$. The derived equation (2.24) is the same form as the equation of motion (2.19) for the parametric pendulum. The derivation implies a correspondence relationship between the parametric pendulum and the coupled pendulums. The static downward position of the parametric pendulum indicates the synchronization of the coupled pendulums. Thus, the periodic librations represent subharmonic motions near the synchronization. On the other hand, the periodic rotations correspond to the synchronization of the different order. For example, for a periodic rotation at which the parametric pendulum rotates once during the excitation period, the synchronization of the order 1 : 2 or 2 : 1 appears in the coupled pendulums. In this way, the periodic motions of the parametric pendulum are associated with the synchronous motions of coupled pendulums.

Chapter 3

Energy Conversion in Frequency Entrainment of Libration

This chapter begins analysis of energy conversion in synchronization. We focus on frequency entrainment for two types of limit cycles on the cylindrical state space. In this chapter, we first introduce the van der Pol oscillator as a model system in which frequency entrainment of libration occurs. Then energy exchanged in the system is examined with response characteristics of periodic librations. The energy is further analyzed in transient phenomenon to the entrainment.

3.1 Van der Pol oscillator

In this section, the van der Pol oscillator [66] is introduced as a model system in which frequency entrainment occurs for a librational limit cycle. We review the entrainment phenomenon and then define the notion of energy in the system for the analysis of energy conversion.

3.1.1 Model system

As a dynamical system with a stable librational limit cycle, we consider the forced van der Pol oscillator described as follows [64]:

$$\frac{\mathrm{d}u}{\mathrm{d}t} = v, \tag{3.1a}$$

$$\frac{\mathrm{d}v}{\mathrm{d}t} = \mu(1 - \beta u - \gamma u^2)v - u + B \sin \nu t, \tag{3.1b}$$

where u and v are the dependent variables of the nondimensional time t. The positive parameter μ determines the magnitude of the nonlinear damping, and β and γ characterize the nonlinearity of the damping. The term $B \sin \nu t$ represents the periodic excitation with the amplitude B and the angular frequency ν. We express the periodic excitation by $e_\mathrm{L}(t) := B \sin \nu t$ and its period by $T_\mathrm{L} := 2\pi/\nu$. In the thesis, the damping
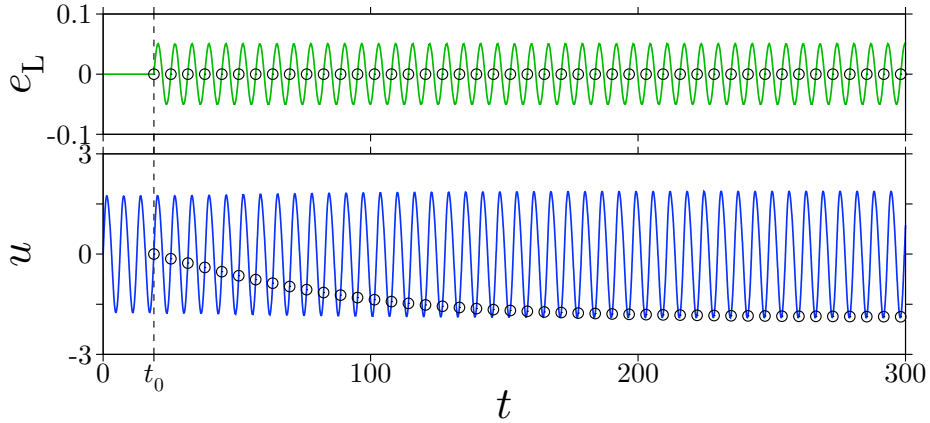
Figure 3.1: Frequency entrainment of libration in the system (3.1) at $\mu = 0.15$, $\beta = \gamma = 4/3$, $B = 0.05$, and $\nu = 0.99$. The periodic excitation $e_L(t - t_0) = B \sin\{\nu(t - t_0)\}$ is applied from $t = t_0$. The convergence of the stroboscopic points, denoted by the circles $\odot$, shows that the librational limit cycle is entrained by the periodic excitation.

parameters are fixed at $\mu = 0.15$, $\beta = 4/3$, and $\gamma = 4/3$ [64] so that a stable limit cycle appears in the system (3.1).

3.1.2 Frequency entrainment

As mentioned in Chapter 2, there exists a stable librational limit cycle or a limit cycle of the first kind [63] in the system (3.1) without the periodic excitation as shown in Fig. 2.5(a). The angular frequency ν_0 of the limit cycle is numerically estimated to be around 0.99. Frequency entrainment can be observed in the situation in which the excitation frequency is close to the frequency of a limit cycle [64]. We briefly review the system behavior that represents the frequency entrainment of libration.

Figure 3.1 shows frequency entrainment caused by the periodic excitation in the system (3.1). The excitation parameters are set at the amplitude $B = 0.05$ and the angular frequency $\nu = 0.99$ for the occurrence of the entrainment phenomenon. In the figure, the limit cycle is first observed. Then the periodic excitation is applied from $t = t_0$. The circles on the waveforms indicate stroboscopic points at every excitation period T_L. The application of the periodic excitation induces frequency entrainment of the limit cycle. The convergence of the stroboscopic points shows that the entrained libration appears.

We confirmed the frequency entrainment of libration in the system (3.1) by using Fig. 3.1. The entrainment phenomenon can be divided into two regimes. One is the entrained regime that is shown by the converged stroboscopic points. The other is the transient regime corresponding to the interval from the application of the periodic excitation to the entrained regime. Since the regimes exhibit different behaviors, we expect different features for the regimes in terms of energy conversion. In this chapter,

22

each of the two regimes is analyzed from the viewpoint of energy conversion.

3.1.3 Energy conversion

The notion of energy is introduced to the system (3.1). We begin with the definition of a function S_L as

$$S_L(u, v) := \frac{1}{2}v^2 + \frac{1}{2}u^2. \tag{3.2}$$

From a physical point of view, we interpret S_L as energy stored in the system (3.1). The temporal change of S_L can be described by using the time derivative of Eq. (3.2). That is,

$$\frac{dS_L}{dt} = \frac{\partial S_L}{\partial u} \cdot \frac{du}{dt} + \frac{\partial S_L}{\partial v} \cdot \frac{dv}{dt} = \mu(1 - \beta u - \gamma u^2)v^2 + Bv\sin\nu t. \tag{3.3}$$

In the transformation, we substituted Eqs. (3.1) and (3.2) into the time and the partial derivatives, respectively. Eq. (3.3) reveals that the temporal change of the stored energy is determined by effect from the damping and the periodic excitation on the system (3.1). Therefore we can evaluate variation of the stored energy during a finite time interval. For any behavior $(u(t), v(t))$ of the system (3.1), integration of Eq. (3.3) in any interval $[t_1, t_2]$, where $t_1 < t_2$, gives

$$S_L(t_2) - S_L(t_1) = \int_{t_1}^{t_2} \mu[1 - \beta u(t) - \gamma\{u(t)\}^2]\{v(t)\}^2 \, dt + \int_{t_1}^{t_2} Bv(t)\sin\nu t \, dt. \tag{3.4}$$

Since the stored energy $S_L(u(t), v(t))$ is a function of time t, we described the stored energy as $S_L(t)$. The left-hand side of Eq. (3.4) represents variation of the stored energy during the interval $[t_1, t_2]$. On the right-hand side, the first term denotes energy dissipated from the system by the damping, and the second term represents energy supplied to the system by the periodic excitation during the interval $[t_1, t_2]$. The relationship (3.4) implies that the variation of the stored energy is equivalent to the sum of the dissipated energy and the supplied energy in any interval.

3.2 Entrained libration

In this section, energy conversion is analyzed for the entrained states in the system (3.1) by using response curves. Before the analysis, we derive an averaged equation for the system (3.1). Response curves help us to associate the energy conversion and response characteristics of the entrained librations. The relationship is verified by the theoretical description from the averaged equation.

3.2.1 Averaged equation

In order to provide a theoretical viewpoint for the analysis, an averaged equation is derived for the system (3.1). In the derivation, we first assume the following for the system (3.1).

(i) The parameters μ and B are sufficiently small.

(ii) The excitation frequency ν is close to the frequency ν_0 of the librational limit cycle.

(iii) The considered domain in the state space is the vicinity of an entrained libration.

These assumptions make it possible to describe any libration $(u(t), v(t))$ which satisfies (iii) as a perturbation of the librational limit cycle,

$$u(t) = b_\mathrm{L}(t) \sin\big(\nu t + \theta_\mathrm{L}(t)\big), \tag{3.5a}$$

$$v(t) = \nu b_\mathrm{L}(t) \cos\big(\nu t + \theta_\mathrm{L}(t)\big), \tag{3.5b}$$

where $b_\mathrm{L}(t)$ is the amplitude of the libration and $\theta_\mathrm{L}(t)$ is the phase difference between the libration and the periodic excitation $B \sin \nu t$. The temporal change of these variables represent the transient behavior in the vicinity of an entrained libration. A stable fixed point of the variables corresponds to an entrained libration. By applying the averaging method [62] to Eq. (3.1) with Eq. (3.5), the following averaged equation is obtained [21]:

$$\frac{\mathrm{d}b_\mathrm{L}}{\mathrm{d}t} = \frac{1}{2}\mu b_\mathrm{L}\left(1 - \frac{1}{4}\gamma b_\mathrm{L}^2\right) - \frac{B}{2\nu}\sin\theta_\mathrm{L}, \tag{3.6a}$$

$$\frac{\mathrm{d}\theta_\mathrm{L}}{\mathrm{d}t} = \frac{1 - \nu^2}{2\nu} - \frac{B}{2\nu b_\mathrm{L}}\cos\theta_\mathrm{L}. \tag{3.6b}$$

In Eq. (3.6b), the frequency of the librational limit cycle is substituted as $\nu_0 = 1$. Equilibrium points of Eq. (3.6), denoted by b_L^* and θ_L^*, approximate the amplitude and phase difference of periodic librations of Eq. (3.1). Therefore, a stable equilibrium point of Eq. (3.6) corresponds to an entrained libration in the system (3.1).

3.2.2 Response curves for supplied energy

Energy conversion at the entrained states in the system (3.1) is analyzed through energy supplied by the periodic excitation. We provide a relationship of energy balance at the periodic librations. Eq. (3.4) describes the energy balance in the system (3.1) during any interval. Substituting $t_1 = 0$, $t_2 = T_\mathrm{L}$ and any periodic libration $(u^*(t), v^*(t))$ into Eq. (3.4) gives the expression for the energy balance at any periodic libration in the system (3.1),

$$0 = \int_0^{T_\mathrm{L}} \mu\big[1 - \beta u^*(t) - \gamma\{u^*(t)\}^2\big]\{v^*(t)\}^2 \,\mathrm{d}t + \int_0^{T_\mathrm{L}} B v^*(t) \sin \nu t \,\mathrm{d}t. \tag{3.7}$$

Since the stored energy during the period T_L is kept constant at any periodic libration, the difference of these functions $S_\mathrm{L}(T_\mathrm{L})$ and $S_\mathrm{L}(0)$ is equal to zero on the left-hand side of Eq. (3.7). On the right-hand side, the first term denotes energy dissipated
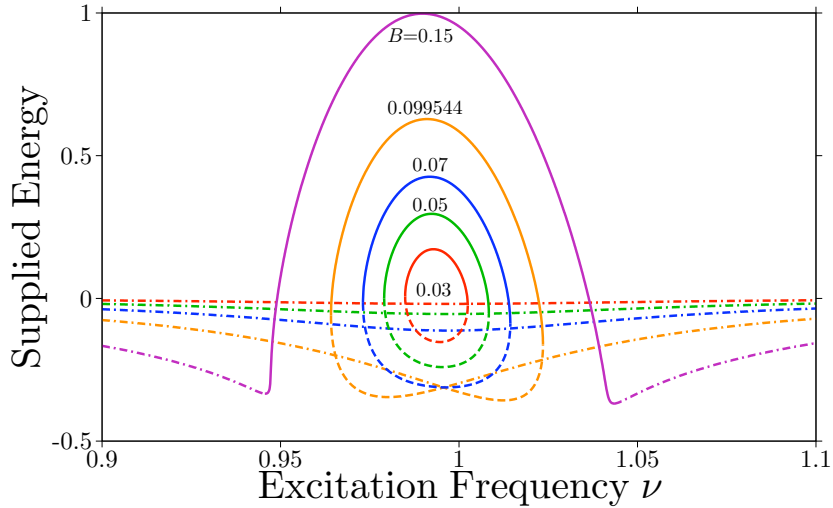
Figure 3.2: Response curves for the energy supplied by the periodic excitation in the system (3.1) at $\nu = 0.15$ and $\beta = \gamma = 4/3$. The supplied energy is calculated from the second term on the right-hand side of Eq. (3.7). The solid lines correspond to completely stable librations, the dashed lines directly unstable ones, and the chain lines completely unstable ones [78]. The detailed classification of the stability of these periodic librations is explained in the appendix of this chapter.

from the system (3.1) by the damping during T_{L}. The second term represents energy supplied to the system by the periodic excitation during T_{L}. Eq. (3.7) clarifies that the supplied energy is equivalent to the dissipated energy at any periodic libration. From the relationship, we focus on the supplied energy to analyze energy conversion at the entrained states of the system (3.1).

Figure 3.2 shows response curves for the energy supplied to the system (3.1) by the periodic excitation. The solid curves depict stable librations which correspond to the entrained states. Thus, the region of the excitation frequency ν for the solid curves implies the entrainment region. For each amplitude B of the excitation, the maximum energy is supplied around the frequency $\nu = \nu_0 \approx 0.99$. On the other hand, the supplied energy indicates negative value around both ends of the entrainment region. Based on Eq. (3.5a), we investigate response characteristics of the entrained librations to associate the supplied energy with the characteristics. Here the response characteristics suggest the amplitude and the phase difference in the fundamental frequency component for the periodic librations. The amplitude and phase difference correspond to a fixed point of the variables b_{L} and θ_{L} in Eq. (3.5a). Fig. 3.3(a) shows response curves for the amplitude of the periodic librations. The solid curves corresponding to the entrained librations manifest resonance phenomenon in the neighborhood of the frequency of the librational limit cycle, denoted by the cross symbol. Furthermore, the excitation frequency ν for the largest amplitude decreases as the excitation amplitude B increases. The corresponding resonance phenomenon is observed in the response curves for the supplied energy. The result indicates a correlation between the supplied energy
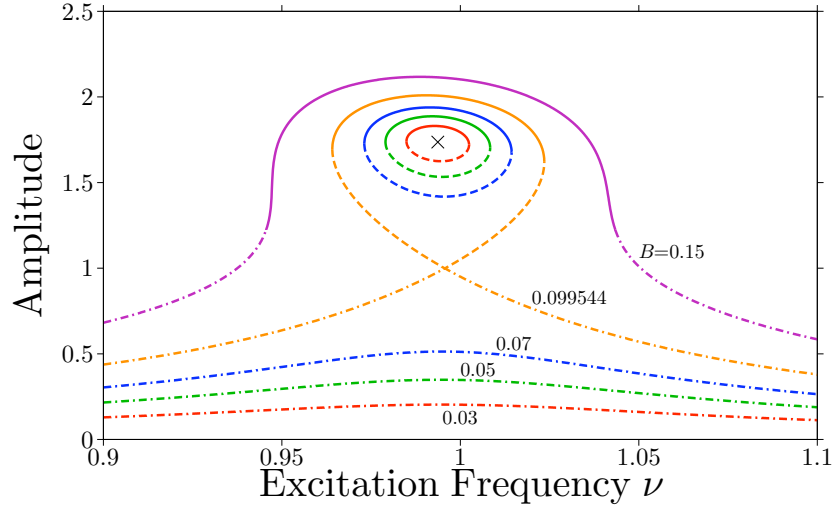
(a) Amplitude.
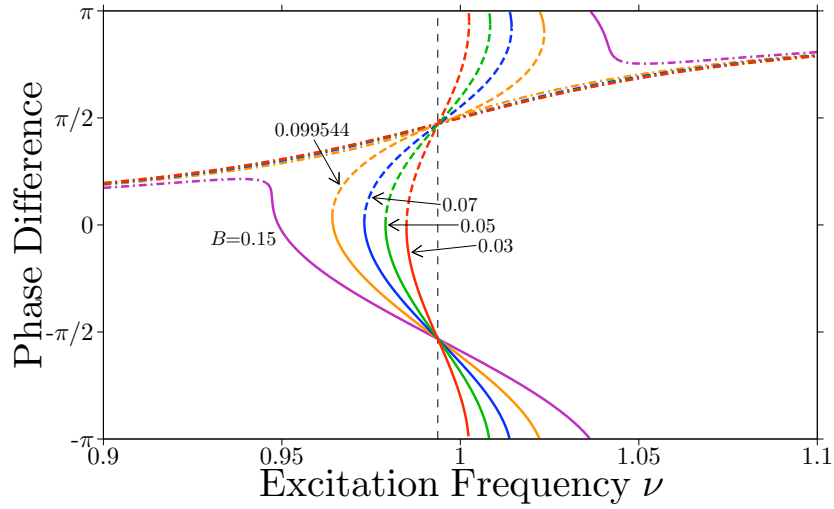
(b) Phase difference.

Figure 3.3: Response curves for (a) the amplitude of the periodic librations and (b) the phase difference between the periodic librations and the periodic excitation by using Eq. (3.1) at $\nu = 0.15$ and $\beta = \gamma = 4/3$. In (a), the cross symbol represents the amplitude of the librational limit cycle. In (b), the vertical dashed line indicates the angular frequency of the limit cycle. Each type of the lines shows the stability of the periodic librations in the same manner as Fig. 3.2.
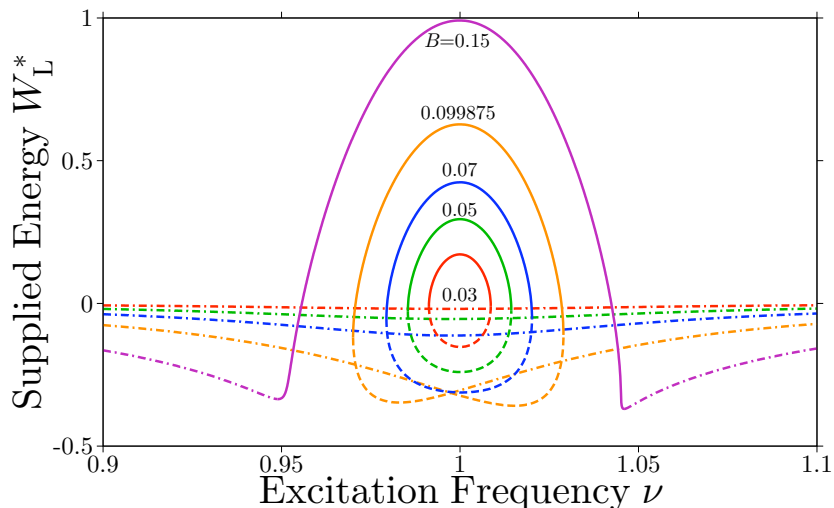
26

Figure 3.4: Response curves for the energy W_L^* supplied by the periodic excitation by using Eqs. (3.6) and $W_L^* = -\pi b^* B \sin \theta_L^*$ at $\nu = 0.15$ and $\beta = \gamma = 4/3$. The solid lines correspond to stable equilibrium points, the dashed and chain lines unstable ones. The instability is classified by the number of positive eigen value of the linearized matrix of Eq. (3.6) at the equilibrium points. The dashed lines denote one positive eigen value, the chain lines two.

and the amplitude at the entrained librations. Fig. 3.3(b) depicts response curves for the phase difference between the periodic librations and the periodic excitation. All solid curves are coincident at the frequency of the librational limit cycle. At the frequency, the phase difference of the stable librations is $-\pi/2$. For the dashed lines, the same coincidence is observed at $\pi/2$. Positive energy is supplied at the phase difference from $-\pi$ to 0.

We verify the numerical results from a theoretical viewpoint. By applying the averaging method to Eq. (3.7) with any periodic libration, that is $u^*(t) = b_L^* \sin(\nu t + \theta_L^*)$ and $v^*(t) = \nu b_L^* \cos(\nu t + \theta_L^*)$, a theoretical expression is obtained for the energy balance at any periodic libration in the system (3.1) as

$$0 = \pi \mu \nu b_L^{*2} \left(1 - \frac{1}{4} \gamma b_L^{*2}\right) - \pi b_L^* B \sin \theta_L^*, \tag{3.8}$$

where the constants b_L^* and θ_L^* correspond to the equilibrium points of the averaged equation (3.6). Eq. (3.8) is a theoretical expression of Eq. (3.7). Thus on the right-hand side of Eq. (3.8), the first term denotes the dissipated energy, and the second term the supplied energy during the period T_L. The equilibrium points of (3.6) give the corresponding supplied energy by using $-\pi b^* B \sin \theta_L^* =: W_L^*$.

Figure 3.4 shows response curves for the supplied energy W_L^* by using Eqs. (3.6) and (3.8). The theoretical result for the supplied energy is consistent with the numerical result shown in Fig. 3.2. In addition, we verify the amplitude and the phase difference of the periodic librations. Figs. 3.5(a) and 3.5(b) show response curves for the ampli-

tude b_L^* and the phase difference θ_L^* obtained by using the equilibrium points of the averaged equation (3.6). The response characteristics are coincident with the numerical results shown in Fig. 3.3. Therefore, under the above assumptions, the equilibrium points of Eq. (3.6) and the theoretical expression (3.8) show response characteristics of the supplied energy and the periodic librations in the system (3.6). This implies that the expression of the supplied energy, that is $W_L^* = -\pi b_L^* B \sin \theta_L^*$, reveals relationships of the supplied energy with the amplitude and the phase difference of the entrained librations. From the theoretical expression, the supplied energy W_L^* increases with the amplitude b_L^*. For the phase difference θ_L^* from $-\pi$ to 0, positive energy is supplied to the system (3.1) by the periodic excitation. These relationships are consistent with the characteristics observed in Figs. 3.2 and 3.3.

3.3 Transient phenomenon of entrainment of libration

In this section, we analyze the transient regime of the frequency entrainment of libration in terms of energy. First a phase equation is derived to describe transient phenomenon of the entrainment in the system (3.1). The theoretical viewpoint clarifies the relationship between the stored energy and the frequency entrainment in the transient regime.

3.3.1 Phase equation

A phase equation is derived which describes the phase dynamics for the frequency entrainment. The phase for the frequency entrainment of libration in the system (3.1) is explicitly identified as the phase difference θ_L defined in Eq. (3.5) because of the following. In the frequency entrainment, the frequency of the limit cycle is entrained by the excitation frequency. The frequency change in the entrainment phenomenon from the limit cycle to the entrained libration can be described by substituting the phase $\theta_L(t) = \nu_0 t - \nu t + \theta_{L0}$ and $\theta_L(t) = \theta_L^*$ into Eq. (3.5), respectively. Here θ_{L0} is the initial phase of the limit cycle. The phase difference θ_L represents the frequency entrainment of libration. In the following, we call the phase difference the phase or the phase variable for the entrainment. We make an additional assumption,

(iv) The temporal change of $b_L(t)$ is fixed at the amplitude of the librational limit cycle, denoted by b_{L0}.

From the assumption, we can focus on the phase dynamics in the transient regime. Then, the expression (3.5) is modified to

$$u(t) = b_{L0} \sin \big(\nu t + \theta_L(t)\big), \tag{3.9a}$$

$$v(t) = \nu b_{L0} \cos \big(\nu t + \theta_L(t)\big). \tag{3.9b}$$

28
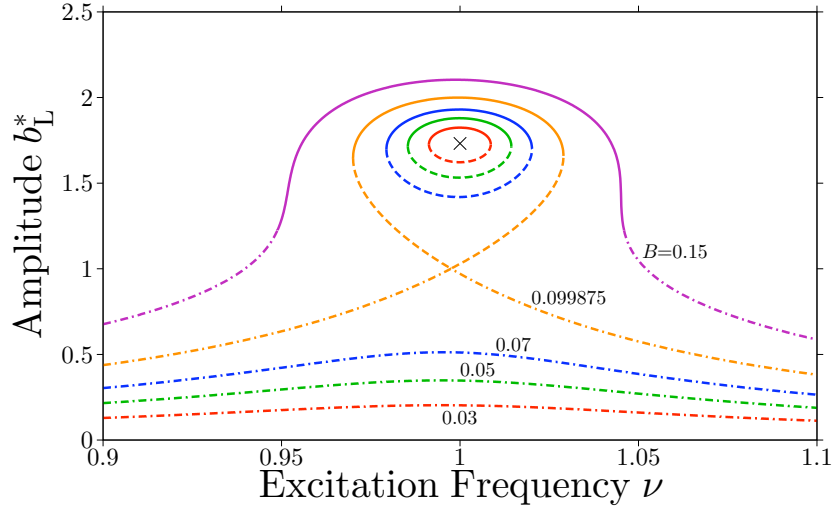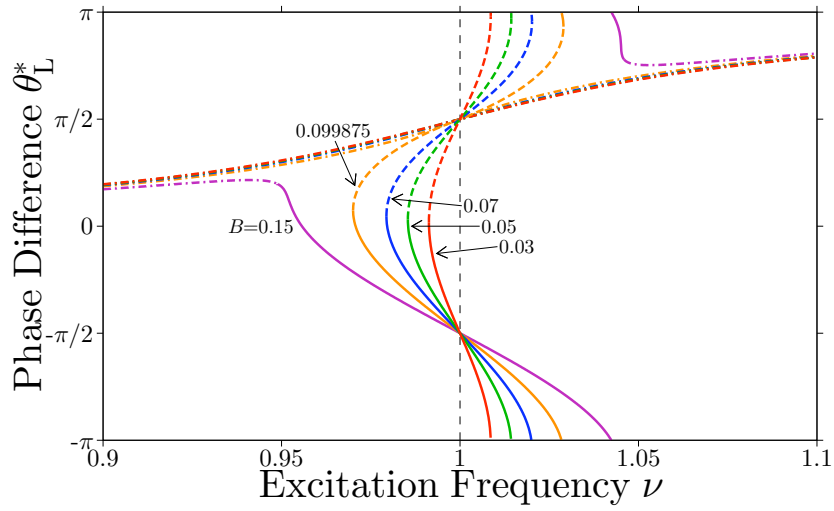
(a) Amplitude b_L^*.

(b) Phase difference θ_L^*.

Figure 3.5: Response curves for (a) the amplitude b_L^* and (b) the phase difference θ_L^* by using Eqs. (3.6) and (3.8) at $\nu = 0.15$, $\beta = \gamma = 4/3$. In (a), the cross symbol represents the amplitude of the librational limit cycle. In (b), the vertical dashed line indicates the angular frequency of the limit cycle. Each type of the lines shows the stability of the equilibrium points in the same manner as Fig. 3.4.

29

The expression (3.9) clearly shows that the dynamics near an entrained libration are governed by the phase variable $\theta_{\mathrm{L}}(t)$. By applying the averaging method to Eq. (3.1) with Eq. (3.9), the following phase equation is obtained:

$$\frac{\mathrm{d}\theta_{\mathrm{L}}}{\mathrm{d}t} = \frac{1 - \nu^2}{2\nu} - \frac{B}{2\nu b_{\mathrm{L0}}}\cos\theta_{\mathrm{L}}. \tag{3.10}$$

On the right-hand side, the first term represents the difference between the frequency of the librational limit cycle $\nu_0 = 1$ and the excitation frequency ν, and the second term the effect of the periodic excitation on the phase dynamics. Eq. (3.10) has the same formulation as the phase equations in [2, 8, 79]. We describe the mechanism of phase regulation in the entrainment phenomenon of libration in terms of the phase equation (3.10). The periodic excitation is applied to the system (3.1), and then the phase θ_{L} undergoes a gradual change according to Eq. (3.10). If the effect of the periodic excitation can compensate the difference between the frequency of the limit cycle and the excitation frequency, the frequency entrainment of libration is observed. Thus the phase equation (3.10) represents how the frequency of the limit cycle is entrained to excitation frequency. In the next chapter, we will obtain the same mechanism for the frequency entrainment of rotation in the phase-locked system (4.1).

3.3.2 Transient behavior of stored energy

The transient regime of the frequency entrainment of libration in the system (3.1) is analyzed in terms of the stored energy. By substituting Eq. (3.9) into Eq. (3.2), the time average of the stored energy is derived as follows:

$$\langle S_{\mathrm{L}}\rangle(\theta_{\mathrm{L}}) := \frac{1}{T_{\mathrm{L}}}\int_{-T_{\mathrm{L}}/2}^{T_{\mathrm{L}}/2} S_{\mathrm{L}}\big(u(t, \theta_{\mathrm{L}}), v(t, \theta_{\mathrm{L}})\big)\,\mathrm{d}t = \frac{1}{4}(1 + \nu^2)b_{\mathrm{L0}}^2 =: \langle S_{\mathrm{L}}\rangle^*, \tag{3.11}$$

where the bracket $\langle\cdot\rangle$ denotes the time average during the excitation period T_{L}. The constant $\langle S_{\mathrm{L}}\rangle^*$ indicates the value of $\langle S_{\mathrm{L}}\rangle$ at the periodic libration. Eq. (3.11) explicitly shows that $\langle S_{\mathrm{L}}\rangle$ is not a function of the phase θ_{L} and remains at $\langle S_{\mathrm{L}}\rangle^*$ in the transient and entrained regimes. This result is originated from the assumption (iv). Eq. (3.11) is significant for the mechanism of the frequency entrainment of libration.

Figure 3.6 shows the stored energy and the phase in the frequency entrainment of libration in the system (3.1). The transient regime is induced by resetting the periodic excitation at $t = t_0$. The solid line on the waveform of u denotes the amplitude which is calculated from $\sqrt{u^2 + (v/\nu)^2}$. The stored energy S_{L} is obtained by using Eq. (3.2). The solid curve on the waveform of S_{L} indicates the time average obtained by averaging S_{L} over the excitation period T_{L}. In addition, the dashed line represents the time average at the entrained libration. Since these lines correspond to b_{L}, $\langle S_{\mathrm{L}}\rangle$, and $\langle S_{\mathrm{L}}\rangle^*$, we indicate these lines by using the corresponding notations in Fig. 3.6. We regard the stroboscopic points of $\tan^{-1}(\nu u/v) =: \phi_{\mathrm{L}}$ as the phase θ_{L}. Figs. 3.6(a) and 3.6(b) are for two different reset time t_0 for $\nu = 0.98$. In Fig. 3.6(a), the deviation $\langle S_{\mathrm{L}}\rangle - \langle S_{\mathrm{L}}\rangle^*$

(a) $t_0 = (3 + 1/4) T_L$ and $\nu = 0.98$.

(b) $t_0 = (3 + 3/4) T_L$ and $\nu = 0.98$.

(c) $t_0 = (3 + 1/4) T_L$ and $\nu = 0.99$.

(d) $t_0 = (3 + 3/4) T_L$ and $\nu = 0.99$.
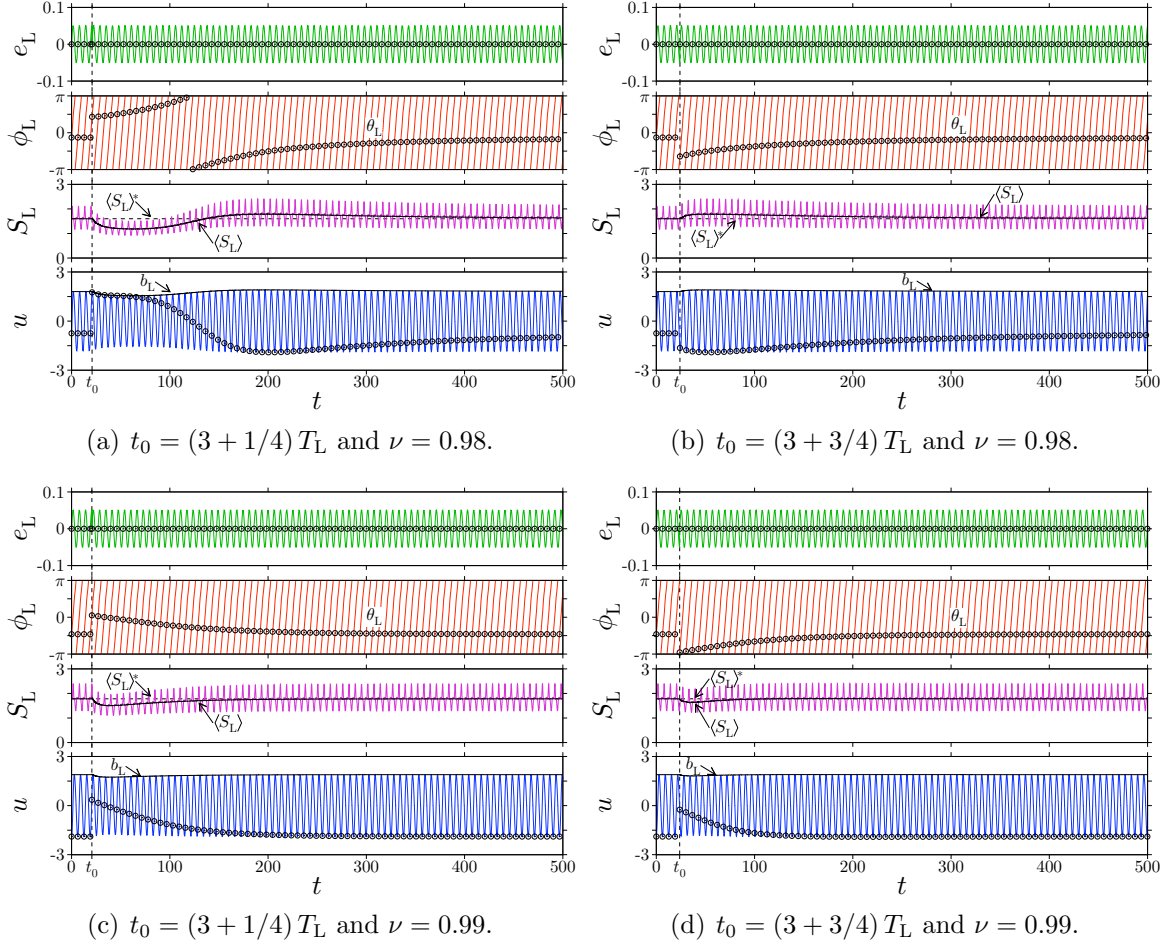
Figure 3.6: Stored energy and phase in the frequency entrainment of libration in the system (3.1) at $\mu = 0.15$, $\beta = \gamma = 4/3$, and $B = 0.05$. The phase of the periodic excitation e_L is reset at $t = t_0$, and then the transient regime of the frequency entrainment appears. The solid lines on the waveforms of u and S_L denote the amplitude and the time average of S_L, respectively. The dashed lines of S_L represent the time average at the entrained libration. Since these lines correspond to b_L, $\langle S_L \rangle$, and $\langle S_L \rangle^*$, we indicate these lines by using the corresponding notation. The phase θ_L is estimated from the stroboscopic points $\odot$ of $\tan^{-1}(\nu u / v) =: \phi_L$.

indicates negative value after the resetting. On the other hand, in Fig. 3.6(b), the positive deviation is observed. These changes of $\langle S_{\mathrm{L}} \rangle$ have no affect on the phase response. Indeed the phase monotonically increases. Rather, we can confirm that b_{L} depends on $\langle S_{\mathrm{L}} \rangle$. The dependence coincides with Eq. (3.11). Here it should be noted that the amplitude $b_{\mathrm{L}}(t)$ is fixed at $b_{\mathrm{L}0}$ in the derivation of the phase equation. Next, we consider the stored energy and the phase at the different excitation frequency, namely $\nu = 0.99$ in Figs. 3.6(c) and 3.6(d). In these figures, the phase θ_{L} increases or decreases for the negative deviation $\langle S_{\mathrm{L}} \rangle - \langle S_{\mathrm{L}} \rangle^*$. The results are consistent with Eq. (3.11). Therefore, the development of the entrainment phenomenon of libration does not depend on the stored energy.

3.4   Remarks

In this chapter, we analyzed energy conversion in frequency entrainment of libration. Here the van der Pol oscillator was employed as a dynamical system with a stable librational limit cycle.

At the entrained states, energy conversion in the system was investigated through energy supplied to the system by the periodic excitation. Response curves were obtained numerically and theoretically for the supplied energy and the characteristics of the entrained librations. The characteristics are the amplitude and the phase difference from the periodic excitation. The theoretical result from the averaged equation for the system is coincident with the numerical one. The coincidence implies that the observed relationships between the response curves are described by the theoretical expression. The magnitude of energy conversion at the entrained librations increases with the amplitude. Since the response curves for the amplitude exhibit resonance phenomenon, the maximum energy is converted near the frequency of the librational limit cycle.

In the transient regime, we considered the development of the entrainment phenomenon by deriving the phase equation which describes the phase dynamics for the entrainment. The theoretical expression for the stored energy does not include the phase. This implies that the development of the entrainment phenomenon of libration does not depend on the energy conversion. We numerically confirmed the energy conversion in the transient regime of the entrainment. Therefore, the phase regulation which governs the frequency entrainment of libration is not essentially affected by any energy supply from the external. The energy conversion determines the amplitude.

Finally, we summarize the energy conversion in the frequency entrainment of libration. The notion of energy was associated with the amplitude. As a relationship between the energy conversion and the response characteristics of the periodic librations, we can take the resonance phenomenon for the supplied energy. The theoretical expression for the supplied energy contains the phase. However, the supplied energy can be replaced with the dissipated energy without the phase from the relationship of energy balance. Therefore in the transient and entrained regimes, the energy conversion can be comprehended through the amplitude.

Appendix to classification of stability

This appendix presents the classification used in the thesis for the stability of hyperbolic periodic orbits or fixed points according to [78, 80].

Consider an n-dimensional non-autonomous T-periodic system

$$\frac{\mathrm{d}\boldsymbol{x}}{\mathrm{d}t} = \boldsymbol{f}(t, \boldsymbol{x}), \quad \boldsymbol{x} \in \mathbb{R}^n \tag{3.12}$$

with a T-periodic orbit $\boldsymbol{x}^*(t) = \boldsymbol{x}^*(t - T)$. We can construct a stroboscopic map P for the system (3.12). The T-periodic orbit $\boldsymbol{x}^*(t)$ corresponds to a fixed point of the map P, that is, $\boldsymbol{x}^* = P(\boldsymbol{x}^*)$. The local behavior of P near $\boldsymbol{x}^*$ is approximated by linearizing the map P at $\boldsymbol{x}^*$. The obtained linear map

$$\boldsymbol{\xi}_{k+1} = DP(\boldsymbol{x}^*)\boldsymbol{\xi}_k \tag{3.13}$$

describes the dynamics in the vicinity of $\boldsymbol{x}^*$, where $\boldsymbol{\xi}_k$ denotes a variation of $\boldsymbol{x}_k$ from $\boldsymbol{x}^*$ for the integer k. The linear map $DP(\boldsymbol{x}^*)$ is an $n \times n$ matrix, where $D := \partial/\partial\boldsymbol{x}$. The eigenvalues λ_i of the matrix $DP(\boldsymbol{x}^*)$ determine the stability of the periodic orbit or fixed points $\boldsymbol{x}^*$ for $i = 1, \cdots, n$. These eigenvalues have been already sorted by the magnitude of the modulus, that is, $|\lambda_1| \geq |\lambda_2| \geq \cdots \geq |\lambda_n|$.

For $n = 2$, the periodic orbit or fixed point $\boldsymbol{x}^*$ is characterized [78] as follows:

$$\begin{cases} completely\ stable & \text{if } |\lambda_2| \leq |\lambda_1| < 1, \\ completely\ unstable & \text{if } |\lambda_1| \geq |\lambda_2| > 1, \\ directly\ unstable & \text{if } \lambda_1 > 1 > \lambda_2 > 0, \\ inversely\ unstable & \text{if } \lambda_1 < -1 < \lambda_2 < 0. \end{cases}$$

For $\boldsymbol{x}^*$, the dimensions of the stable and the unstable manifolds are denoted by n_{s} and n_{u}, respectively. Here $n_{\mathrm{s}} + n_{\mathrm{u}} = n$. For $n \geq 3$ and $n_{\mathrm{u}} \leq 1$, we extend the classification as follows:

$$\begin{cases} completely\ stable & \text{if } |\lambda_1| < 1, \\ directly\ unstable & \text{if } \lambda_1 > 1 \text{ and } |\lambda_2| < 1, \\ inversely\ unstable & \text{if } \lambda_1 < -1 \text{ and } |\lambda_2| < 1. \end{cases}$$

This extended classification is determined by the eigenvalue λ_1 with the maximum modulus for $|\lambda_i| < 1$ $(i = 2, \cdots, n)$.

Chapter 4

Energy Conversion in Frequency Entrainment of Rotation

In this chapter, we analyze energy conversion in frequency entrainment for the rotational limit cycle. The phase-locked system is introduced as a dynamical system with a stable rotational limit cycle. In the same manner as Chapter 3, energy conversion in the system is investigated at the entrained rotations. Then, the transient regime of the frequency entrainment is analyzed in terms of energy. We associate the dynamics of phase for the entrainment phenomenon with energy stored in the system. Finally, the frequency entrainment phenomena of libration and rotation are compared from the viewpoint of energy conversion.

4.1   Phase locked system

This section explains the phase-locked system in which frequency entrainment appears for a rotational limit cycle or a limit cycle of the second kind [63]. The frequency entrainment of rotation is reviewed, and the notion of energy is introduced into the system.

4.1.1   Model system

We consider frequency entrainment of rotation in the phase locked system given by

$$\frac{\mathrm{d}\phi}{\mathrm{d}t} = y, \tag{4.1a}$$

$$\frac{\mathrm{d}y}{\mathrm{d}t} = -ky - \sin\phi + N + A\sin\Omega t, \tag{4.1b}$$

where ϕ and y are the dependent variables of the nondimensional time t. The positive parameter k denotes the damping coefficient and N the constant torque. The term $A\sin\Omega t$ represents the periodic excitation with the amplitude A and the angular frequency Ω. Here we express the periodic excitation by $e_{\mathrm{R}}(t) := A\sin\Omega t$ and its
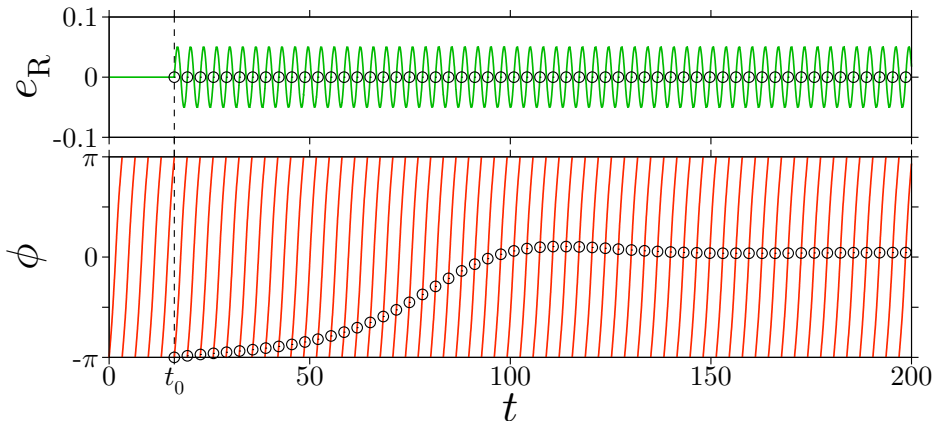
Figure 4.1: Frequency entrainment of rotation in the system (4.1) at $k = 0.1$, $N = 0.2$, $A = 0.05$, and $\Omega = 1.93$. The periodic excitation $e_R(t - t_0) = A\sin\{\Omega(t - t_0)\}$ is applied from $t = t_0$. The convergence of the stroboscopic points, denoted by the circles $\odot$, shows that the rotational limit cycle is entrained by the periodic excitation.

period by $T_R := 2\pi/\Omega$. The damping coefficient and the constant torque are fixed at $k = 0.1$ and $N = 0.2$ so that there exists a stable rotational limit cycle in the system (4.1). The parameter setting satisfies the condition, namely $N > 4k/\pi$, which describes the existence of a stable rotational limit cycle. The condition is obtained from the Melnikov's method [65].

4.1.2   Frequency entrainment

In Chapter 2, we already confirmed the existence of a stable rotational limit cycle in the system (4.1) without the periodic excitation. The angular frequency Ω_0 of the limit cycle is numerically estimated to be around 1.93. Frequency entrainment of rotation can be observed in the same situation as the phenomenon of libration. Frequency entrainment of rotation has been observed in a single driven pendulum [81] and the Josephson junction circuit [69, 70, 72, 82]. We briefly review the frequency entrainment of rotation in the system (4.1).

Figure 4.1 shows frequency entrainment by the periodic excitation in the system (4.1). The excitation parameters are fixed at $A = 0.05$ and $\Omega = 1.93$ to induce the entrainment phenomenon. In the figure, we observe the rotational limit cycle without the periodic excitation for $t < t_0$. From $t = t_0$, the periodic excitation is applied to the system. The circles on the lines denote the stroboscopic points at every excitation period T_R. After $t = t_0$, the stroboscopic points converge. Since the convergent stroboscopic points represent the appearance of a periodic rotation, we can observe that the frequency of the rotational limit cycle is entrained by the excitation frequency.

As confirmed for the frequency entrainment of libration in Chapter 3, we also confirm two regimes of the entrainment phenomenon of rotation in the system (4.1). After

the application of the periodic excitation, the transient regime appears. Then the entrained regime is observed. In the same manner as Chapter 3, energy conversion in the system (4.1) is investigated for the entrained rotations and for the transient phenomenon, respectively.

4.1.3 Energy conversion

We define the energy stored in the system (4.1) as the following function S_R:

$$S_\mathrm{R}(\phi, y) := \frac{1}{2}y^2 - \cos\phi. \tag{4.2}$$

The temporal change of the stored energy S_R is represented by the time derivative,

$$\frac{\mathrm{d}S_\mathrm{R}}{\mathrm{d}t} = \frac{\partial S_\mathrm{R}}{\partial\phi} \cdot \frac{\mathrm{d}\phi}{\mathrm{d}t} + \frac{\partial S_\mathrm{R}}{\partial y} \cdot \frac{\mathrm{d}y}{\mathrm{d}t} = -ky^2 + Ny + Ay\sin\Omega t. \tag{4.3}$$

In the transformation, we substituted Eqs. (4.1) and (4.2) into the time and the partial derivatives, respectively. Eq. (4.3) explains that the temporal change of the stored energy is determined by effect from the damping, the constant torque, and the periodic excitation on the system (4.1). Next, variation of the stored energy S_R during a finite time interval is obtained. For any behavior $(\phi(t), y(t))$ of the system (4.1), by integrating Eq. (4.3) in any interval $[t_1, t_2]$, the following equation is given:

$$S_\mathrm{R}(t_2) - S_\mathrm{R}(t_1) = \int_{t_1}^{t_2} \left[-k\{y(t)\}^2 \right] \mathrm{d}t + \int_{t_1}^{t_2} Ny(t)\,\mathrm{d}t + \int_{t_1}^{t_2} Ay(t)\sin\Omega t\,\mathrm{d}t, \tag{4.4}$$

where we regarded the stored energy $S_\mathrm{R}(\phi(t), y(t))$ as the function of time t, that is $S_\mathrm{R}(t)$. The left-hand side of Eq. (4.4) represents the variation of the stored energy during the interval $[t_1, t_2]$. On the right-hand side, the first term denotes energy dissipated from the system by the damping, and the second and third terms represent energy supplied to the system by the constant torque and the periodic excitation during the interval $[t_1, t_2]$. Therefore, Eq. (4.4) implies that the stored energy changes by the sum of the dissipated energy and the supplied energy in any interval. The similar relationship (3.4) was obtained for the system (3.1).

4.2 Entrained rotation

This section describes analysis of energy conversion at the entrained states of the system (4.1) by using response curves. In order to provide a theoretical viewpoint to the analysis, we derive an averaged equation for the system (4.1). The response curves obtained numerically and theoretically allow us to understand features of the energy conversion with the entrained rotations. As the notion of energy, energy supplied to the system by the periodic excitation is considered.

4.2.1 Averaged equation

Before analyzing energy conversion at the entrained rotations, an averaged equation is derived for the system (4.1). First we make the following assumptions for the system (4.1).

(v) The parameters k, N, and A are sufficiently small.

(vi) The excitation frequency Ω is close to the angular frequency Ω_0 of the rotational limit cycle.

(vii) The vicinity of a stable periodic rotation representing an entrained state is addressed.

From these assumptions, we can describe any rotation $(\phi(t), y(t))$ which satisfies (vii) as a perturbation of the rotational limit cycle. However, the general expression of rotation is not established because of the nonlinearity. A few researchers have given expressions to periodic rotations from various viewpoints [38, 39, 74, 83].

We begin with an expression for the rotational limit cycle. From the temporal change and the periodic orbit in the state space shown in Fig. 2.7(a), the rotational limit cycle, denoted by $\phi_0(t)$, can be approximated as the sum of the rotatory component and the fundamental oscillatory one,

$$\phi_0(t) = \Omega_0 t + \theta_{R0} + a_{R0} \sin\left(\Omega_0 t + \psi_{R0}\right). \tag{4.5}$$

On the right-hand side, the first two terms denote the rotatory component, and the last term represents the fundamental oscillatory component with the amplitude a_{R0} and the phase difference ψ_{R0}. The second term θ_{R0} is an arbitrary constant obtained from the time average of $\phi_0(t) - \Omega_0 t$. Here the rotatory component $\Omega_0 t + \theta_{R0}$ remains at constant difference from the phase of the oscillatory component, $\Omega_0 t + \psi_{R0}$, because the periodic orbit for the limit cycle is identified in the cylindrical state space. We explicitly describe the constant phase deviation $\delta_{R0} := \psi_{R0} - \theta_{R0}$ as

$$\phi_0(t) = \Omega_0 t + \theta_{R0} + a_{R0} \sin\left(\Omega_0 t + \theta_{R0} + \delta_{R0}\right). \tag{4.6}$$

In Eq. (4.6) the amplitude a_{R0} and the phase deviation δ_{R0} are uniquely determined for the fixed parameters k and N.

From the above assumptions, we can describe any rotation $(\phi(t), y(t))$ which satisfies (vii) as a perturbation of the rotational limit cycle and its time derivative,

$$\phi(t) = \Omega t + \theta_R(t) + a_R(t) \sin\left(\Omega t + \theta_R(t) + \delta_R(t)\right), \tag{4.7a}$$

$$y(t) = \Omega + \omega_R(t) + \Omega a_R(t) \cos\left(\Omega t + \theta_R(t) + \delta_R(t)\right). \tag{4.7b}$$

The perturbation of θ_{R0}, a_{R0}, and δ_{R0} produces the corresponding variables $\theta_R(t)$, $a_R(t)$, and $\delta_R(t)$. In addition, we should consider the perturbation of the rotatory component in y, denoted by $\omega_R(t)$, because of the assumption (vii). Therefore, the temporal

change of these variables represents transient behavior in the vicinity of an entrained rotation, and a stable fixed point of these variables corresponds to an entrained rotation. Applying the averaging method [62] to Eq. (4.1) with Eq. (4.7) gives the averaged equation

$$\frac{\mathrm{d}\theta_\mathrm{R}}{\mathrm{d}t} = \omega_\mathrm{R}, \tag{4.8a}$$

$$\frac{\mathrm{d}\omega_\mathrm{R}}{\mathrm{d}t} = -k\big(\Omega + \omega_\mathrm{R}\big) - J_1(a_\mathrm{R})\sin\delta_\mathrm{R} + N, \tag{4.8b}$$

$$\frac{\mathrm{d}a_\mathrm{R}}{\mathrm{d}t} = \frac{J_0(a_\mathrm{R}) + J_2(a_\mathrm{R})}{2\Omega}\sin\delta_\mathrm{R} - \frac{1}{2}ka_\mathrm{R} - \frac{A}{2\Omega}\sin\big(\theta_\mathrm{R} + \delta_\mathrm{R}\big), \tag{4.8c}$$

$$\frac{\mathrm{d}\delta_\mathrm{R}}{\mathrm{d}t} = -\omega_\mathrm{R} + \frac{J_0(a_\mathrm{R}) - J_2(a_\mathrm{R})}{2a_\mathrm{R}\Omega}\cos\delta_\mathrm{R} - \frac{1}{2}\Omega - \frac{A}{2a_\mathrm{R}\Omega}\cos\big(\theta_\mathrm{R} + \delta_\mathrm{R}\big), \tag{4.8d}$$

where $J_n(\cdot)$ is the Bessel function of the first kind for the integer n. The detailed derivation is given in the appendix of this chapter. Equilibrium points of Eq. (4.8), denoted by θ_R^*, ω_R^*, a_R^*, and δ_R^*, approximate the components of the periodic rotations in the system (4.1). Thus, a stable equilibrium point of the averaged equation (4.8) corresponds to an entrained rotation in the system (4.1). Here we already know $\omega_\mathrm{R}^* = 0$ because the perturbation creates the variable $\omega_\mathrm{R}(t)$.

4.2.2 Response curves for supplied energy

Using the same approach as Chapter 3, we analyze energy conversion at the entrained rotations in the system (4.1). Energy balance is described at the entrained rotations. We already derived the energy balance (4.4) in the system (4.1) during any interval. For any periodic rotation $(\phi^*(t), y^*(t))$, by substituting $t_1 = 0$ and $t_2 = T_\mathrm{R}$ into Eq. (4.4), the energy balance at any periodic rotation in the system (4.1) is given by

$$\begin{aligned}
0 &= \int_0^{T_\mathrm{R}}\Big[-k\{y^*(t)\}^2\Big]\,\mathrm{d}t + \int_0^{T_\mathrm{R}} Ny(t)\,\mathrm{d}t + \int_0^{T_\mathrm{R}} Ay^*(t)\sin\Omega t\,\mathrm{d}t \\
&= \int_0^{T_\mathrm{R}}\Big[-k\{y^*(t)\}^2\Big]\,\mathrm{d}t + 2\pi N + \int_0^{T_\mathrm{R}} Ay^*(t)\sin\Omega t\,\mathrm{d}t.
\end{aligned} \tag{4.9}$$

For any periodic rotation $(\phi^*(t), y^*(t))$, the corresponding stored energy S_R changes periodically. The difference of the stored energy, $S_\mathrm{R}(T_\mathrm{R}) - S_\mathrm{R}(0)$, is equal to zero on the left-hand side of Eq. (4.9). On the right-hand side, the first term denotes energy dissipated from the system (4.1) by the damping during the excitation period T_R. The remaining terms correspond to energy supplied to the system by the constant torque and the periodic excitation during T_R. Eq. (4.9) shows that the supplied energy is equivalent to the dissipated energy at the entrained rotations. Since the second term $2\pi N$ on the right-hand side of Eq. (4.9) is constant, the energy supplied by the constant torque is invariant for the periodic excitation. Thus we consider the energy supplied by the periodic excitation to analyze the energy conversion at the entrained rotations in the system (4.1).
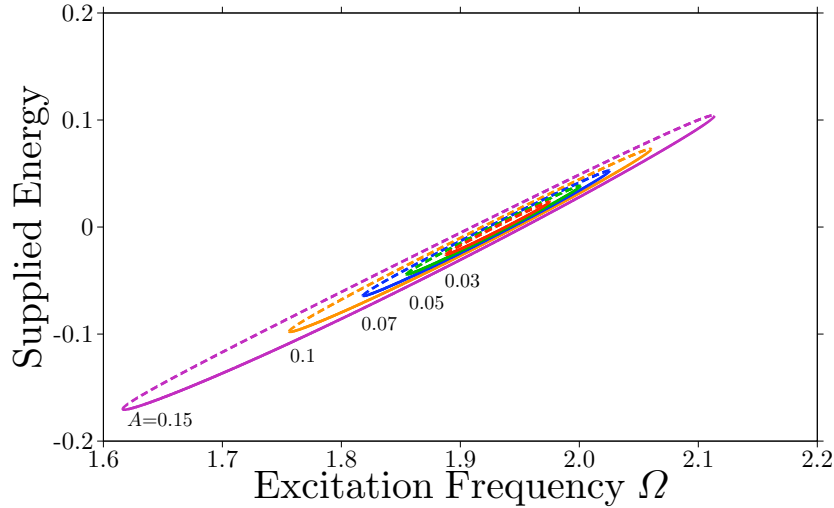
Figure 4.2: Response curves for the energy supplied by the periodic excitation in the system (4.1) at $k = 0.1$ and $N = 0.2$. The supplied energy is calculated from the last term on the right-hand side of Eq. (4.9). The solid lines correspond to completely stable rotations and the dashed lines directly unstable ones [78]. The detailed classification of the stability of these periodic rotations is explained in the appendix of Chapter 3.

Figure 4.2 shows response curves for the energy supplied to the system (4.1) by the periodic excitation. The solid curves denote stable rotations which correspond to the entrained states. Thus the region of the excitation frequency Ω for the solid curves shows the entrainment region. The supplied energy increases with the excitation frequency. The periodic excitation with the large amplitude A can entrain the rotational limit cycle at high frequency. A large amount of energy can be supplied by the large amplitude excitation at high frequency. At low frequency, the periodic excitation extracts energy from the system (4.1). In order to associate the supplied energy with the components of the entrained rotations, we show response characteristics of the entrained rotations based on the variables θ_R, a_R, and δ_R in Eq. (4.7a). Fig. 4.3(a) shows response curves for the phase of the rotatory component corresponding to θ_R. For the solid curves representing entrained rotations, the phase is restricted between $-\pi/2$ and $\pi/2$. Positive energy is supplied for the phase from $-\pi$ to 0. The response curves show similar structure with the curves for the phase difference of the entrained librations in Fig. 3.3(b). All solid and dashed curves are coincident at the frequency of the rotational limit cycle, respectively. Fig. 4.3(b) shows response curves for the amplitude of the fundamental oscillatory component in the periodic rotations. The solid curves show that antiresonance phenomenon appears at higher frequency than the rotational limit cycle. For most of the frequency region, the amplitude decreases as the excitation frequency increases. The amplitude exhibits opposite response characteristics from the supplied energy. Fig. 4.3(c) represents response curves for the phase deviation of the fundamental oscillatory component from the rotatory component. The phase deviation shows little change in comparison with the phase. All curves except
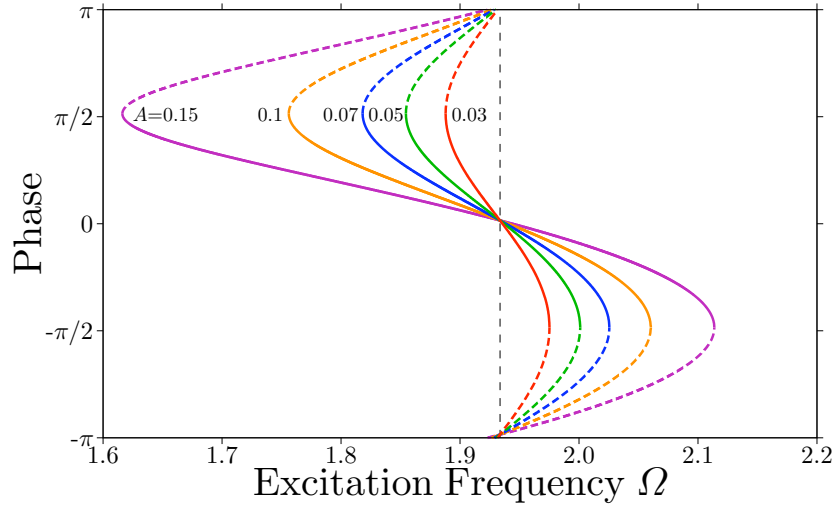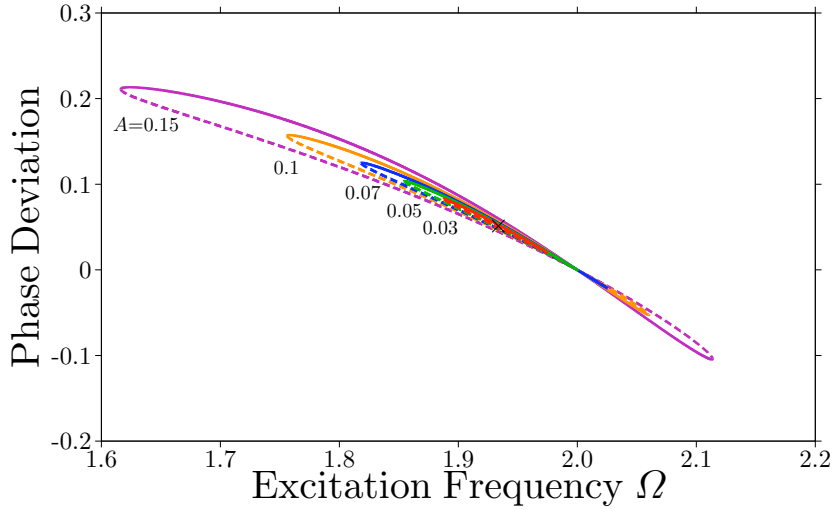
(a) Phase.
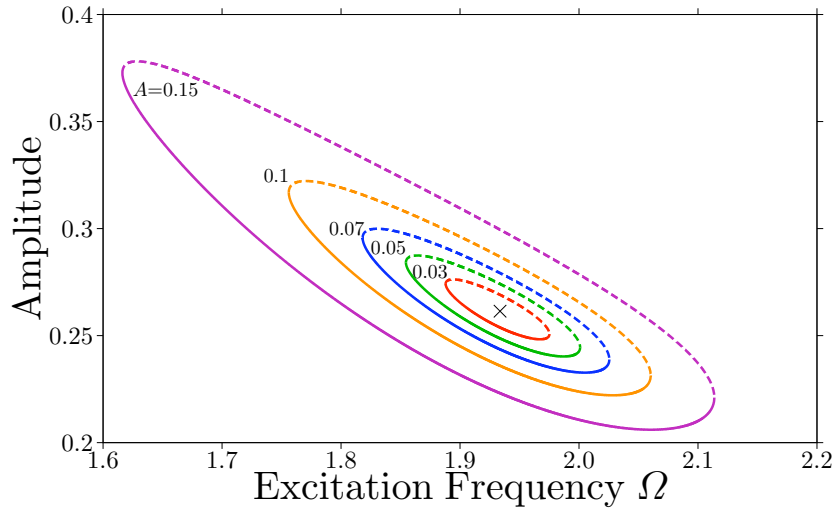
(b) Amplitude.

Figure 4.3: Response curves for the periodic rotations in the system (4.1) at $k = 0.1$ and $N = 0.2$: (a) the phase, (b) the amplitude, and (c) the phase deviation. In (a), the vertical dashed line indicates the angular frequency of the rotational limit cycle. In (b) and (c), the cross symbol represents the amplitude and the phase deviation of the rotational limit cycle. Each type of the lines shows the stability of the periodic rotations in the same manner as Fig. 4.2.

(c) Phase deviation.

Figure 4.3: *Continued.*

$A = 0.03$ are coincident at $\Omega = 2$.

These numerical results are verified by the theoretical study based on the averaged equation (4.8). By applying the averaging method to Eq. (4.9) with any periodic rotation, that is $\phi^*(t) = \Omega t + \theta_R^* + a_R^* \sin(\Omega t + \theta_R^* + \delta_R^*)$ and $y^*(t) = \Omega + \omega_R^* + \Omega a_R^* \cos(\Omega t + \theta_R^* + \delta_R^*)$, a theoretical expression for the energy balance at a periodic rotation in the system (4.1) is derived as

$$0 = -\pi k \Omega (2 - a_R^{*2}) + 2\pi N - \pi a_R^* A \sin(\theta_R^* + \delta_R^*), \qquad (4.10)$$

where the constants θ_R^*, $\omega_R^* = 0$, a_R^*, and δ_R^* are the equilibrium values of the averaged equation (4.8). Eq. (4.10) theoretically describes Eq. (4.9). Thus on the right-hand side of Eq. (4.10), the first term denotes the dissipated energy, and the second and third terms correspond to the supplied energy during the period T_R. The equilibrium points of the averaged equation (4.8) give the corresponding supplied energy by using $-\pi a_R^* A \sin(\theta_R^* + \delta_R^*) =: W_R^*$.

Figure 4.4 shows response curves for the supplied energy W_R^*. The theoretical result of the supplied energy approximates the numerical one shown in Fig. 4.2. In addition, we verify the response characteristics shown in Fig. 4.3 theoretically. Figs. 4.5(a), (b), and (c) represent response curves for the phase θ_R^*, the amplitude a_R^*, and the phase deviation δ_R^* in Eq. (4.8), respectively. These theoretical results are consistent with the numerical ones shown in Fig. 4.3. Under the above assumptions, the equilibrium points of Eq. (4.8) and the relationship (4.10) show response characteristics of the periodic rotations and the supplied energy in the system (4.1). From the results, it is obvious that the expression of the supplied energy, $W_R^* = -\pi a_R^* A \sin(\theta_R^* + \delta_R^*)$, describes relationships of the energy with the entrained rotation. The magnitude of the supplied energy W_R^* increases with the amplitude a_R^*. Since the phase deviation δ_R^* undergoes
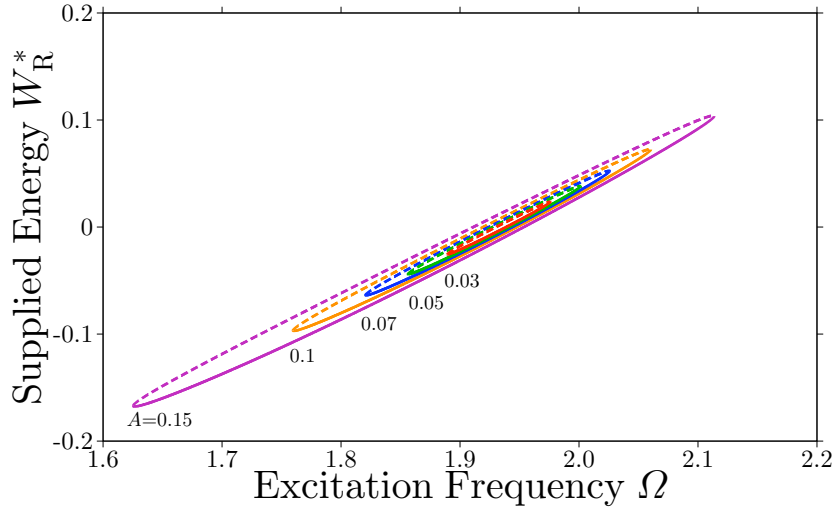
42

Figure 4.4: Response curves for the energy W_R^* supplied by the periodic excitation by using Eqs. (4.8) and $W_R^* = -\pi a_R^* A \sin(\theta_R^* + \delta_R^*)$ at $k = 0.1$ and $N = 0.2$. The solid lines correspond to stable equilibrium points and the dashed lines unstable ones.

little change for the excitation frequency Ω, the phase θ_R^* determines effect of the periodic excitation on the system (4.1). That is, the periodic excitation supplies energy to the system (4.1) for $-\pi/2 < \theta_R < 0$ at the entrained rotations. For $0 < \theta_R < \pi/2$, energy is extracted from the system (4.1) by the excitation. These relationships can be confirmed by using the response curves in Figs. 4.2 and 4.3. Moreover, we observe that the amplitude a_R^* and the phase deviation δ_R^* remain at almost constant in comparison with the phase θ_R^*. The supplied energy W_R^* is governed by the phase θ_R^*. Here we recall the energy balance (4.10). Because of the almost constant amplitude a_R^*, the dissipated energy $-\pi k \Omega (2 - a_R^{*2})$ is governed by the excitation frequency Ω. Considering the constant supplied energy $2\pi N$, we conclude that energy supplied to the system is determined by the phase θ_R^* or the excitation frequency Ω. The validity is confirmed from the response curves for the phase θ_R^*. Indeed for increase of the excitation frequency Ω, $\sin(\theta_R^* + \delta_R^*) \approx \sin \theta_R^*$ monotonically decreases.

4.3 Transient phenomenon of entrainment of rotation

This section presents a relationship between the energy conversion and the transient regime of the frequency entrainment of rotation. The dynamics for the entrainment phenomenon can be represented by a phase equation. We first derive the phase equation for the system (4.1). The stored energy is associated with the dynamics of phase for the frequency entrainment.
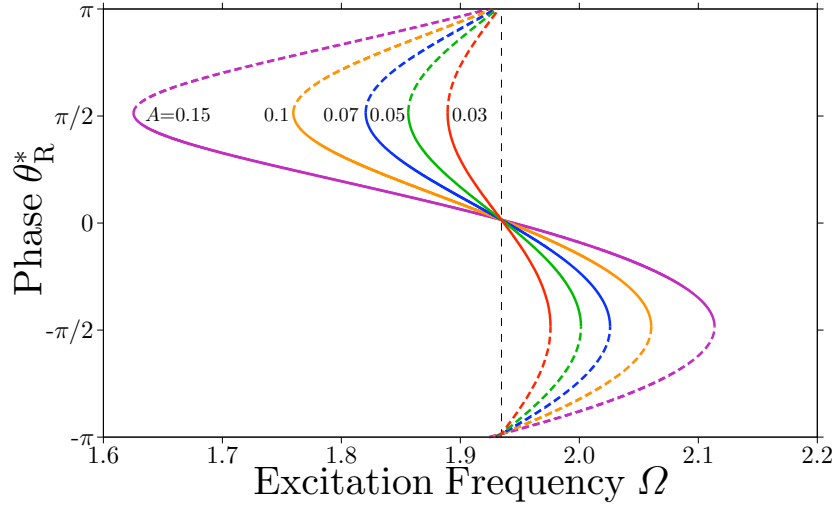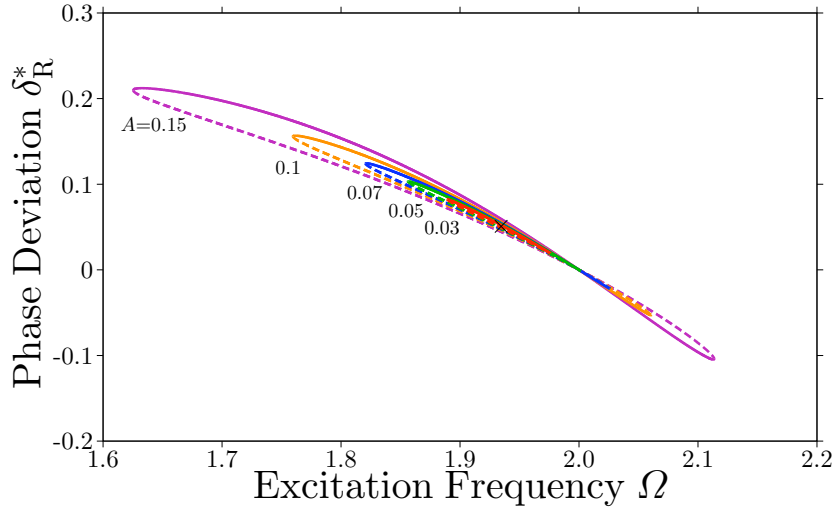
(a) Phase θ_{R}^*.
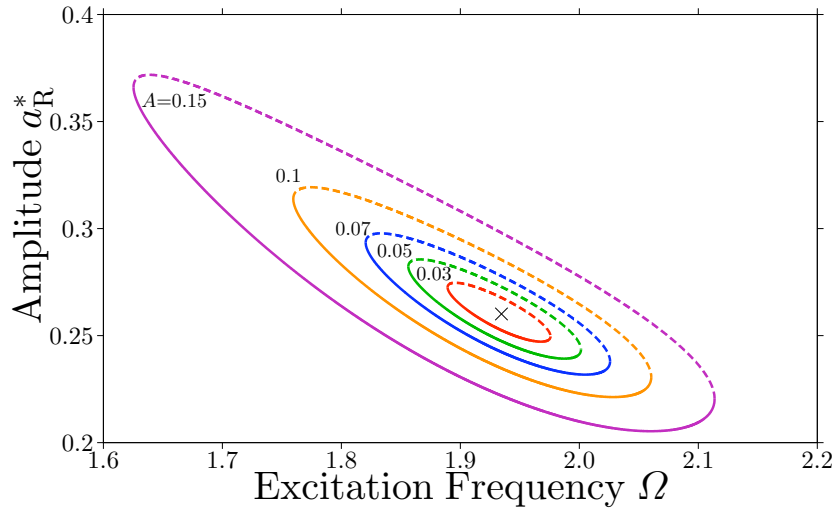
(b) Amplitude a_{R}^*.

Figure 4.5: Response curves for the equilibrium points of Eq. (4.8) at $k = 0.1$ and $N = 0.2$: (a) the phase θ_{R}^*, (b) the amplitude a_{R}^*, and (c) the phase deviation δ_{R}^*. In (a), the vertical dashed line indicates the angular frequency of the rotational limit cycle. In (b) and (c), the cross symbol represents the amplitude $a_{\mathrm{R}0}$ and the phase deviation $\delta_{\mathrm{R}0}$ of the rotational limit cycle. Each type of the lines shows the stability of the equilibrium points in the same manner as Fig. 4.4.

(c) Phase deviation δ_{R}^*.

Figure 4.5: *Continued.*

4.3.1 Phase equation

A phase equation is derived so that we focus on the dynamics of phase for the transient phenomenon in the frequency entrainment of rotation. For the phase-locked system or a rotator, the phase equation has been derived under the condition of overdamping [2]. We derive the phase equation without the condition. In order to derive the phase equation, the phase is identified for the frequency entrainment of rotation. It is possible to identify the phase by using the perturbation of the rotational limit cycle. We add the following assumption:

(viii) The amplitude $a_{\mathrm{R}}(t)$ and the phase deviation $\delta_{\mathrm{R}}(t)$ do not change from the rotational limit cycle, denoted by $a_{\mathrm{R}0}$ and $\delta_{\mathrm{R}0}$.

Eq. (4.7) describes a perturbation of the rotational limit cycle. By modifying Eq. (4.7), another perturbation of the rotational limit cycle is given by

$$\phi(t) = \Omega t + \theta_{\mathrm{R}}(t) + a_{\mathrm{R}0} \sin\left(\Omega t + \theta_{\mathrm{R}}(t) + \delta_{\mathrm{R}0}\right), \tag{4.11a}$$

$$y(t) = \Omega + \omega_{\mathrm{R}}(t) + \Omega a_{\mathrm{R}0} \cos\left(\Omega t + \theta_{\mathrm{R}}(t) + \delta_{\mathrm{R}0}\right). \tag{4.11b}$$

The expression (4.11) clearly shows that any rotation satisfying (vii) is governed by the variable $\theta_{\mathrm{R}}(t)$ and the time derivative $\omega_{\mathrm{R}}(t) = \mathrm{d}\theta_{\mathrm{R}}/\mathrm{d}t$. Hence θ_{R} is the phase variable for the frequency entrainment of rotation.

Now we derive a phase equation that governs the temporal change of θ_{R}. By applying the averaging method to Eq. (4.1) with Eq. (4.11), we obtain the following phase equation:

$$\frac{\mathrm{d}\theta_{\mathrm{R}}}{\mathrm{d}t} = \frac{N}{k} \cdot \frac{\Omega_0 - \Omega}{\Omega_0} - \frac{A a_{\mathrm{R}0}}{2k} \sin\left(\theta_{\mathrm{R}} + \delta_{\mathrm{R}0}\right). \tag{4.12}$$

The detailed derivation is given in the appendix of this chapter. On the right-hand side of Eq. (4.12), the first term represents the difference between the frequency Ω_0 of the rotational limit cycle and the excitation frequency Ω, and the second term effect of the periodic excitation on the phase dynamics. The phase equation (4.12) for the frequency entrainment of rotation has the same form as Eq. (3.10) for the entrainment of libration. This suggests that the entrainment phenomena for the topologically different limit cycles are governed by a common mechanism of phase regulation.

4.3.2 Energy description of transient phenomenon

We identify a relationship between the transient phenomenon of the frequency entrainment of rotation and the energy conversion in the system (4.1). This gives a new description for behavior of the frequency entrainment. We consider the stored energy S_R again to introduce the notion of energy. The stored energy S_R is defined as a function of the fast variables $\phi(t)$ and $y(t)$. On the other hand, the phase θ_R for the frequency entrainment is a slow variable, because the phase variable θ_R is produced on the perturbation and the averaging. The purpose of this section is to associate the notion of energy and the phase dynamics. We need to extract the response of the stored energy S_R with the same time scale as θ_R. It is obvious that the time scale is longer than the excitation period T_R. This operation is achieved by averaging the function S_R over T_R. By substituting Eq. (4.11) into Eq. (4.2) and averaging the equation over T_R, we obtain the following function $\langle S_\mathrm{R} \rangle$ that depends on the phase variable θ_R:

$$
\begin{aligned}
\langle S_\mathrm{R} \rangle(\theta_\mathrm{R}) &:= \frac{1}{T_\mathrm{R}} \int_{-T_\mathrm{R}/2}^{T_\mathrm{R}/2} S_\mathrm{R}\big(\phi(t,\theta_\mathrm{R}), y(t,\theta_\mathrm{R},\omega_\mathrm{R})\big)\mathrm{d}t \\
&= \frac{1}{2}\Omega^2 + \frac{1}{4}\Omega^2 a_\mathrm{R0}^2 + J_1(a_\mathrm{R0})\cos\delta_\mathrm{R0} + \Omega\omega_\mathrm{R} \\
&= \langle S_\mathrm{R} \rangle^* + \Omega\frac{\mathrm{d}\theta_\mathrm{R}}{\mathrm{d}t},
\end{aligned}
\tag{4.13}
$$

where $J_1(\cdot)$ is the Bessel function of the first kind. The bracket $\langle\cdot\rangle$ denotes the time average during the excitation period T_R. The value $\langle S_\mathrm{R} \rangle(\theta_\mathrm{R})$ slowly changes with the slow variable θ_R. The constant $\langle S_\mathrm{R} \rangle^*$ indicates the value of $\langle S_\mathrm{R} \rangle$ at the entrained rotation. Eq. (4.13) can be transformed into

$$
\frac{\mathrm{d}\theta_\mathrm{R}}{\mathrm{d}t} = \frac{1}{\Omega}\big(\langle S_\mathrm{R} \rangle(\theta_\mathrm{R}) - \langle S_\mathrm{R} \rangle^*\big).
\tag{4.14}
$$

The time evolution of the phase θ_R represents transient phenomenon of the entrainment of rotation. Eq. (4.14) implies that the entrainment phenomenon develops according to the change of the stored energy.

The direct consequence of Eq. (4.14) unveils the energy conversion in the transient regime of the frequency entrainment of rotation. From the energy balance (4.4), the variation of the stored energy is equivalent to the sum of the supplied energy and
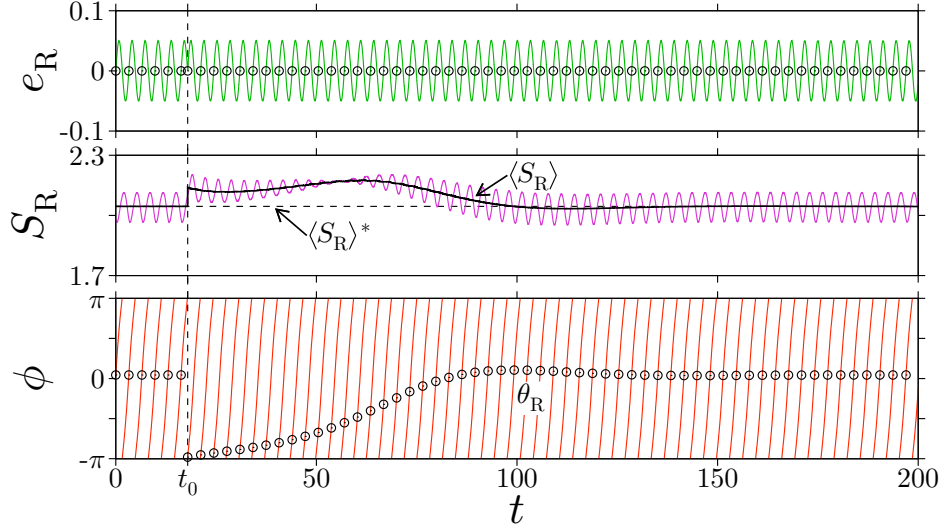
(a) $t_0 = (5 + 1/2)T_R$.
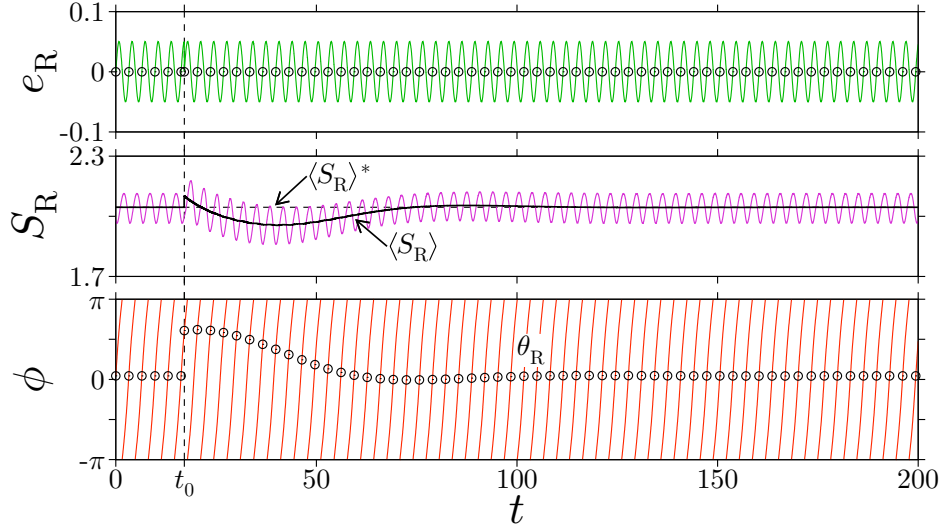
(b) $t_0 = (5 + 1/4)T_R$.

Figure 4.6: Stored energy and phase in the frequency entrainment of rotation in the system (4.1) at $k = 0.1$, $N = 0.2$, $A = 0.05$, and $\Omega = 1.93$. The phase of the periodic excitation e_R is reset at $t = t_0$ and then transient regime of the frequency entrainment appears. The solid line on the waveform of S_R denote the time average over T_R which corresponds to $\langle S_R \rangle$. The dashed lines of S_R indicate the time average at the entrained rotation. Since these lines correspond to $\langle S_R \rangle$ and $\langle S_R \rangle^*$, we indicate these lines by using the corresponding notation. The phase θ_R is estimated from the stroboscopic points $\odot$ of ϕ.

the dissipated energy. Eq. (4.14) implies that the energy exchange induces the phase regulation or the entrainment phenomenon of rotation. Fig. 4.6 shows the stored energy and the phase at the transient regime of the frequency entrainment of rotation in the system (4.1) at $A = 0.05$ and $\Omega = 1.93$. We reset the phase of the periodic excitation e_R at $t = t_0$ so that the transient regime appears. The stroboscopic points of ϕ, marked by the circles, extract the time response of the phase θ_R. The solid and dashed lines on the waveform of S_R correspond to the time average of S_R, that is $\langle S_R \rangle$ and $\langle S_R \rangle^*$, respectively. These lines are calculated by averaging the waveform of S_R during the excitation period T_R. In Fig. 4.6(a), the phase of the periodic excitation e_R changes by π at $t = t_0 = (5 + 1/2)T_R$. At the same moment the phase shifts by around $-\pi$, and then the averaged energy $\langle S_R \rangle$ increases. The phase which can be estimated by using the stroboscopic points increases while the averaged energy $\langle S_R \rangle$ is higher than $\langle S_R \rangle^*$. Fig. 4.6(b) shows transient behavior caused by resetting the excitation e_R at $t = t_0 = (5+1/4)T_R$. At that time the phase shifts by around $\pi/2$. The deviation of the averaged energy $\langle S_R \rangle$ from $\langle S_R \rangle^*$ becomes positive, and the phase slightly increases. In the meantime the deviation $\langle S_R \rangle - \langle S_R \rangle^*$ becomes negative, and then the phase decreases. We confirmed the dynamic relationship between the phase and the averaged energy. The temporal change of the phase is proportional to the magnitude of the time average of the stored energy.

Moreover, we examine the relationship between the phase shift and the deviation of the stored energy. By integrating Eq. (4.14) in the interval $[t_0, \infty)$, we obtain the following relationship between the phase shift and the total of the deviation of the stored energy:

$$\theta_R(t_0) - \theta_R^* = -\frac{1}{\Omega} \int_{t_0}^{\infty} \left\{ \langle S_R \rangle \big(\theta_R(t) \big) - \langle S_R \rangle^* \right\} \, \mathrm{d}t, \qquad (4.15)$$

where θ_R^* is the phase at an entrained rotation. Fig. 4.7 shows the total of the deviation of the stored energy against the phase shift. The dashed line is the theoretical result obtained by using Eq. (4.15). The dots show the numerical result obtained by using Eq. (4.1). Here the phase shift is estimated through the application of $\phi(t_0) - \Omega t_0$ in Eq. (4.1). The theoretical result quantitatively corresponds to the numerical one. The phase shift is proportional to the total of the deviation of the stored energy from the steady value.

4.4 Summary of frequency entrainment of rotation

We analyzed energy conversion in frequency entrainment of rotation. The phase-locked system is considered as a dynamical system with a stable rotational limit cycle.

At the entrained states, the energy conversion in the system was studied by using energy supplied to the system by the periodic excitation. Response curves were obtained numerically and theoretically for the supplied energy and the characteristics of the entrained rotations. That is, the phase difference of the rotatory component from
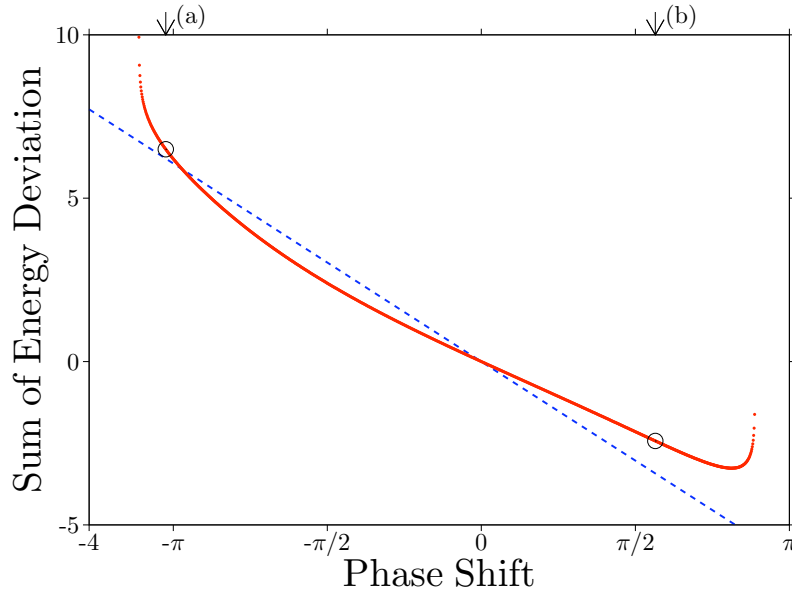
Figure 4.7: Relationship between the total of the deviation of the stored energy and the phase shift in the system (4.1) at $k = 0.1$, $N = 0.2$, $A = 0.05$, and $\Omega = 1.93$. The dashed line is the theoretical result obtained from Eq. (4.15), and the dots show the numerical one from Eq. (4.1). The arrows (a) and (b) show the situations in Figs. 4.6(a) and (b), respectively.

the periodic excitation, and the amplitude and the phase deviation of the fundamental oscillatory component. For the theoretical result, we derived the averaged equation for the system. The averaged equation is valid for the periodic rotations and the stability. The theoretical result from the averaged equation is coincident with the numerical one. The coincidence implies that the observed relationships between the response curves are described by the theoretical expression. The energy conversion at the entrained rotations depends on the phase difference of the rotatory component or the phase for the entrainment. In addition, the supplied energy increases with the excitation frequency.

In the transient regime, we associated the development of the entrainment phenomenon with the energy conversion in the system. The phase equation was derived to represent the dynamics of phase for the frequency entrainment of rotation. The stored energy is described as a form including the temporal change of the phase variable. This implies that the entrainment phenomenon develops according to the change of the stored energy. The energy conversion in the transient regime of the entrainment is confirmed numerically. The obtained energy description of the phase regulation implies the possibility to regulate the phase by changing the stored energy. In other words, we can regulate the phase of rotation by energy exchange.

The energy conversion is summarized in the frequency entrainment of rotation. The notion of energy was associated with the phase difference of the rotatory component or the phase for the frequency entrainment in the transient and entrained regime.

4.5 Comparison with frequency entrainment of libration

In this section, the frequency entrainment of rotation in this chapter is compared with the phenomenon of libration in Chapter 3 from the viewpoint of energy conversion. Before the discussion, we summarize the frequency entrainment phenomena of libration and rotation again. Frequency entrainment occurs for a limit cycle. The entrainment phenomena analyzed in the thesis occur for the topologically different limit cycles. The entrained oscillations, namely the entrained librations and rotations, are also topologically different. The difference reflects the forms of theoretical expressions for the entrained oscillations. Since the corresponding phase is defined from an expression of the entrained oscillation, the defined phase depends on the form of the expression. For each of the entrainment phenomena, the phase was identified and then the phase equation was derived. The obtained phase equations are described as the sum of the difference between the frequency of the limit cycle and the periodic excitation and the effect of the excitation on the phase dynamics. Therefore, the entrainment phenomena of libration and rotation are governed by the same mechanism of phase regulation. The type of the entrained oscillation does not essentially reflect the frequency entrainment in terms of phase.

In the following, we discuss the energy conversion in the frequency entrainment phenomena of libration and rotation. First, we focus on the energy conversion at the entrained states. For the frequency entrainment of libration, the energy conversion is associated with the amplitude of the entrained librations. The magnitude of energy conversion increases with the amplitude. Since the response curves for the amplitude exhibit resonance phenomenon, the maximum energy can be converted at the resonance frequency or the frequency of the librational limit cycle. For the entrainment phenomenon of rotation, the energy conversion is associated with the phase for the phenomenon. From the response curves for the phase, the energy conversion monotonically increases with the excitation frequency. The two entrained oscillations are compared in terms of the magnitude of energy conversion in a pendulum. In a pendulum, the amplitude of the periodic librations can increase to π with the energy conversion. We can regard the periodic libration with the amplitude π as a periodic rotation with the half period. Further increase of the amplitude produces rotation. In this sense, the rotation can be regarded as a periodic libration with the amplitude π and with twice the period. Therefore, a larger amount of energy can be converted at the entrained rotations than at the entrained librations. From the response curves for the supplied energy at the entrained rotations, we conclude that the entrained rotations at high frequency are suited for the energy conversion by a pendulum.

Next, we consider the frequency entrainment phenomena of libration and rotation from the viewpoint of phase regulation by the energy exchange. For the entrainment phenomenon of libration, it was confirmed that the dynamics of phase were not affected by the energy supply. On the other hand, we could associate the notion of energy with the phase for the frequency entrainment of rotation. The result suggests the possibility

to regulate the phase for the entrainment of rotation. The energy-based regulation of phase may be obvious because the stored energy for rotation is directly related to the angular velocity $\Omega + \omega_{\mathrm{R}}$ or the temporal change of the phase $\omega_{\mathrm{R}} = \mathrm{d}\theta_{\mathrm{R}}/\mathrm{d}t$ in Eq. (4.13). The point that we should raise is the relationship between the stored energy and the temporal change of the phase, described by Eq. (4.14). Eq. (4.14) indicates a strategy to regulate the phase of rotation. For rotation of a pendulum, energy exchange is realized by the application of torque in the direction of rotation and inverse rotation. The possibility to regulate the phase is applied to the start control of a periodic rotation of the parametric pendulum in Chapter 5.

Finally, we summarize the energy conversion in frequency entrainment. The entrainment phenomena of libration and rotation exhibit different properties of energy conversion. Energy conversion is associated with amplitude for libration and with phase for rotation. Thus, the entrainment phenomena with the common mechanism of phase regulation can be characterized in terms of energy conversion in the systems.

Appendix to detailed derivation of averaged equation

This appendix provides the detailed derivation of the averaged equation (4.8) for the system (4.1). By substituting Eq. (4.7) into Eq. (4.1), we obtain

$$
\Omega + \frac{\mathrm{d}\theta_{\mathrm{R}}}{\mathrm{d}t} + \frac{\mathrm{d}a_{\mathrm{R}}}{\mathrm{d}t} \sin\left(\Omega t + \theta_{\mathrm{R}} + \delta_{\mathrm{R}}\right) + \left(\Omega + \frac{\mathrm{d}\theta_{\mathrm{R}}}{\mathrm{d}t} + \frac{\mathrm{d}\delta_{\mathrm{R}}}{\mathrm{d}t}\right) a_{\mathrm{R}} \cos\left(\Omega t + \theta_{\mathrm{R}} + \delta_{\mathrm{R}}\right)
$$
$$
= \Omega + \omega_{\mathrm{R}} + \Omega a_{\mathrm{R}} \cos\left(\Omega t + \theta_{\mathrm{R}} + \delta_{\mathrm{R}}\right),
$$
(4.16)

and

$$
\frac{\mathrm{d}\omega_{\mathrm{R}}}{\mathrm{d}t} + \Omega \frac{\mathrm{d}a_{\mathrm{R}}}{\mathrm{d}t} \cos\left(\Omega t + \theta_{\mathrm{R}} + \delta_{\mathrm{R}}\right) - \left(\Omega + \frac{\mathrm{d}\theta_{\mathrm{R}}}{\mathrm{d}t} + \frac{\mathrm{d}\delta_{\mathrm{R}}}{\mathrm{d}t}\right) \Omega a_{\mathrm{R}} \sin\left(\Omega t + \theta_{\mathrm{R}} + \delta_{\mathrm{R}}\right)
$$
$$
= -k\left\{\Omega + \omega_{\mathrm{R}} + \Omega a_{\mathrm{R}} \cos\left(\Omega t + \theta_{\mathrm{R}} + \delta_{\mathrm{R}}\right)\right\}
$$
$$
- \sin\left\{\Omega t + \theta_{\mathrm{R}} + a_{\mathrm{R}} \sin\left(\Omega t + \theta_{\mathrm{R}} + \delta_{\mathrm{R}}\right)\right\} + N + A \sin \Omega t.
$$
(4.17)

Averaging the above equations over the excitation period $T_{\mathrm{R}} = 2\pi/\Omega$ gives the following equations:

$$
\frac{\mathrm{d}\theta_{\mathrm{R}}}{\mathrm{d}t} = \omega_{\mathrm{R}},
$$
(4.18)

and

$$
\frac{\mathrm{d}\omega_{\mathrm{R}}}{\mathrm{d}t} = -k\left(\Omega + \omega_{\mathrm{R}}\right) - J_1(a_{\mathrm{R}}) \sin \delta_{\mathrm{R}} + N,
$$
(4.19)

where $J_n(\cdot)$ is the Bessel function of the first kind for the integer n. In addition, averaging $(4.16) \times \sin(\Omega t + \theta_{\mathrm{R}} + \delta_{\mathrm{R}}) + (4.17) \times \cos(\Omega t + \theta_{\mathrm{R}} + \delta_{\mathrm{R}})/\Omega$ over T_{R}, we obtain

$$
\frac{\mathrm{d}a_{\mathrm{R}}}{\mathrm{d}t} = \frac{J_0(a_{\mathrm{R}}) + J_2(a_{\mathrm{R}})}{2\Omega} \sin \delta_{\mathrm{R}} - \frac{1}{2} k a_{\mathrm{R}} - \frac{A}{2\Omega} \sin\left(\theta_{\mathrm{R}} + \delta_{\mathrm{R}}\right),
$$
(4.20)

and averaging $(4.16) \times \cos(\Omega t + \theta_R + \delta_R) - (4.17) \times \sin(\Omega t + \theta_R + \delta_R)/\Omega$ over T_R gives

$$\frac{d\theta_R}{dt} + \frac{d\delta_R}{dt} = \frac{J_0(a_R) - J_2(a_R)}{2a_R\Omega} \cos\delta_R - \frac{1}{2}\Omega - \frac{A}{2a_R\Omega}\cos\left(\theta_R + \delta_R\right). \qquad (4.21)$$

From the above equations (4.18), (4.19), (4.20), and (4.21), we obtain the averaged equation (4.8).

Appendix to detailed derivation of phase equation

We describe the derivation of the phase equation (4.12). Under the assumption (viii), Eqs. (4.16) and (4.17) are modified as

$$\Omega + \frac{d\theta_R}{dt} + \left(\Omega + \frac{d\theta_R}{dt}\right)a_{R0}\cos\left(\Omega t + \theta_R + \delta_{R0}\right) = \Omega + \omega_R + \Omega a_{R0}\cos\left(\Omega t + \theta_R + \delta_{R0}\right), \quad (4.22)$$

and

$$\begin{aligned}
\frac{d\omega}{dt} - \left(\Omega + \frac{d\theta_R}{dt}\right)\Omega a_{R0}\sin\left(\Omega t + \theta_R + \delta_{R0}\right) \\
= -k\left\{\Omega + \omega_R + \Omega a_{R0}\cos\left(\Omega t + \theta_R + \delta_{R0}\right)\right\} \\
- \sin\left\{\Omega t + \theta_R + a_{R0}\sin\left(\Omega t + \theta_R + \delta_{R0}\right)\right\} + N + A\sin\Omega t.
\end{aligned} \qquad (4.23)$$

Averaging the above equations over the excitation period T_R gives

$$\frac{d\theta_R}{dt} = \omega_R, \qquad (4.24)$$

and

$$\frac{d\omega_R}{dt} = -k\left(\Omega + \omega_R\right) - J_1(a_{R0})\sin\delta_{R0} + N, \qquad (4.25)$$

where $J_n(\cdot)$ is the Bessel function of the first kind for the integer n. Since the fundamental oscillatory component can be regarded as an additional one of the rotatory component, we remove the effect of the oscillatory component on the phase dynamics. By averaging $(4.22) \times \sin(\Omega t + \theta_R + \delta_{R0}) + (4.23) \times \cos(\Omega t + \theta_R + \delta_{R0})/\Omega$ over T_R, we do not have to consider the effect and obtain

$$J_1(a_{R0})\sin\delta_{R0} = \frac{1}{2}k\Omega a_{R0}^2 + \frac{Aa_{R0}}{2}\sin\left(\theta_R + \delta_{R0}\right), \qquad (4.26)$$

where the relationship $2J_1(a_{R0})/a_{R0} = J_0(a_{R0}) + J_2(a_{R0})$ is used. Substitution of Eq. (4.26) into Eq. (4.25) gives

$$\frac{d\omega_R}{dt} = -k\left(\Omega + \omega_R\right) - \frac{1}{2}k\Omega a_{R0}^2 - \frac{Aa_{R0}}{2}\sin\left(\theta_R + \delta_{R0}\right) + N. \qquad (4.27)$$

Here the assumption (v) is explicitly formulated as $k = \epsilon k'$, $N = \epsilon N'$, and $A = \epsilon A'$ with the small parameter ϵ, where the constants k', N', and A' are of the same order. Then we can rewrite Eq. (4.27) as

$$\frac{\mathrm{d}\omega_\mathrm{R}}{\mathrm{d}t} = \epsilon\left\{ -k'\left(\Omega + \omega_\mathrm{R}\right) - \frac{1}{2}k'\Omega a_\mathrm{R0}^2 - \frac{A'a_\mathrm{R0}}{2}\sin\left(\theta_\mathrm{R} + \delta_\mathrm{R0}\right) + N'\right\}. \qquad (4.28)$$

This equation indicates that the time derivative of ω_R is sufficiently small. Thus we can regard it as zero. Using Eq. (4.24), we obtain the following equation which describes the time derivative of θ_R:

$$\frac{\mathrm{d}\theta_\mathrm{R}}{\mathrm{d}t} = \frac{N}{k} - \Omega - \frac{1}{2}\Omega a_\mathrm{R0}^2 - \frac{A a_\mathrm{R0}}{2k}\sin\left(\theta_\mathrm{R} + \delta_\mathrm{R0}\right). \qquad (4.29)$$

This derivation can be applied for the rotational limit cycle at $A = 0$. The similar equation for θ_R0 is obtained as

$$\frac{\mathrm{d}\theta_\mathrm{R0}}{\mathrm{d}t} = \frac{N}{k} - \Omega_0 - \frac{\Omega_0 a_\mathrm{R0}^2}{2} = 0, \qquad (4.30)$$

where the excitation frequency Ω is changed into the frequency Ω_0 of the rotational limit cycle. This equation gives the description for Ω_0. By substituting Eq. (4.30) into Eq. (4.29), the phase equation (4.12) is derived.

# Appendix to verification of phase equation

In this chapter, we derived the phase equation (4.12) for the frequency entrainment of rotation in the system (4.1) without a condition of overdamping. This appendix numerically confirms the validity of the phase equation.

First, the transient regime represented by the phase equation (4.12) is confirmed. Fig. 4.8 shows transient regime of the entrainment obtained by using Eqs. (4.12) and (4.1). As for the initial condition, we set the initial value of Eq. (4.12). Then, by using Eq. (4.11), the corresponding initial value is determined for Eq. (4.1). Note that the initial value of Eq. (4.1) is not uniquely determined because Eq. (4.1) is non-autonomous. However the non-uniqueness of the initial value does not change the numerical result shown in Fig. 4.8. In Fig. 4.8(a) the initial value of Eq. (4.12) is set at $\theta_\mathrm{R}(0) = -3$. The initial deviation $\theta_\mathrm{R}(0)$ is negative in comparison with the steady state. In Fig. 4.8(b) the initial deviation $\theta_\mathrm{R}(0) = 2$ is positive. The predicted value of the phase is consistent with the value obtained from Eq. (4.1).

In addition to the transient regime, we examine the entrained states by using response curves for the phase variable. Fig. 4.9 shows the response curves obtained (a) theoretically by using Eq. (4.12) and (b) numerically by using Eq. (4.1). For sufficiently small value of the amplitude A, the response curves show a good agreement with each other. At $A = 0.1$, however, the existence regions of steady states which correspond to the entrainment regions are not consistent. This indicates the limitation
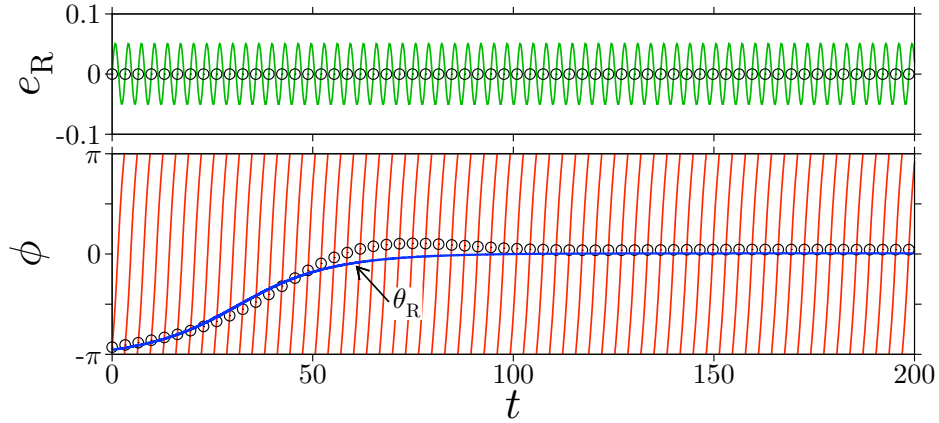
(a) $\theta_R(0) = -3$.
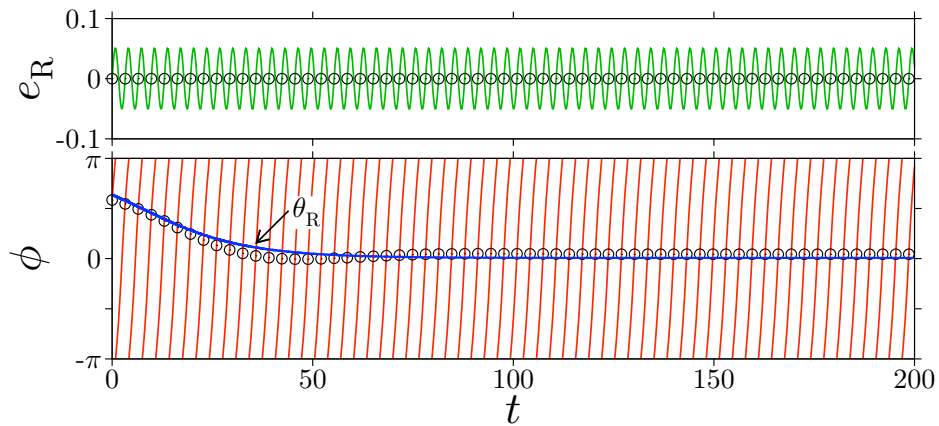
(b) $\theta_R(0) = 2$.

Figure 4.8: Transient regime of the entrainment phenomenon of rotation by using Eqs. (4.12) and (4.1) at $k = 0.1$, $N = 0.2$, $A = 0.05$, and $\Omega = 1.93$. The initial conditions of Eq. (4.12) are (a) $\theta_R(0) = -3$ and (b) $\theta_R(0) = 2$, and the conditions of Eq. (4.1) are set at the corresponding values by employing Eq. (4.11). The curves denoted by θ_R show the phase obtained from Eq. (4.12). The stroboscopic points $\odot$ represent the phase estimated from Eq. (4.1).
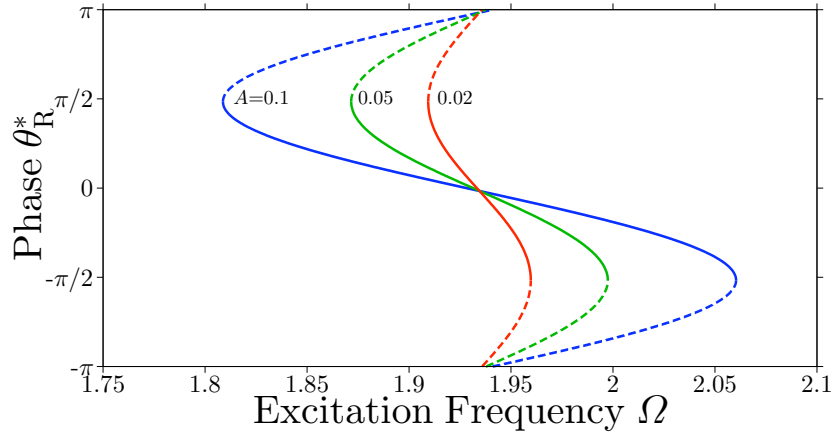
(a) Theoretical result.
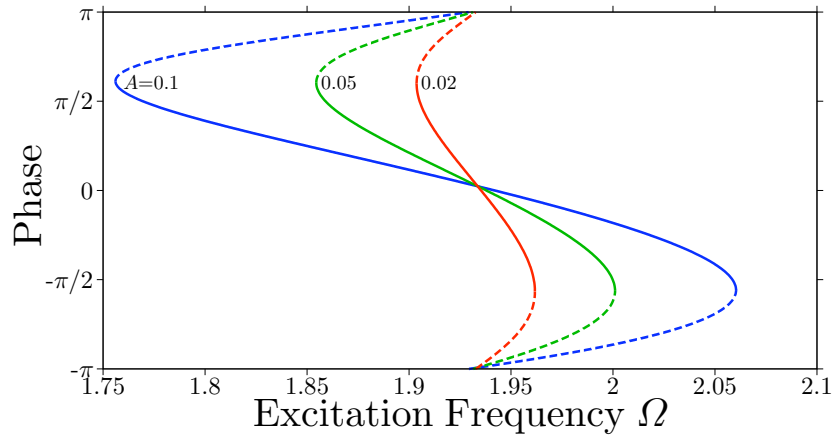
(b) Numerical result.

Figure 4.9: Response curves for the phase obtained (a) theoretically by using Eq. (4.12) and (b) numerically by using Eq. (4.1) at $k = 0.1$ and $N = 0.2$. The steady states correspond to equilibrium points of Eq. (4.12) and the time average of $\phi(t) - \Omega t$ at periodic rotations of Eq. (4.1).

of the validity of Eq. (4.12). The limitation originates from the assumption (v). The numerical results show that the phase equation (4.12) provides good approximation of the transient regime and the steady states of Eq. (4.1).

Chapter 5

Start Control of Periodic Rotation

This chapter presents a control method for starting the periodic rotation inherent in the parametric pendulum. First, properties of the target periodic rotations are explained. The requirements are clarified for the control method. Then, the start control is constructed on the basis of the possibility to regulate the phase of rotation discussed in Chapter 4. We numerically investigate the performance of the control.

5.1 Parametric pendulum

In this section, the periodic rotations inherent in the parametric pendulum are explained. The periodic rotations are suited for applications such as energy scavenging. A problem arises in applications of the periodic rotations.

5.1.1 Equation of motion and periodic steady states

The dynamics of the parametric pendulum are described by the following equation of motion with the nondimensional time t, the angular displacement $\theta(t)$, and the velocity $v(t)$:

$$\frac{\mathrm{d}\theta}{\mathrm{d}t} = v, \tag{5.1a}$$

$$\frac{\mathrm{d}v}{\mathrm{d}t} = -cv - \left(1 + p\cos\omega t\right)\sin\theta, \tag{5.1b}$$

where c is the damping coefficient. The term $p\cos\omega t$ denotes the parametric excitation with the amplitude p and the angular frequency ω. We express the parametric excitation by $e_\mathrm{P}(t) := p\cos\omega t$ and its period by $T_\mathrm{P} := 2\pi/\omega$.

Periodic steady states of the parametric pendulum are represented with a natural number n and an integer r by

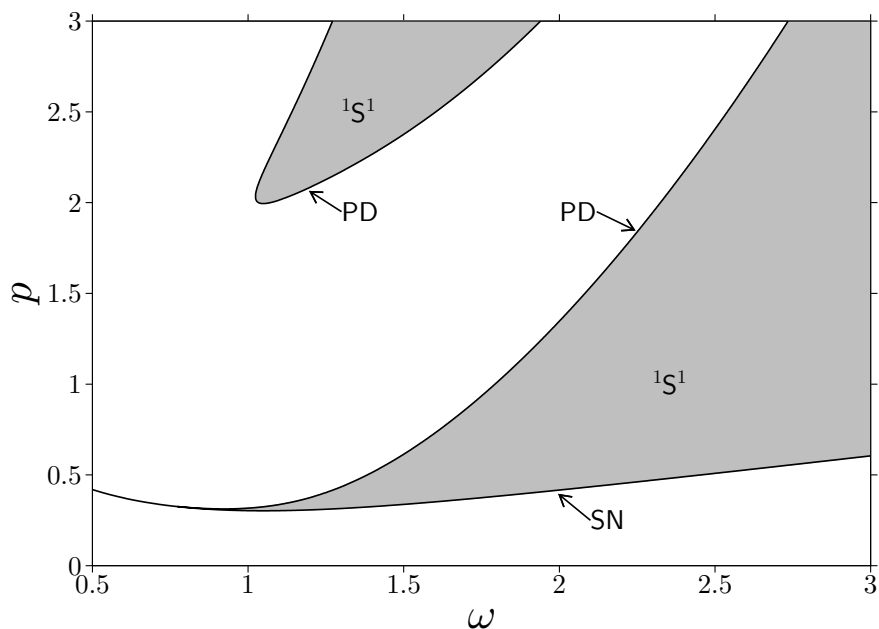$$\theta(t) = \theta(t - nT_\mathrm{P}) + 2\pi r. \tag{5.2}$$

Figure 5.1: Existence domain of the periodic rotations $(1, 1)$ in the excitation parameter space (p, ω) for the parametric pendulum (5.1) at $c = 0.1$. SN denotes the saddle-node bifurcation and PD the period-doubling bifurcation. The gray corresponds to the existence domain of the periodic rotations $(1, 1)$.

A combination of n and r corresponds to a state in which the pendulum rotates r times during n periods. The positive (negative) value of r shows that the pendulum rotates in the direction to increase (decrease) the angular displacement θ. Periodic librations are expressed as $r = 0$. We describe a periodic steady state at which the pendulum rotates r times during n periods as a periodic rotation (n, r) for $r \neq 0$ [32] and an nT_{P}-periodic libration for $r = 0$. In the following figures, completely stable, directly unstable, and inversely unstable periodic steady states or fixed points are symbolized by ${}^{n}\mathsf{S}^{r}$, ${}^{n}\mathsf{D}^{r}$, and ${}^{n}\mathsf{I}^{r}$. In particular, for $n \geq 2$, the periodic points are numbered as ${}^{n}\mathsf{S}_{i}^{r}$ for $i = 1, \cdots, n$.

5.1.2 Periodic rotation

In Chapters 3 and 4, we clarified periodic rotations can convert larger amount of energy than periodic librations. This suggests that the periodic rotations are useful for energy scavenging by the parametric pendulum. We explain properties of the periodic rotations of the parametric pendulum.

First, the dependence of the periodic rotations $(1, 1)$ on the excitation parameters is examined. Fig. 5.1 shows the existence domain of the periodic rotations $(1, 1)$, denoted by ${}^{1}\mathsf{S}^{1}$, in the excitation parameter space for the parametric pendulum (5.1) at $c = 0.1$. Small amplitude excitation cannot sustain the periodic rotations. For high excitation
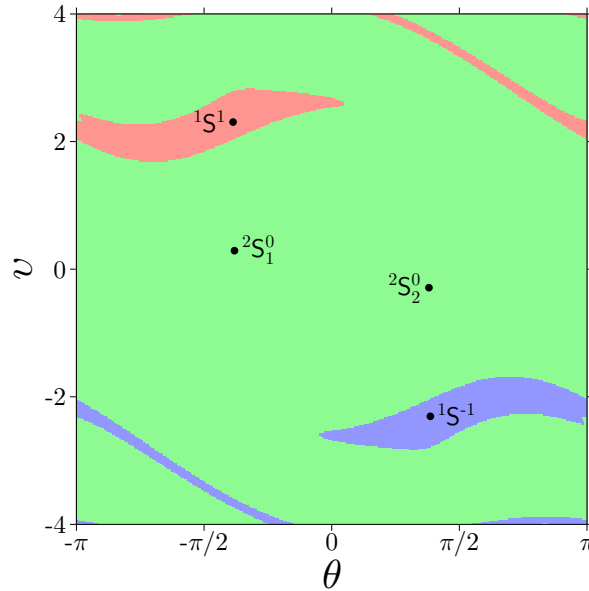
Figure 5.2: Domain of attraction for the parametric pendulum (5.1) at $c = 0.1$, $p = 0.5$, and $\omega = 2$. The fixed points ${}^{1}\mathsf{S}^{\pm 1}$ correspond to stable periodic rotations $(1, \pm 1)$, respectively. The pair of periodic points ${}^{2}\mathsf{S}^{0}_{1,2}$ denote a stable $2T_{\mathrm{P}}$-periodic libration.

frequency, the existence domain extends to large amplitude. The existence domain for small amplitude is bounded by the saddle-node bifurcation SN and the period-doubling bifurcation PD. On the other hand, for large amplitude and low frequency, there is another existence domain of the periodic rotations $(1, 1)$. The domain is surrounded by the period-doubling bifurcation PD.

Next, we investigate the dependence of the periodic rotations on the initial condition. Fig. 5.2 shows the domain of attraction for the parametric pendulum at $c = 0.1$, $p = 0.5$, and $\omega = 2$. At the parameter setting, there exist three periodic steady states: a periodic rotation $(1, 1)$, a $2T_{\mathrm{P}}$-periodic libration, and a periodic rotation $(1, -1)$. These states are denoted by ${}^{1}\mathsf{S}^{1}$, ${}^{2}\mathsf{S}^{0}_{1,2}$, and ${}^{1}\mathsf{S}^{-1}$, respectively. Because the boundaries $\theta = \pm\pi$ are identified on the plane, we can image a simply-connected domain in the cylindrical state space for each attractor. Since Eq. (5.1) is invariant with respect to the transformation $(\theta, \upsilon) \mapsto (-\theta, -\upsilon)$, the domain of attraction exhibits rotational symmetry. Thus we have only to consider one of the periodic rotations $(1, \pm 1)$. In this chapter, we focus on the periodic rotation $(1, 1)$. Fig. 5.2 shows that the onset of the periodic rotations $(1, \pm 1)$ depends on the initial state. Moreover, the basin of the rotations locates on limited region of high angular velocity υ.

These numerical results give us some remarks for the periodic rotations of the parametric pendulum from the viewpoint of applications such as energy scavenging. Fig. 5.1 suggests that the periodic rotations are applicable to energy scavenging over a wide range of the excitation parameters. On the other hand, Fig. 5.2 brings up the dependence of the onset on the initial state for the periodic rotations. The pendulum

at the static downward position requires enough energy supply to rotate. In addition, the pendulum has to be controlled for the periodic rotations.

5.2 Start control

In this section, we propose a control method for starting the periodic rotation inherent in the parametric pendulum. The possibility to regulate the phase of rotation by energy exchange in Chapter 4 presents a concept of the control method. The concrete scheme of the start control is constructed.

We describe requirements for the control for starting the periodic rotation. In Fig. 5.2, the basin of the periodic rotation $(1, 1)$ does not cover all the region with large velocity. This implies that increasing the angular velocity is not sufficient for the onset of the periodic rotation. The control is required to locate the state point inside the basin of the target. It is difficult to find a theoretical condition for the basin because of the nonlinearity. Thus the desired control makes the state point approach the target periodic rotation without any information about the target. In addition, the control input must become null after the onset of the periodic rotation inherent in the parametric pendulum.

5.2.1 Strategy based on phase regulation by energy exchange

In Chapter 4, we indicated the possibility to regulate the phase of rotation by exchanging energy with the considered system. The possibility is originated from Eq. (4.14). That is, the temporal change of phase is governed by the deviation of the stored energy from the criterion value at the entrained rotation. The relationship (4.14) can be interpreted as follows. Energy supply to the system increases the phase or the frequency of rotation, and energy extraction from the system decreases the phase or the frequency. In this sense, the phase of rotation can be regulated by exchanging energy. The energy supply and extraction can be easily carried out by applying the constant torque in the direction of the rotation and the inverse rotation, respectively.

Then we shift an issue about how to identify the current state of phase. In the analysis for the frequency entrainment phenomena of libration and rotation, the phase was estimated by the stroboscopic measurement. The temporal change of stroboscopic points for the angular displacement corresponds to the change of phase. It is effective to identify the current state of phase by using the difference between the two adjacent stroboscopic points for the angular displacement. Since the measurement of stroboscopic points is operated at a constant time interval, it is not suited for continuous control. Now identifying the absolute value of phase is not required for the regulation of phase because we focus on the temporal change of phase. We extend the above discrete measurement to a continuous one. The extension is performed by employing at every moment the difference between two states at a distance of the time interval of stroboscopic measurement.
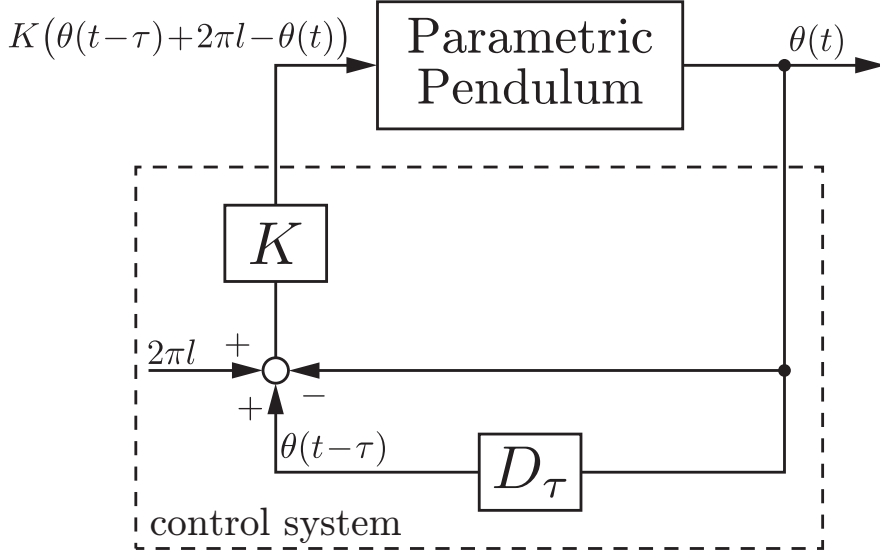
Figure 5.3: Block diagram of the proposed control for the periodic rotation inherent in the parametric pendulum (5.1).

For the parametric pendulum (5.1), we follow the above strategy to design a control method for starting an inherent periodic rotation. We target the periodic rotation (n, r). The period of the target rotation is nT. The temporal change of the phase is estimated by using $\theta(t) - \theta(t - nT) - 2\pi r$, where we consider the rotation number r of the target rotation. Thus the control input torque $u(t)$ to the parametric pendulum is designed with the estimated phase shift and the control gain K as

$$u(t) = -K\big(\theta(t) - \theta(t - nT) - 2\pi r\big), \tag{5.3}$$

where the minus sign reflects the relationship between the phase and the energy exchange. The control gain K is introduced to adjust the magnitude of the control torque.

The control method has been known as the delayed feedback control which was proposed by Pyragas for controlling chaos [51]. The delayed feedback control does not require the exact model for the controlled system [52–55] and can establish the motion inherent in the system. These properties satisfy the above requirements. The control scheme is designed as a general form based on the delayed feedback control.

5.2.2 Construction of control scheme

Based on the delayed feedback control, we construct the start control for the periodic rotation inherent in the parametric pendulum as a general formulation. The block diagram of the proposed method is shown in Fig. 5.3. In the control scheme at a moment t, the current angular displacement $\theta(t)$ is input to the delay block D_τ, and then the angular displacement delayed by time τ, that is $\theta(t - \tau)$, is output from

the block. The control input $u(t)$ affects the pendulum as torque in the direction of rotation. The equation governing the controlled parametric pendulum is described as

$$\frac{\mathrm{d}\theta}{\mathrm{d}t} = v, \tag{5.4a}$$

$$\frac{\mathrm{d}v}{\mathrm{d}t} = -cv - \left(1 + p\cos\omega t\right)\sin\theta + u(t), \tag{5.4b}$$

$$u(t) = K\left(\theta(t-\tau) + 2\pi l - \theta(t)\right). \tag{5.4c}$$

The performance of the control method is determined by the control gain K, the delay time τ, and the rotation number l.

5.3   Control behavior

This section begins numerical investigation into the proposed control for the periodic rotation inherent in the parametric pendulum. In this chapter, the parameter setting for Eq. (5.1) is fixed at

$$c = 0.1, \quad p = 0.5, \quad \text{and} \quad \omega = 2 \tag{5.5}$$

so that the parametric pendulum exhibits a stable periodic rotation $(1,1)$. The periodic rotation $(1,1)$ coexists with a periodic rotation $(1,-1)$ and a $2T_\mathrm{P}$-periodic libration at the parameter setting. From the symmetry of the parametric pendulum with respect to the transformation $(\theta, v) \mapsto (-\theta, -v)$, we focus on the periodic rotation $(1,1)$ as the target rotation of the proposed control. As for the control parameters, the delay time and the rotation number are fixed at $\tau = T_\mathrm{P} = 2\pi/\omega$ and $l = r = 1$, respectively. This setting corresponds to targeting the stable periodic rotation $(1,1)$.

First of all, we numerically show how the proposed method controls the parametric pendulum to the target rotation. The time delay component extends the dimension of the state space of the system from the inherent two to infinity. Now we fix the initial condition at the stable $2T_\mathrm{P}$-periodic libration inherent in the parametric pendulum (5.1), that is $(\theta(s), v(0))$ for $s \in (-T_\mathrm{P}, 0]$. Fig. 5.4 shows control behaviors in the system (5.4) from $t = t_0 = 3T_\mathrm{P}$. The circles on the curves denote the stroboscopic points at the excitation period T_P in order to evaluate the periodicity of the motion. A transient behavior at the control gain $K = 0.1$ is shown in Fig. 5.4(a). The initial state is one of the periodic points with $\theta < 0$, as symbolized by ${}^2\mathsf{S}_1^0$ in Fig. 5.2. After applying the start control, the control input $u(t)$ operates as driving torque and then the angular displacement $\theta(t)$ begins to increase. At around $t = 11T_\mathrm{P}$, $\theta(t)$ shows periodicity and the control input $u(t)$ disappears. This result indicates the achievement of the start control. The null control input at the achievement satisfies the requirement for the start control. Fig. 5.4(b) shows another control behavior at $K = 0.1$. The initial state is the other periodic point ${}^2\mathsf{S}_2^0$ with $\theta > 0$. In this situation, the proposed method cannot start the target rotation. The angular displacement $\theta(t)$ does not reach $\theta = \pi/2$. The state approaches to a periodic libration. Then, the control continues
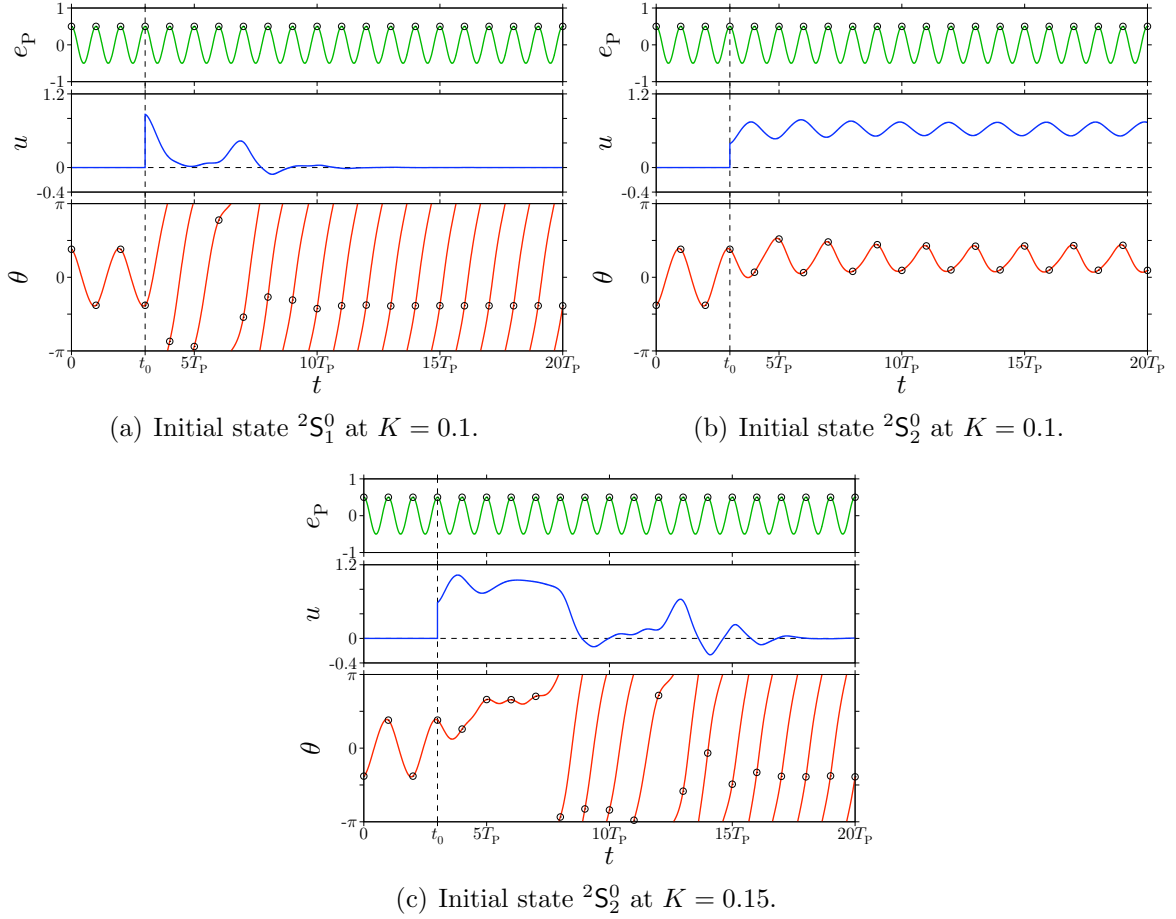
(a) Initial state $^2\mathsf{S}_1^0$ at $K = 0.1$.

(b) Initial state $^2\mathsf{S}_2^0$ at $K = 0.1$.

(c) Initial state $^2\mathsf{S}_2^0$ at $K = 0.15$.

Figure 5.4: Behaviors of the controlled parametric pendulum (5.4). The other parameters are fixed at $c = 0.1$, $p = 0.5$, $\omega = 2$, $\tau = T_\mathrm{P} = 2\pi/\omega$, and $l = 1$. The initial condition for the time delay component is set at the coexisting $2T_\mathrm{P}$-periodic libration. The start control is applied from $t = t_0 = 3T_\mathrm{P} = 3 \cdot 2\pi/\omega$. The initial state is one of the periodic points corresponding to the $2T_\mathrm{P}$-periodic libration, namely $^2\mathsf{S}_{1,2}^0$ shown in Fig. 5.2. The circles $\odot$ on the curves denote the stroboscopic points at the excitation period T_P.

to apply torque to the pendulum. Compared with Fig. 5.4(a), the initial condition directly affects the performance of start control. Fig. 5.4(c) shows a control behavior at $K = 0.15$ for the same initial condition as Fig. 5.4(b). The control swings up the pendulum over $\theta = \pm\pi$ at around $t = 8T_\mathrm{P}$, and then the pendulum rotates periodically at around $t = 18T_\mathrm{P}$. The control input indicates null after establishing the target rotation. The result shows the accomplishment of the proposed method. Figs. 5.4(b) and (c) show control behaviors from the same initial condition. However, the difference of the control gain K changes the performance of the control method. For the large control gain, the control can swing up the pendulum over $\theta = \pi/2$. Therefore, it is expected that the control method with the larger control gain starts the periodic rotation inherent in the parametric pendulum (5.1).

5.4 Domain of attraction

The performance of the start control directly depends on the control gain K. On the other hand, even though the small control gain, it is easily expected that the start control is achieved if the initial state is in the vicinity of the target rotation. This suggests that the achievement also depends on the initial condition. In the following, we study the basin of the target periodic rotation $(1,1)$ for the controlled parametric pendulum (5.4).

Figure 5.5 shows the domain of attraction for the system (5.4) at the control gain $K = 0.05$, 0.1, 0.15, 0.2, and 0.25. The initial condition for the time delay component is given as the inherent behavior of the parametric pendulum (5.1). The start control is applied from $t = 0$. Hence the figures display the domain at the beginning moment of the start control. Increasing the control gain expands the basin of the target rotation $(1,1)$. At $K = 0.05$, the basin of the target rotation contains the vicinity of the state point at $(\theta, \upsilon) = (\pi, 0)$. The state point represents the static pendulum at the upward position. From the position the pendulum can rotate with small energy supply because the state point lies on the boundary between librations and rotations in an undamped free pendulum. In Fig. 5.2, the vicinity of the state point is contained in the basin of the $2T_\mathrm{P}$-periodic libration. This implies that the parametric excitation does not supply energy at the neighborhoods of the point. Fig. 5.5(a) shows that these neighborhoods can be controlled for the target rotation. Thus the basin of the periodic rotation $(1,1)$ possibly contains state points representing transient rotation. Indeed, Figs. 5.5(a), (b), and (c) show that there appear state points with enough angular velocity to rotate outside of the basin of the target. It should be noted that transient rotation is not a sufficient condition for the onset of the target rotation. For the small control gain, the achievement of the control strongly depends on the initial condition. In contrast, the periodic rotation $(1,1)$ becomes only one attractor on the domain at $K = 0.2$ as shown in Fig. 5.5(d). At the control gain, the proposed method can start the target rotation from any initial state. Further increase of the control gain breaks the achievement at $K = 0.2$ and the target rotation disappears. The stability of the
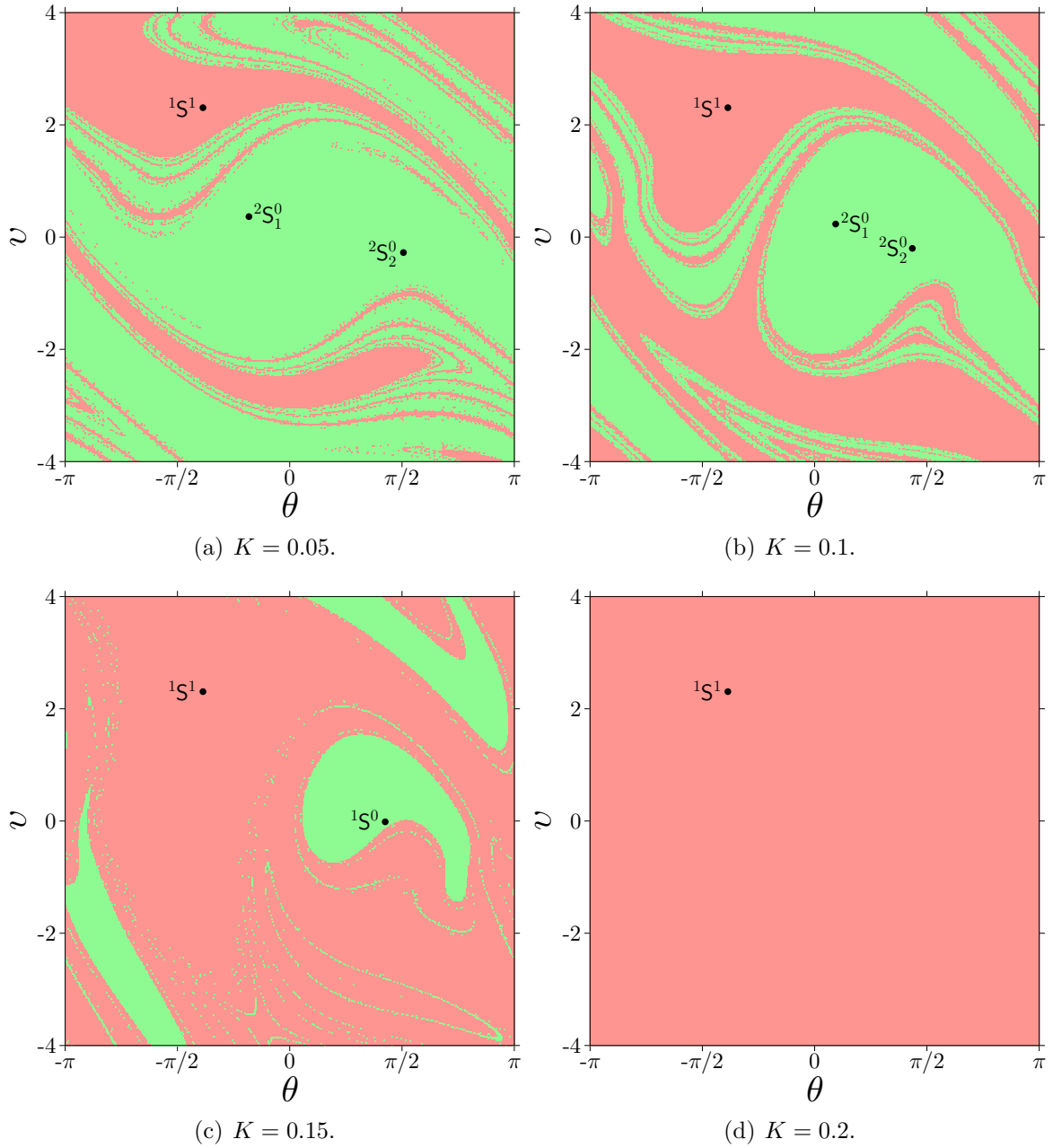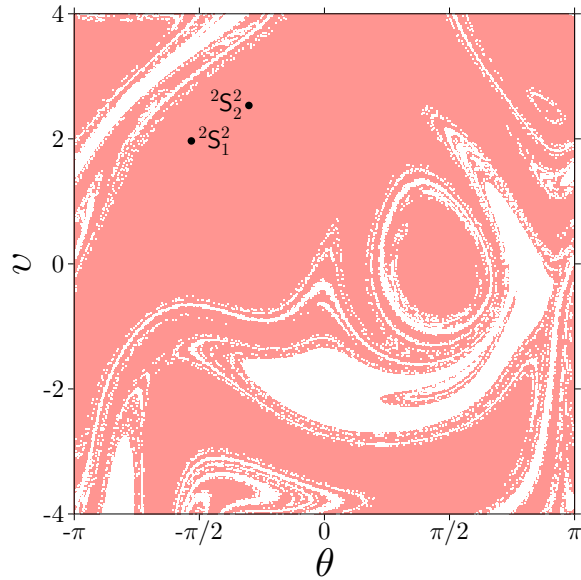
Figure 5.5: Domain of attraction for the controlled parametric pendulum (5.4) at $c = 0.1$, $p = 0.5$, $\omega = 2$, $\tau = T_\mathrm{P} = 2\pi/\omega$, and $l = 1$. The start control is applied from $t = 0$. The initial condition for the time delay component is given as the inherent behavior of the parametric pendulum (5.1) for $t < 0$. The target rotation is indicated by the fixed point $^1\mathsf{S}^1$.

(e) $K = 0.25$.

Figure 5.5: *Continued.*

target rotation changes by the increase of the control gain. In Fig. 5.5(e), the white corresponds to the basin of a periodic state generated through a bifurcation.

From the numerical investigation into the domain of attraction, we confirmed that a range of the control gain K exists to operate the start control regardless of the initial condition. The detailed range is identified through studying the bifurcation structure with respect to the control gain in the next section.

5.5 Bifurcation structure with respect to control gain

The control gain is a parameter to govern the performance of the start control. It has been reported that the stabilization of an unstable periodic orbit depends on the control gain in the delayed feedback control [51]. In addition, increasing the control gain may change the stability of the target. This implies that the proposed method, which is based on the delayed feedback control, possibly induces the stability change of the target rotation. We confirmed the stability change of the target rotation shown in Fig. 5.5(e). On the other hand, the previous section showed that starting the periodic rotation requires enough torque or the control gain to swing up the pendulum. Thus even the control with the large control gain does not always start the target rotation. It is important to understand the two features of the proposed method associated with the control gain K: the accessibility to the target and the stability change of the target.

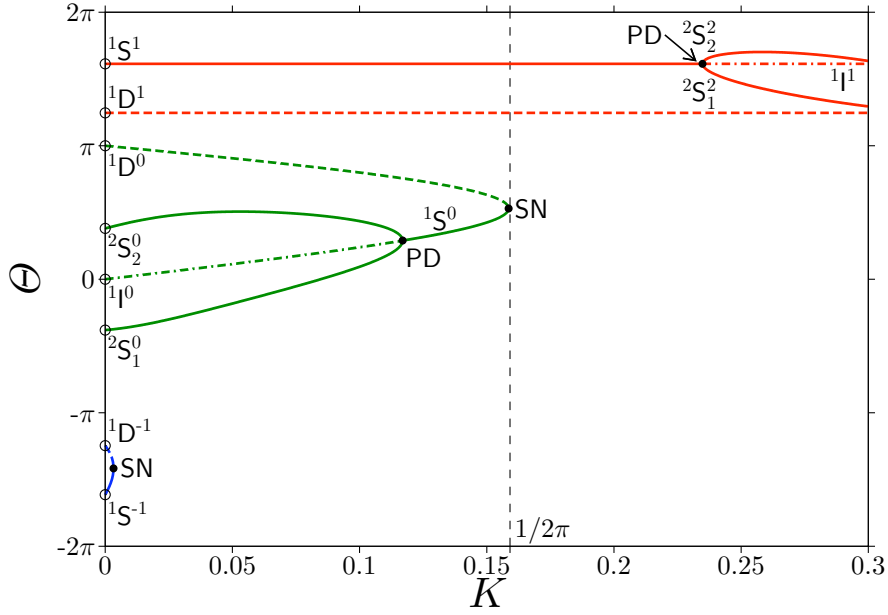Before studying the bifurcation structure, the following notation is introduced for

Figure 5.6: Bifurcation diagram with respect to the control gain K in the controlled parametric pendulum (5.4) at $c = 0.1$, $p = 0.5$, $\omega = 2$, $\tau = T_\mathrm{P} = 2\pi/\omega$, and $l = 1$. PD denotes the period-doubling bifurcation and SN the saddle-node bifurcation. The type of line shows the stability of the periodic states; the solid lines denote completely stable states, the dashed lines directly unstable ones, and the chain lines inversely unstable ones. The detailed classification of the stability is explained in the appendix of Chapter 3.

displaying the bifurcation diagram:

$$\Theta := \theta + 2\pi r, \tag{5.6}$$

where θ denotes the angular displacement at the stroboscopic point and r indicates the rotation number of the periodic rotation in the positive direction. The notation divides periodic rotations and librations.

The bifurcation diagram with respect to the control gain K is shown in Fig. 5.6. At $K = 0$, there exist seven fixed points and a pair of periodic points: the fixed points $^1\mathsf{S}^{\pm1}$ and $^1\mathsf{D}^{\pm1}$ for completely stable and directly unstable periodic rotations $(1, \pm1)$, the fixed points $^1\mathsf{D}^0$ and $^1\mathsf{I}^0$ for directly and inversely unstable equilibrium points, and the periodic points $^2\mathsf{S}^0_{1,2}$ for a completely stable $2T_\mathrm{P}$-periodic libration. Since Eq. (5.4) at $K = 0$ is equivalent to Eq. (5.1), the stable points $^1\mathsf{S}^{\pm1}$ and $^2\mathsf{S}^0_{1,2}$ correspond to those in Fig. 5.2. Increasing the control gain first induces the saddle-node bifurcation which annihilate the branches $^1\mathsf{S}^{-1}$ and $^1\mathsf{D}^{-1}$. The domain of attraction after the bifurcation changes as shown in Figs. 5.5(a) and (b). For additional increase of the control gain, the period-doubling bifurcation occurs. As a result, $^2\mathsf{S}^0_{1,2}$ and $^1\mathsf{I}^0$ disappear and a completely stable libration $^1\mathsf{S}^0$ appears as the alternative attractor. At $K = 0.1586$, the system encounters the saddle-node bifurcation. The stable T_P-periodic libration

coexisting with the target disappears with the paired unstable libration $^1\mathsf{D}^0$. The domain of attraction in the interval of K was shown in Fig. 5.5(c). We describe the value of the control gain K at the saddle-node bifurcation as K_0. The value K_0 is a critical point that all the inherent steady states coexisting with the target disappear through the bifurcations for $K < K_0$. Fig. 5.5(d) shows that the target rotation becomes only one attractor at $K = 0.2 > K_0$. However, further increase of the control gain bifurcates the target rotation $(1,1)$ to the periodic rotation $(2,2)$. The period doubling bifurcation is confirmed as the stability change of the target. Fig. 5.5(e) shows the bifurcated periodic rotation $(2,2)$, denoted by $^2\mathsf{S}_{1,2}^2$ at $K = 0.25$. On the other hand, the directly unstable periodic rotation $^1\mathsf{D}^1$ is invariant for the change of K because of the odd number condition [84, 85].

For the control gain $K > K_0$, the proposed control establishes the periodic rotation regardless of the initial condition. However, the control gain K larger than the critical point K_0 does not give a necessary and sufficient condition for the achievement of the control. The reason is that the large control gain possibly changes the stability of the target. Indeed, we confirmed the stability change by the numerical investigation. Thus, the critical point K_0 does not give a sufficient condition. The point still provides valuable information to the design of the control parameter because it is a necessary condition for the control from any initial condition. For any parameter setting, it is difficult to determine the critical point K_0. We can present the inequality $K_0 \leq 1/2\pi$ by a brief consideration. In the system (5.4) without the parametric excitation, the control input $u(t) = 2\pi K > 1$ breaks the static and periodic potential. As a result, the stable equilibrium point disappears for the control gain $K > 1/2\pi$. There exists no periodic libration bifurcated from the equilibrium point due to the parametric excitation.

5.6   Remarks

In this chapter, we proposed a control method for starting the periodic rotation inherent in the parametric pendulum (5.1) and numerically examined the performance. The analysis of energy conversion in frequency entrainment clarified that periodic rotations can convert larger amount of energy than periodic librations. This implies that the periodic rotation is suited for applications such as energy scavenging by the parametric pendulum.

We began with investigation into the properties of the periodic rotations. As a result, the onset of the periodic rotations depends on the initial state of the pendulum and requires energy supply because the periodic rotations are motions with high energy. The investigation suggests the need for a control method to start the periodic rotation. The possibility to regulate the phase of rotation by energy exchange in Chapter 4 gives a strategy to construct the control method. That is, supplying energy to the system increases the phase or the frequency of rotation, and extracting energy from the system decreases the phase or the frequency. Energy exchange can be realized by applying the constant torque to a rotating pendulum. Identifying the temporal change of the phase

is carried out by using at every moment the difference between the states at a distance of the excitation period. In this way, we proposed the start control for the periodic rotation inherent in the parametric pendulum.

The proposed control method was numerically studied. The control behaviors show that the expected control can be achieved. The domain of attraction and the bifurcation structure indicate that the control gain governs the performance of the control method. For an initial state with low energy, the control method first has to swing up the pendulum over the upward position for the target periodic rotation. This operation requires large control input torque. In addition, the stability change of the target orbit, depending on the control gain, occurs in the control method because the control is based on the delayed feedback control. On the other hand, we could find the range of the control gain in which the control method is achieved from any initial state of the pendulum.

The proposed method with time delay operates as a control to cross over a separatrix which forms a boundary between basins of steady states. The control generates a pass to the target by adding dimensions to the inherent state space. For the delayed feedback control which is the framework of the proposed method, the extended and the generalized schemes have been reported [58, 86]. It is obvious that the extension and the generalization are valid for the proposed onset control. These concepts imply that the proposed start control is applicable to periodic rotations in complicated systems.

Chapter 6

Controlled States of Mechanical Pendulum under Delayed Feedback

This chapter experimentally investigates the start control proposed in the previous chapter. First, a mechanical pendulum excited vertically by shaker is introduced as an experimental setup for the parametric pendulum. Next, the control scheme is implemented to the setup. The feasibility of the control is confirmed experimentally. Experiments elucidate the performance of the control method depending on the control parameters. Finally, a verification experiment manifests energy scavenging by a periodic rotation of the mechanical pendulum.

6.1 Vertically excited mechanical pendulum

A vertically excited mechanical pendulum is introduced as an experimental setup for the parametric pendulum. We observe periodic rotations of the mechanical pendulum with the coexisting motions to verify the start control and the energy scavenging.

6.1.1 Experimental setup

We construct the experimental setup for the parametric pendulum by exciting a mechanical pendulum vertically. Fig. 6.1 illustrates the rod and the bob which constitute the mechanical pendulum. The rod is perforated for the rotary shaft and the bob. The holes for the bob is opened at $10\,\mathrm{mm}$ intervals to adjust and fix the position of the bob. The adjustment determines the length and the moment of inertia of the mechanical pendulum. In the bob, the hole which the rod is inserted into and the corresponding holes to fix the position are opened. In Fig. 6.1, the gray corresponds to the holes. The mechanical pendulum is constructed by inserting the rod into the bob as shown in Fig. 6.2. The position of the bob is explained by center-to-center distance between the rotary shaft and the bob.

Figure 6.3 shows a photograph of the experimental setup. The pendulum is supported by the mechanical rig mounted on an electromagnetic shaker. The electromag-
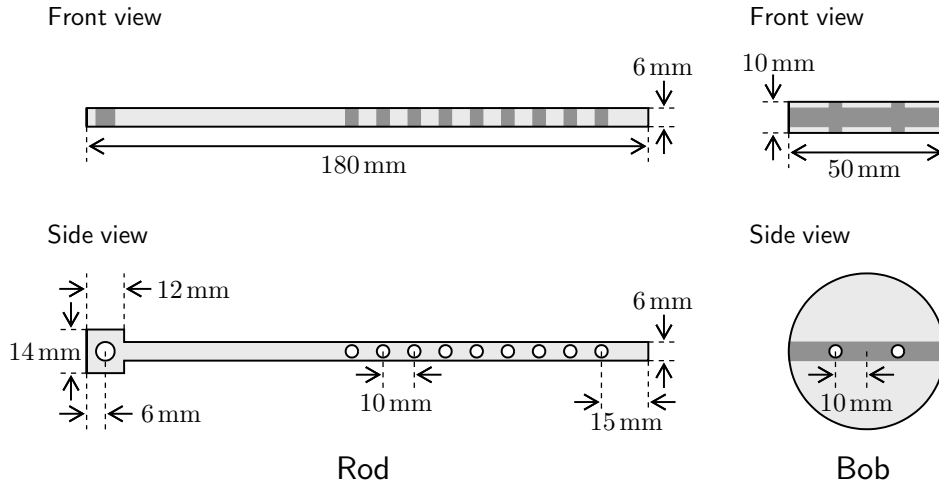
Figure 6.1: Schematic illustration of the parts of the mechanical pendulum: the rod and the bob. The gray corresponds to the holes.
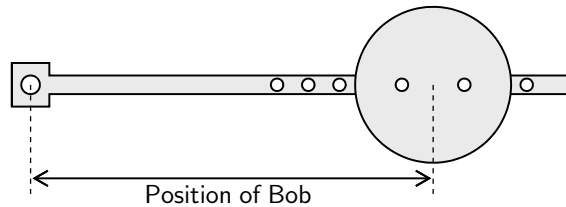

Figure 6.2: Schematic illustration of the mechanical pendulum. The pendulum is constructed by inserting the rod in the hole of the bob and fixing the position. The position of the bob is described as center-to-center distance between the rotary shaft and the bob.

netic shaker generates vertical excitation which corresponds to the parametric excitation. In addition, the experimental setup includes an accelerometer, angle sensors, and DC motors. The accelerometer measures the vertical acceleration of the rig or the pendulum. The angle sensor is fixed at the rotary shaft of the mechanical pendulum to measure the angular displacement of the pendulum. The DC motor is connected with the shaft by the gears for applying torque and generating electricity. Fig. 6.4 shows a schematic diagram of the experimental setup. The electromagnetic shaker is regulated through the V/I converter and the current amplifier at excitation frequency generated by the function generator. Here it is not expected that the shaker vertically excites the mechanical pendulum in ideal sinusoidal waveform, because the experimental setup behaves as a coupled system of the mechanical pendulum and the electromagnetic shaker [87].
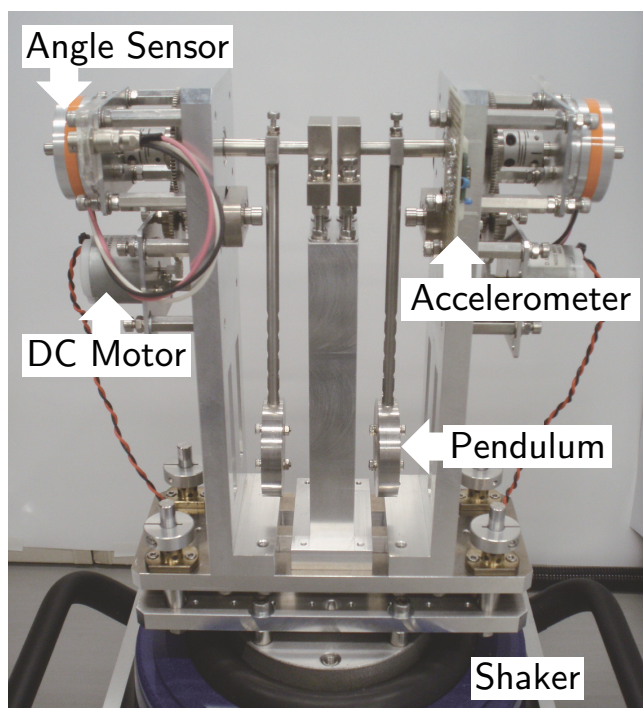
Figure 6.3: Photograph of the experimental setup for the parametric pendulum. The experimental setup consists of the mechanical rig supporting the pendulums mounted on the electromagnetic shaker which generates vertical excitation.

6.1.2   Observation of motions

Typical motions are observed for the vertically excited mechanical pendulum. In particular, we confirm the existence of periodic rotations and the system parameters at which the rotations appear. The system parameters correspond to the specification of the mechanical pendulum and the amplitude and the frequency of the vertical excitation. Periodic rotations observed here are employed as the target of the start control and perform energy scavenging from the vertical excitation in the following section. Throughout this experimental study, two kinds of setups are used for the mechanical pendulum in order to adjust the range of rotatory torque induced by the DC motor.

One is the mechanical pendulum with the smallest moment of inertia which can be realized in the experimental setup. The specification is listed as Setting 1 in Table 6.1. At this setup, the DC motor can generate the largest torque relative to the moment of inertia of the pendulum. However motions of the mechanical pendulum are damped strongly by the connected DC motor. As a result, two steady states appear for various vertical excitations. Fig. 6.5 shows the steady states at sinusoidal excitation with amplitude $5.6\,\mathrm{m/s^2}$ and frequency $5\,\mathrm{Hz}$. The two states are (a) a periodic rotation $(1,1)$ and (b) the static downward position.

At the other setup the mechanical pendulum possesses the largest moment of inertia listed as Setting 2 in Table 6.1. The damping effect which is caused by the connected
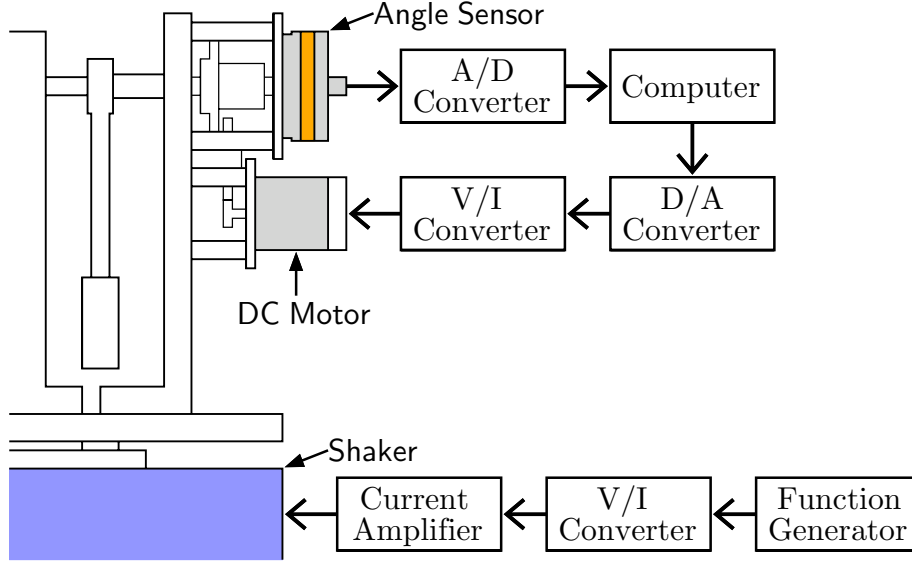
Figure 6.4: Schematic diagram of the experimental setup.

Table 6.1: Two kinds of specifications of the mechanical pendulum.

Setting	1	2
Mass of Rod		39.6 g
Mass of Bob	50.6 g	144.9 g
Position of Bob	89.0 mm	149.0 mm
Mass	94.8 g	189.1 g
Length	88.2 mm	138.3 mm
Moment of Inertia	7.37×10^{-4} kg·m^2	3.62×10^{-3} kg·m^2
Natural Frequency	1.68 Hz	1.34 Hz
Damping Coefficient	7×10^{-5} kg·m^2/s	1×10^{-4} kg·m^2/s

DC motor is suppressed at the smallest level. There appear a variety of periodic steady motions of the vertically excited mechanical pendulum. Fig. 6.6(a) shows a periodic rotation $(1,1)$ and (b) a $2T_\mathrm{P}$-periodic libration at sinusoidal excitation with amplitude 1.1 m/s^2 and frequency 2 Hz, where T_P denotes the excitation period. Fig. 6.7(a) shows a periodic rotation $(1,1)$ and (b) a $4T_\mathrm{P}$-periodic libration. The excitation parameters are regulated to the amplitude 2.1 m/s^2 and the frequency 3.5 Hz. Fig. 6.8 shows two periodic rotations which possess different periods. One has the same period as the vertical excitation and the other twice the period. The vertical excitation is generated at sinusoidal waveform with amplitude 2.0 m/s^2 and frequency 4 Hz.

We can observe the static downward position of the vertically excited mechanical pendulum for any vertical excitation. The observation is different from the numerical results for the physical model in Chapter 5. The difference is caused by the assumption

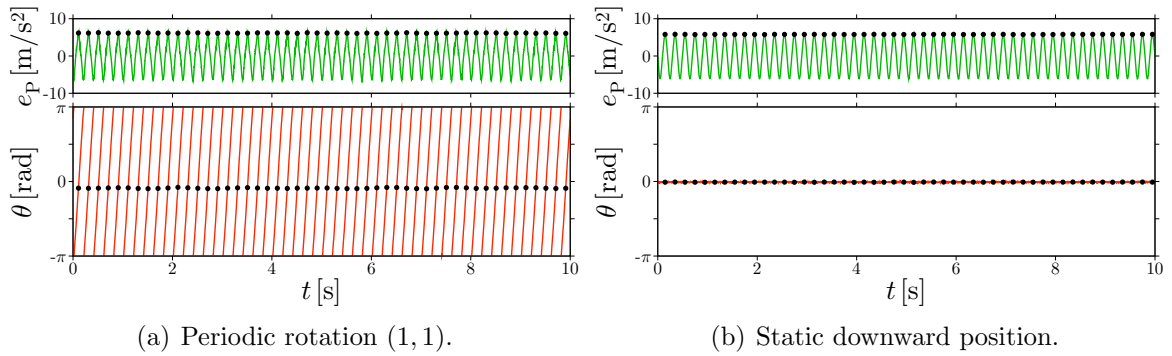(a) Periodic rotation $(1,1)$.

(b) Static downward position.

Figure 6.5: Steady states of the vertically excited mechanical pendulum with the smallest moment of inertia. The vertical excitation of the shaker is regulated to sinusoidal waveform with amplitude $5.6\,\mathrm{m/s^2}$ and frequency $5\,\mathrm{Hz}$. The dots denote the stroboscopic points at every excitation period.

(a) Periodic rotation $(1,1)$.

(b) $2T_\mathrm{P}$-periodic libration.
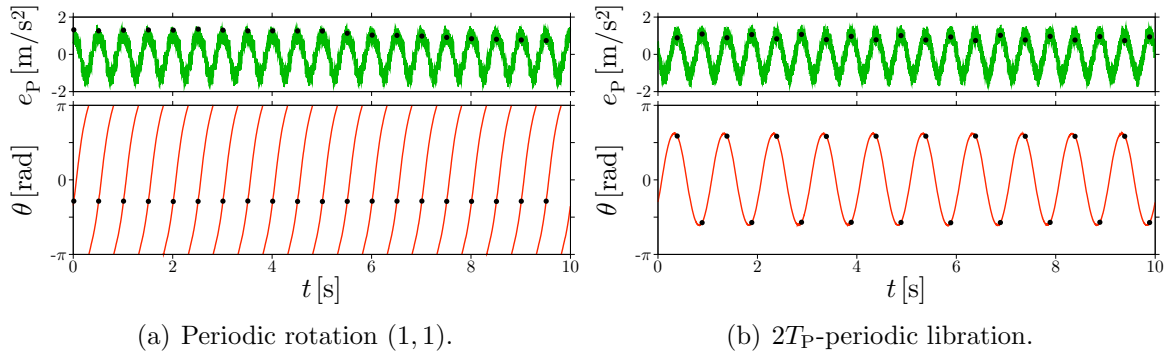
Figure 6.6: Steady motions of the mechanical pendulum at sinusoidal excitation with amplitude $1.1\,\mathrm{m/s^2}$ and frequency $2\,\mathrm{Hz}$. The mechanical pendulum is assembled with the largest moment of inertia.

of the linear viscous damping in the model. Nonlinearity of the damping appears in real mechanical systems. Moreover, the mechanical pendulum is connected with the DC motor. This induces complicated nonlinearity of the damping. In the thesis, we do not consider the damping characteristics. Instead of the detailed modeling and identification of the damping, we estimate the approximate value of the linear component of the damping through the logarithmic decrement method [87] for the reference. It should be noted that the modeling and identification are significant for applications such as energy scavenging because the damping characteristics directly related to dissipative energy due to the damping and the converted energy. The modeling and identification have been known as much complicated work [59, 60]. Indeed, the start control with delay operates properly without the exact mathematical model of the experimental setup [52, 55].
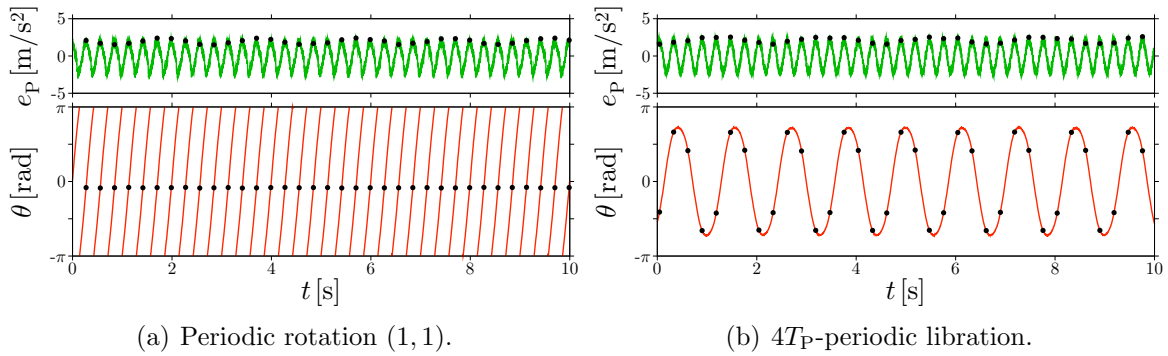
(a) Periodic rotation $(1, 1)$.

(b) $4T_\mathrm{P}$-periodic libration.

Figure 6.7: Steady motions of the mechanical pendulum at sinusoidal excitation with amplitude $2.1\,\mathrm{m/s^2}$ and frequency $3.5\,\mathrm{Hz}$. The mechanical pendulum is assembled with the largest moment of inertia.
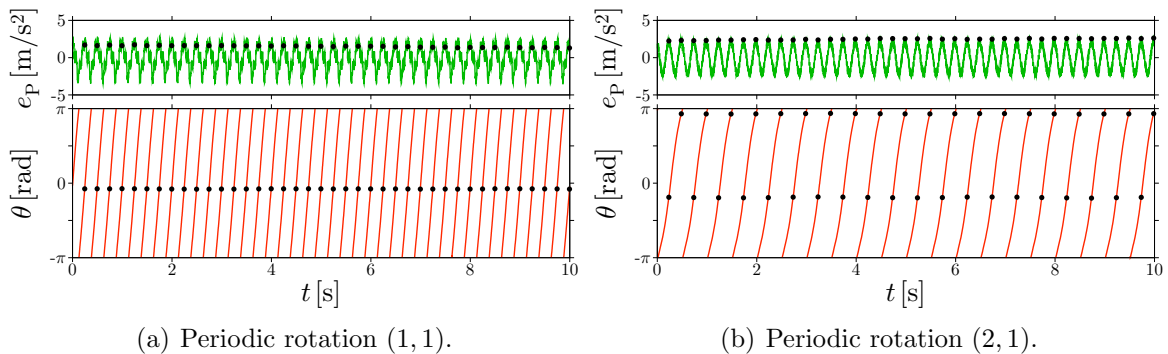

(a) Periodic rotation $(1, 1)$.

(b) Periodic rotation $(2, 1)$.

Figure 6.8: Two periodic rotations of the mechanical pendulum at sinusoidal excitation with amplitude $2.0\,\mathrm{m/s^2}$ and frequency $4\,\mathrm{Hz}$. The mechanical pendulum is assembled with the largest moment of inertia. The periodic rotations have rotation frequency different from each other.

6.2 Start control for periodic rotation

The control method proposed in the previous chapter is implemented in the experimental setup. The preliminary experiment showed that the mechanical pendulum connected with the DC motor rotates periodically. Since the DC motor is used in the control scheme, we should regard the mechanical pendulum with the DC motor as the experimental setup including the control system. However, the DC motor cannot be removed after the onset of the target rotation because of the following two reasons. One is that the DC motor is necessary for generating electric power in the energy scavenging. The other reason is that disconnecting the DC motor causes discontinuous change in the inertia and damping of the mechanical pendulum. The change possibly breaks the target periodic rotation. The DC motor should be regarded as a part of the mechanical pendulum which is now controlled. In other words, the periodic rotation observed in the previous section is the target motion of the proposed start control.

This section experimentally verifies the feasibility of the proposed control.

6.2.1   Installation of control system

The block diagram shown in Fig. 5.3 illustrates a flow of the start control. The flow is implemented in the experimental setup as shown in Fig. 6.4. Data acquisition of the angular displacement for the control is carried out by using the angle sensor. The control input is calculated by a computer according to the block diagram. The output voltage corresponding to the control input is converted to current for regulating the DC motor. The DC motor induces torque through the gears by 0.179 N·m/A. In the following, we use the control gain K and the delay time τ as well as the vertical excitation e_P and its period T_P with the corresponding dimension. In particular, the delay time is displayed at its reciprocal, that is, frequency. We call it control frequency.

6.2.2   Controlled behavior

We show behaviors of the mechanical pendulum under the start control. The observed periodic rotations are established by the start control from the coexisting motions.

First, we observe the start control for a periodic rotation from the static downward position. Based on the previous observation in Fig. 6.5, the mechanical pendulum is fixed at Setting 1 in Table. 6.1, and the vertical excitation is regulated to sinusoidal waveform with amplitude $5.6\,\mathrm{m/s^2}$ and frequency $5\,\mathrm{Hz}$. As for the control parameters, the control gain K is $0.072\,\mathrm{A/rad}$, the delayed time τ is the same as the excitation period $1/(5\,\mathrm{Hz}) = 2\,\mathrm{s}$, and the rotation number l is unit. Fig. 6.9 shows the behavior of the mechanical pendulum controlled for the periodic rotation. At the beginning of the control, the control operates for swinging up the pendulum and then the pendulum rotates. The stroboscopic points, denoted by the dots on the curves, show that the amount of change in the angular displacement increases at first and then converge. At around $3\,\mathrm{s}$ after the operation, the control input disappears and the target periodic rotation appears.

Next, the target periodic rotations are established from the coexisting periodic librations or rotations. We have already observed periodic motions coexisting with the corresponding target periodic rotations. Fig. 6.10(a) shows the system behavior under the start control from the $2T_P$-periodic libration to the target rotation in Fig. 6.6. Fig. 6.10(b) depicts the start control from the $4T_P$-periodic libration to the target rotation in Fig. 6.7. As shown in Fig. 6.10(c) the mechanical pendulum is controlled from the periodic rotation $(2, 1)$ to the target rotation $(1, 1)$ in Fig. 6.8. In addition, the start control can target the periodic rotation $(2, 1)$ in Fig. 6.8 by adjusting the delay time. The delay time is fixed at twice the excitation period. Fig. 6.10(d) shows the start control from the unstable static upward position to the target rotation $(2, 1)$ in Fig. 6.8. In this case, we empirically confirmed that the initial condition for starting the target rotation is strict. However, the proposed control can realize the target rotation.

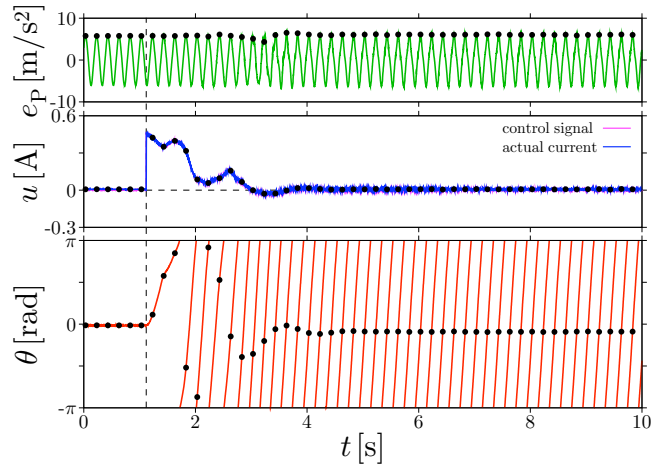These experiments verify the feasibility of the proposed control. Here we showed

Figure 6.9: Start control of the vertically excited mechanical pendulum from the static downward position to the periodic rotation. The mechanical pendulum is assembled at Setting 1 in Table 6.1. In order to generate the inherent periodic rotation, the vertical excitation is regulated to sinusoidal waveform with amplitude $5.6\,\mathrm{m/s^2}$ and frequency $5\,\mathrm{Hz}$. As the control parameters, the control gain K is $0.072\,\mathrm{A/rad}$, the delayed time τ is the same as the excitation period $1/(5\,\mathrm{Hz}) = 2\,\mathrm{s}$, and the rotation number is fixed at $l = 1$. The vertical dashed line indicates the beginning time of the start control.

the achieved results of the control scheme. As discussed in the previous chapter, the magnitude of the control gain and the initial condition govern the establishment of the target rotation in experiments. From a practical point of view, the limitation of the maximum torque generated by the DC motor might become a main cause of the failure. However, this point is not essential for the proposed method because the advantage is to make the motion of the pendulum approach to the target rotation.

6.3   Bifurcation with respect to control gain

This section experimentally confirms that the performance of the proposed control, which was numerically studied in the previous chapter, depends on the control gain. We focus on the stability of the target rotation. In the following, the mechanical pendulum is adjusted at Setting 2 in Table 6.1.

Figure 6.11 shows a bifurcation diagram of a periodic rotation with respect to the control gain K. The vertical excitation is regulated to sinusoidal waveform with amplitude $1.1\,\mathrm{m/s^2}$ and frequency $2\,\mathrm{Hz}$. As for the control parameters, the delay time is fixed at the excitation period and the rotation number is unit. The diagram is plotted through the stroboscopic observation. With increase of the control gain, the periodic rotation bifurcates at around $K = 0.15\,\mathrm{A/rad}$. Fig. 6.12 shows the system behaviors around the bifurcation. Before the bifurcation as shown in Fig. 6.12(a), the start
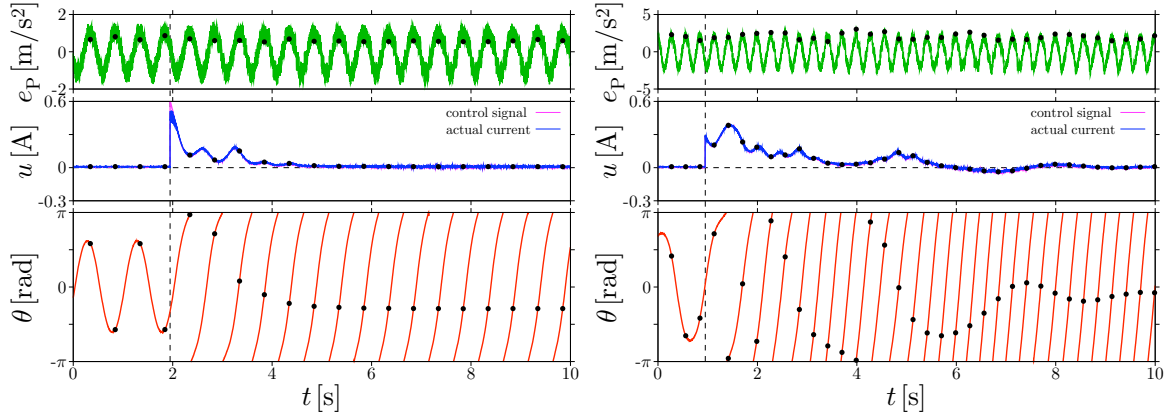
(a) From the $2T_P$-periodic libration in Fig. 6.6.

(b) From the $4T_P$-periodic libration in Fig. 6.7.
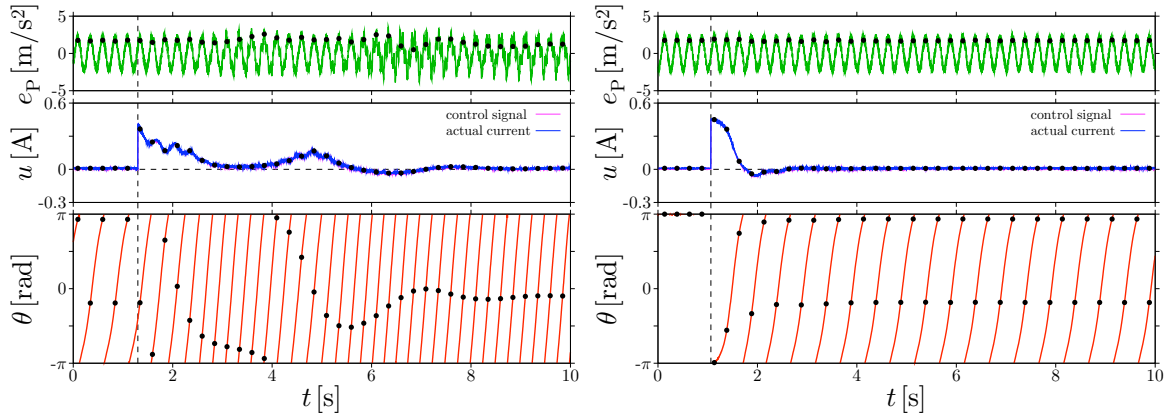
(c) From the periodic rotation $(2, 1)$ in Fig. 6.8.

(d) From the unstable static upward position to the periodic rotation $(2, 1)$ in Fig. 6.8.

Figure 6.10: Start control of the vertically excited mechanical pendulum assembled at Setting 2 in Table 6.1. The vertical excitation is regulated as the same as Figs. 6.6, 6.7, and 6.8. As the control parameters, the control gain K is $0.072\,\mathrm{A/rad}$ and the delayed time τ is the same as the excitation period in (a) and (b). In (c), the control gain K is increased to $0.11\,\mathrm{A/rad}$. In (d), the delay time τ is regulated to twice the period in order to target the periodic rotation $(2, 1)$. The rotation number is fixed at $l = 1$.
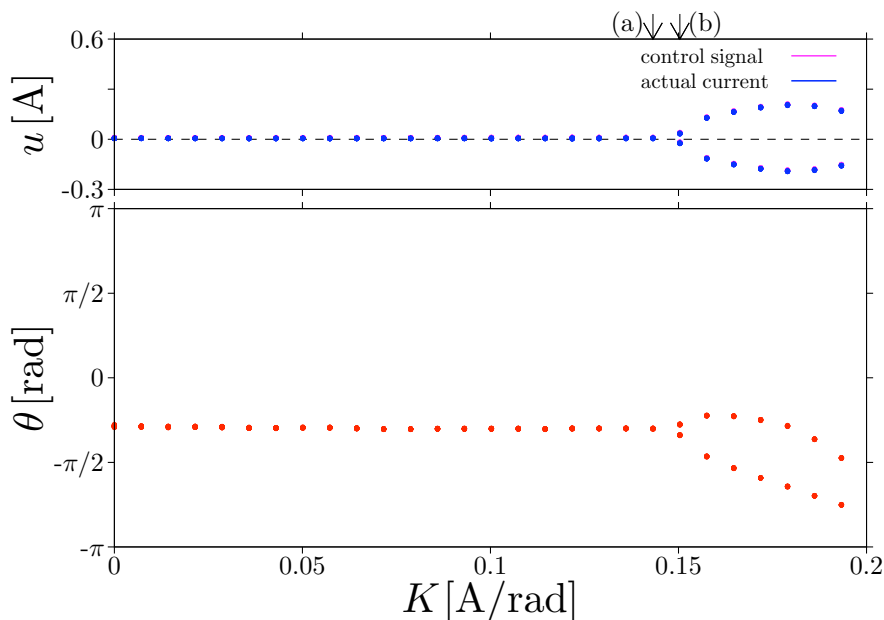
Figure 6.11: Bifurcation diagram with respect to the control gain K for the periodic rotation of the vertically excited mechanical pendulum under the start control. The vertical excitation is regulated to sinusoidal waveform with amplitude $1.1\,\mathrm{m/s^2}$ and frequency $2\,\mathrm{Hz}$. As for the control parameters, the delay time is fixed at the excitation period and the rotation number is unit. The data are measured through the stroboscopic observation.

control performs the desired operation. This is confirmed from the null control input. The mechanical pendulum exhibits the target periodic rotation. After the bifurcation in Fig. 6.12(b), the control input appears and the period is twice the excitation period. The pendulum rotates with twice the excitation period. This implies the occurrence of the period-doubling bifurcation. The experimental result is consistent with the numerical result in the previous chapter.

6.4 Bifurcation with respect to delay time

In this section, we examine bifurcation with respect to the delay time τ as another control parameter. In the applications of the controlled parametric pendulum, no exact information can be obtained for the frequency of external vibration in nature. The bifurcation diagram with respect to the delay time elucidates the existence range of a periodic rotation in the domain of delay. The range possibly represents the tolerance of the proposed control with the mistuned delay. In addition, it is confirmed that synchronization governs the existence and the width. The result assures that synchronization overcomes the mistuned difference of delay through entrainment.
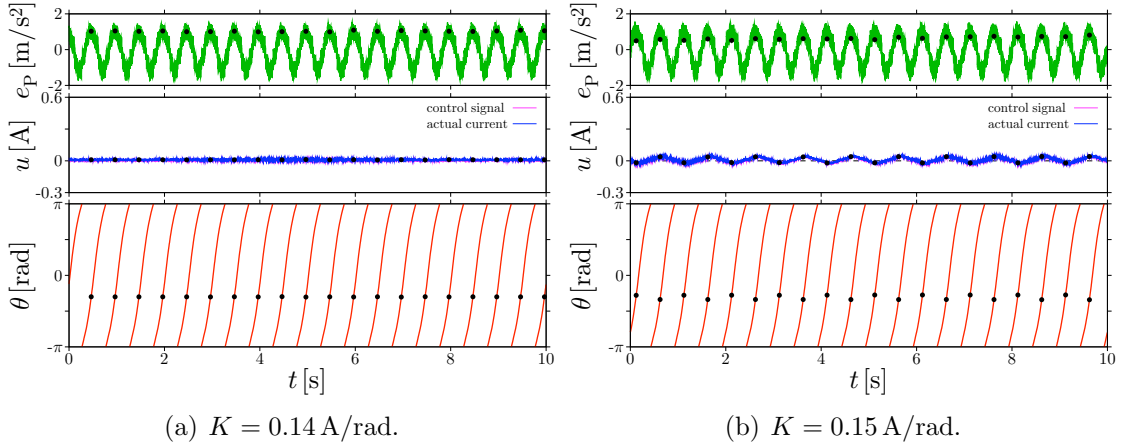
(a) $K = 0.14 \, \text{A/rad}$.   (b) $K = 0.15 \, \text{A/rad}$.

Figure 6.12: Behaviors of the vertically excited mechanical pendulum under the start control at the different control gain K in Fig. 6.11.

6.4.1 Experimental observation

Figure 6.13 shows a bifurcation diagram of rotation with respect to the delay time τ in the vertically excited mechanical pendulum under the start control. The shaker is calibrated to generate sinusoidal excitation with amplitude $1.2 \, \text{m/s}^2$ and frequency $2.3 \, \text{Hz}$. The control gain is fixed at $0.072 \, \text{A/rad}$ and the rotation number at unit. The diagram is measured by downward and upward shift of the delay time from the excitation period $1/2.3 \, \text{s}$. The points are plotted through the stroboscopic observation. According to the experimental procedure, we display the bifurcation parameter at the reciprocal of the delay time, denoted by $1/\tau$ in Fig. 6.13. For some of the delay time, controlled behaviors are shown in Fig. 6.14. At $\tau = 1/2.3 \, \text{s}$, the delay time is the same as the excitation period. In this case, the periodic rotation inherent in the vertically excited mechanical pendulum appears as shown in Fig. 6.14(c). The null control input implies the achievement of the desirable operation.

Increasing the control frequency, corresponding to decreasing the delay time τ, shifts the stroboscopic point of θ in the positive direction. Figs. 6.14(d) and (e) show that the start control can maintain the periodic rotation. Each of the periodic rotations is denoted by a single stroboscopic point in Fig. 6.13, which implies that the period or the rotations is coincident with the excitation period. Then, the control input remains and vibrates periodically. Average of the control input increases with the control frequency. Further increase of the control frequency induces a bifurcation. At around $1/\tau = 3.3 \, \text{Hz}$, the periodic rotation disappears and a quasiperiodic rotation appears. The quasiperiodic rotation is depicted by a number of the stroboscopic points in Fig. 6.13. Fig. 6.14(f) shows the the quasiperiodic behavior of the mechanical pendulum and the control input. The frequency of the quasiperiodic rotation is larger than the excitation frequency. On the other hand, decreasing the control frequency shifts the stroboscopic point of θ in the negative direction in a symmetric fashion. Small decrease induces a bifurcation at which the periodic rotation disappears. For the control frequency
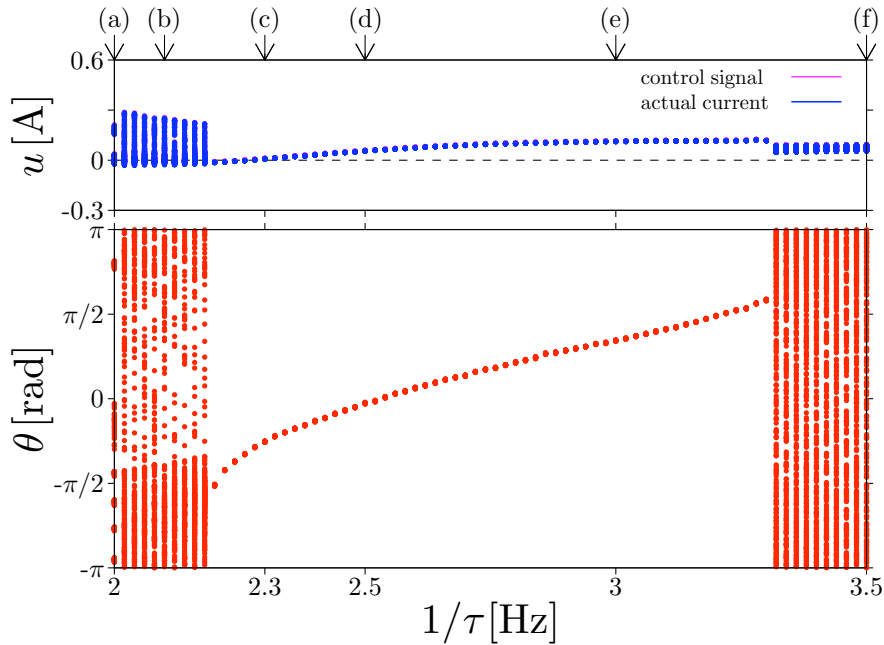
Figure 6.13: Bifurcation diagram of rotation with respect to the control frequency as the reciprocal of the delay time τ in the vertically excited mechanical pendulum under the start control. The vertical excitation is regulated to sinusoidal waveform with amplitude $1.2\,\mathrm{m/s^2}$ and frequency $2.3\,\mathrm{Hz}$. The control gain is regulated to $0.072\,\mathrm{A/rad}$ and the rotation number is fixed at unit. This diagram is measured by downward and upward shift of the control frequency from the excitation frequency $2.3\,\mathrm{Hz}$.

lower than the critical value of the bifurcation, the mechanical pendulum exhibits quasiperiodic rotations. Figs. 6.14(a) and (b) show the quasiperiodic rotations with the frequency lower than the excitation frequency. Here we compare the quasiperiodic behaviors which appear by loosing the stability under the control. In Fig. 6.14(f), the stroboscopic points of θ increases at almost the same distance. The control input is almost constant. In Figs. 6.14(a) and (b), the shift of the stroboscopic points greatly changes at every 6 periods. At the change, the control input increases. This result implies that the control rotates the mechanical pendulum if the rotation frequency is lower than the control frequency. As a result, the quasiperiodic rotation appears.

Figure 6.15 shows a bifurcation diagram at the control gain $K = 0.14\,\mathrm{A/rad}$. The other condition is not changed from Fig. 6.13. The bifurcation diagram displays qualitatively the same structure as the diagram in Fig. 6.13. The range of the delay time in which the periodic rotation is maintained becomes narrow with the increase of the control gain. For increasing the control gain, the bifurcation which annihilates the periodic rotation is induced by smaller difference between the angular displacement at the current and the delay because the difference is amplified by the larger control gain. This result possibly shows that the control gain governs the window of the periodic rotation in the domain of the delay time. Further increase of the control gain may

(a) $1/\tau = 2\,\mathrm{Hz}$.

(b) $1/\tau = 2.1\,\mathrm{Hz}$.

(c) $1/\tau = 2.3\,\mathrm{Hz}$.

(d) $1/\tau = 2.5\,\mathrm{Hz}$.

(e) $1/\tau = 3\,\mathrm{Hz}$.

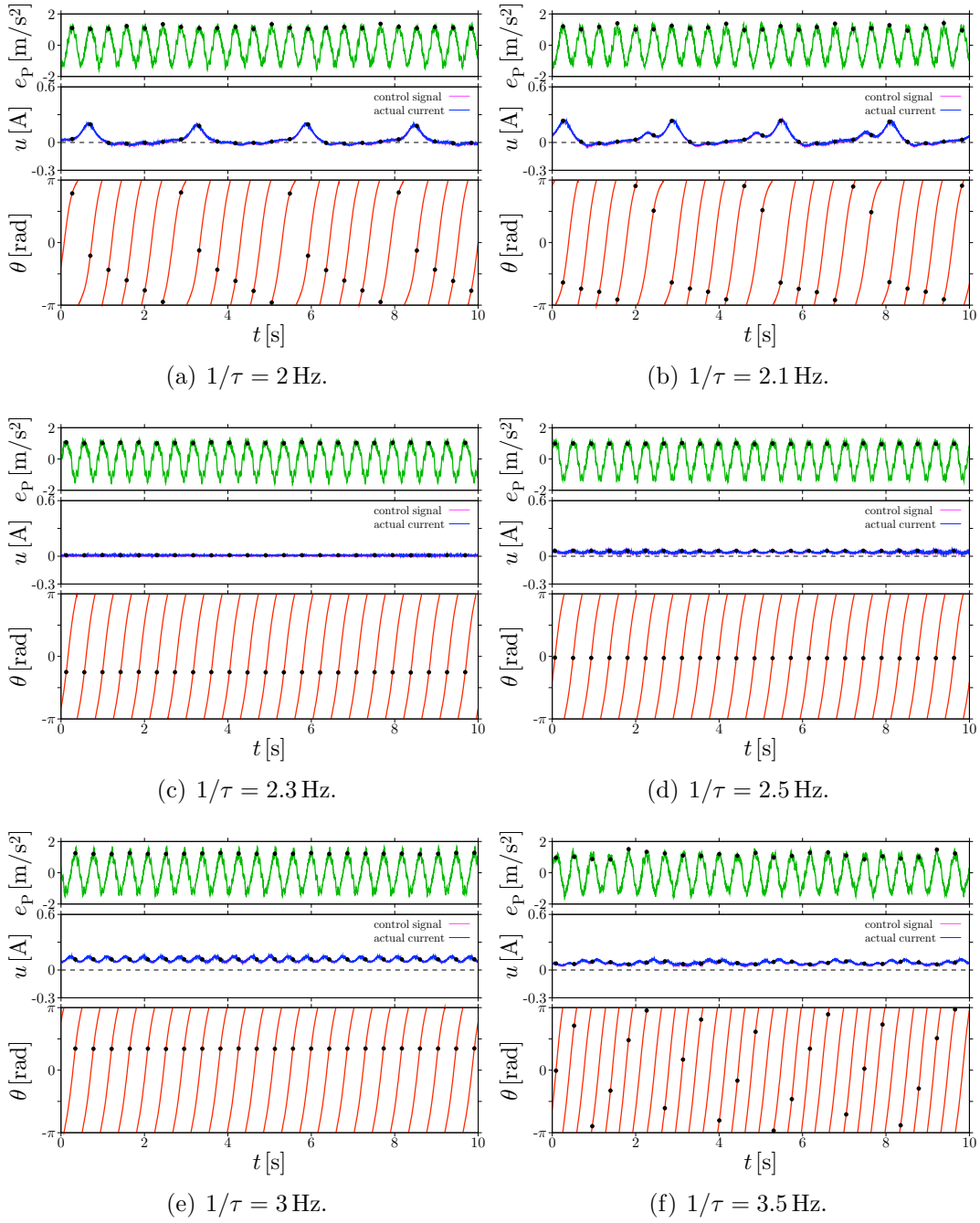(f) $1/\tau = 3.5\,\mathrm{Hz}$.

Figure 6.14: Behaviors of the vertically excited mechanical pendulum under the start control at different delay time in Fig. 6.13.
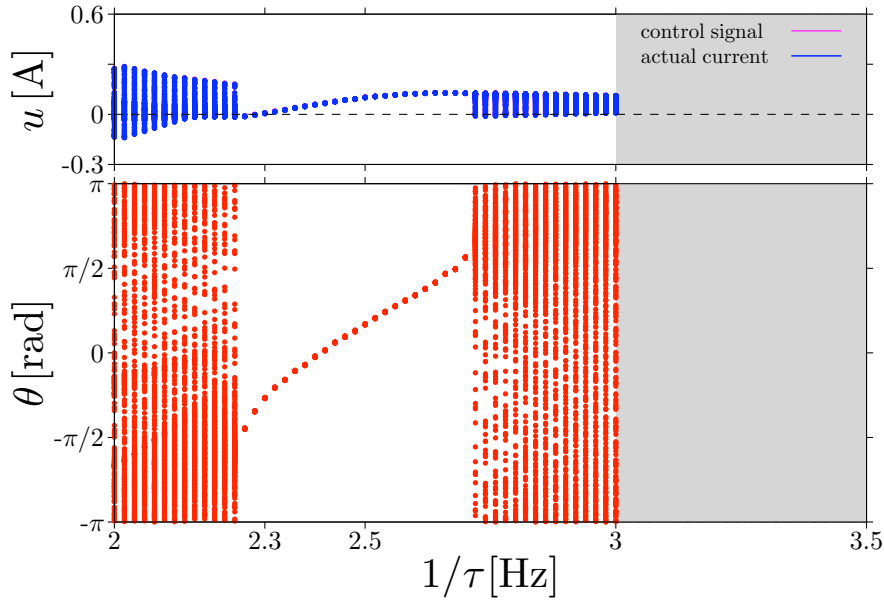
Figure 6.15: Bifurcation diagram of rotation with respect to the delay time τ in the vertically excited mechanical pendulum with the start control. The vertical excitation is regulated to sinusoidal waveform with amplitude $1.2\,\mathrm{m/s^2}$ and frequency $2.3\,\mathrm{Hz}$. The control gain is $0.14\,\mathrm{A/rad}$ and the rotation number at unit.

break the tolerance of the the proposed control toward the inaccurate delay time. The critical value of the control gain is consistent with the period-doubling bifurcation with respect to the control gain K in the previous chapter.

In addition, we confirm the bifurcation structure for different vertical excitation. Fig. 6.16 shows the bifurcation diagram with respect to the control frequency at the excitation amplitude $2.2\,\mathrm{m/s^2}$ and the frequency $4\,\mathrm{Hz}$. The control gain K is fixed at $0.14\,\mathrm{A/rad}$ and the rotation number at unit. This bifurcation diagram also shows qualitatively the same structure as Figs. 6.13 and 6.15. The bifurcating structure appears for any periodic rotation inherent in the vertically excited mechanical pendulum.

6.4.2 Comparison with entrainment region

The start control is tolerant toward the mistuned delay time. The bifurcation diagram with respect to the delay time elucidated the window of the periodic rotation in the domain of the delay. The experiments showed the common bifurcation structure. The window extends to the direction of high control frequency more widely than to low frequency. We here clarify that the feature is closely associated with the region of frequency entrainment.

In order to explain the bifurcation structures, we introduce a simple model below. The bifurcation diagrams shown in Figs. 6.13, 6.15, and 6.16 indicate that the control input u increases with the increase of the control frequency inside of the window.
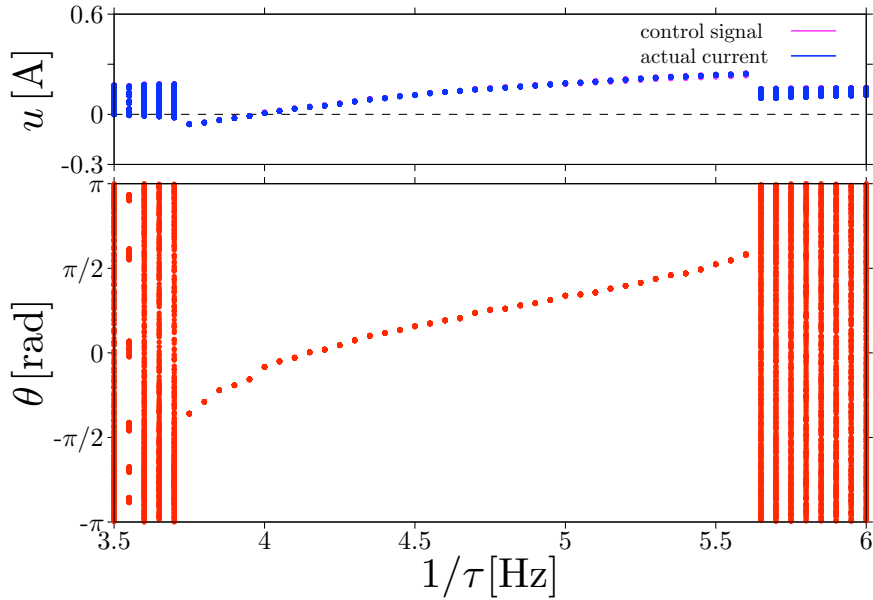
Figure 6.16: Bifurcation diagram of rotation with respect to the control frequency $1/\tau$ in the vertically excited mechanical pendulum under the start control. The vertical excitation is regulated to sinusoidal waveform with amplitude $2.2\,\mathrm{m/s^2}$ and frequency $4\,\mathrm{Hz}$. The control gain K is fixed at $0.14\,\mathrm{A/rad}$ and the rotation number at unit. This diagram is measured by downward and upward shift of the control frequency from the excitation frequency $4\,\mathrm{Hz}$.

Fig. 6.14 shows that the control input can be expressed as the sum of a sinusoidal waveform and a constant. The vibration of the control input can be regarded as a perturbation because the vibration amplitude is sufficiently small. From the experimental point of view, we simplify the controlled pendulum as the following parametric pendulum (5.1) driven by a constant torque N:

$$\frac{\mathrm{d}\theta}{\mathrm{d}t} = v, \tag{6.1a}$$

$$\frac{\mathrm{d}v}{\mathrm{d}t} = -cv - \left(1 + p\cos\omega t\right)\sin\theta + N. \tag{6.1b}$$

Figure 6.17 shows a bifurcation diagram of rotation with respect to the torque N at $c = 0.1$, $p = 0.5$, and $\omega = 2$. The bifurcation diagram shows qualitatively similar structure to the window in the domain of the delay time τ. By regarding the vibration of the control input as a perturbation, we qualitatively identify both bifurcations. The stable periodic rotation disappears by the saddle-node bifurcation at both sides of the existence range of the periodic rotation in Fig. 6.17. The existence range is widely extended to the direction of large torque. For appropriate torque N, no parametric excitation implies the existence of a stable rotational limit cycle. The Melnikov's method [65] gives the existence condition $N > 4c/\pi \approx 0.127$. Frequency entrainment
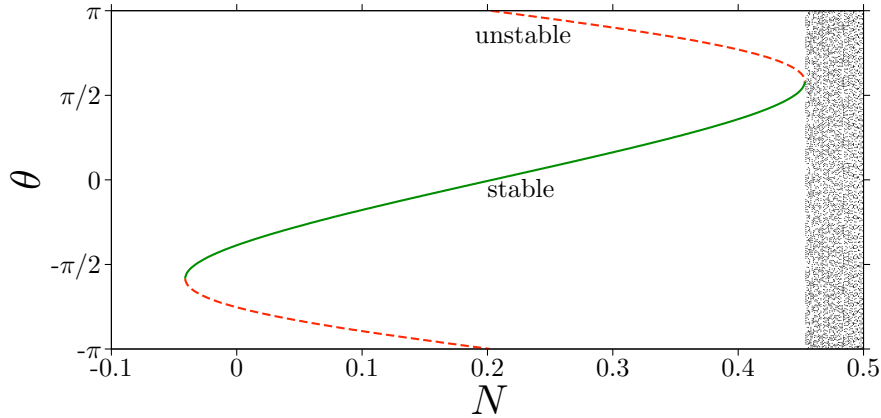
85

Figure 6.17: Bifurcation diagram of rotation with respect to the torque N in the driven parametric pendulum (6.1) at $c = 0.1$, $p = 0.5$, and $\omega = 2$. The branches consist of the stroboscopic points.

of the rotational limit cycle occurs by the parametric excitation in the range which satisfies the condition. The periodic rotations correspond to the entrained rotations. On the other hand, for $N \leq 4c/\pi$, the entrainment does not arise because the required limit cycle does not exist [2, 64]. However, the existence range is extended to a certain negative value of torque because the parametric excitation can compensate energy dissipated by the negative torque. In terms of frequency entrainment, we can give different interpretations for saddle-node bifurcations. The bifurcation at the positive torque corresponds to out of the entrained state. As a result, quasiperiodic rotation appears after the bifurcation [17, 64]. For the negative torque, rotation cannot be maintained because the torque works in the opposite direction of the rotation.

From the above discussion, the window of the periodic rotation is widely extended to shorter delay because of the effect of frequency entrainment. Frequency entrainment or synchronization governs the tolerance of the start control with the mistuned delay time. This result implies that the start control operates to a periodically excited system without the exact information of the excitation frequency. A periodic rotation is established by regulating the delay time shorter than the expected value. The controlled periodic rotation is not the target rotation. However, decreasing the control gain or the control frequency corresponds to the decrease of the control input. Then, the periodic rotation approaches to the target rotation. Furthermore, the tolerance of the start control with mistuned delay is efficient for vibration of nature which includes a variety of frequency. The control method is expected to extract the frequency component suited for the periodic rotation from the window.
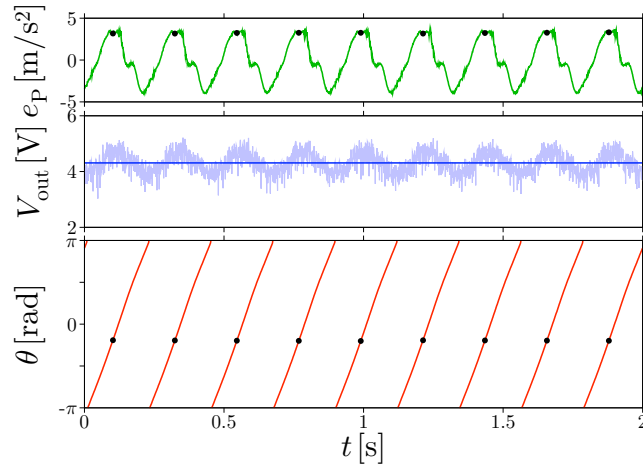
Figure 6.18: Energy scavenging by a periodic rotation of the mechanical pendulum with the DC motor from the vertical vibration. The vertical excitation is regulated to sinusoidal waveform with amplitude $3.4\,\mathrm{m/s^2}$ and frequency $4.5\,\mathrm{Hz}$. The electric load is resistance $500\,\Omega$.

6.5 Energy scavenging from vertical vibration

In this chapter, we have observed the periodic rotations of the vertically excited mechanical pendulum connected with the DC motor. At the end, we demonstrate energy scavenging from the vertical vibration by the mechanical pendulum. Here the DC motor works as an electric generator and the electric load is a resistance. Fig. 6.18 shows the energy scavenging through a periodic rotation of the mechanical pendulum with the DC motor from the vertical excitation of the shaker. The vertical vibration is fixed at sinusoidal waveform with amplitude $3.4\,\mathrm{m/s^2}$ and frequency $4.5\,\mathrm{Hz}$. The DC motor generates electricity at $4.3\,\mathrm{V}$ for the resistance $500\,\Omega$. The experimental result manifests the possibility of energy scavenging by a periodic rotation of the parametric pendulum.

6.6 Remarks

This chapter was devoted to the experimental investigation into the controlled states of the mechanical pendulum under the delayed feedback. First, the vertically excited mechanical pendulum was introduced as an experimental system for the parametric pendulum. The mechanical pendulum connected with the DC motor exhibited periodic rotations and the coexisting motions. For the experimental setup, we mounted the control system for stating a periodic rotation proposed in the previous chapter. The experiments verified the feasibility of the proposed method.

In addition, the performance which depends on the control parameters was confirmed through examining the bifurcation structure. The increase of the control gain

induced the loss of stability of the target rotation. The feature has been already predicted by the numerical study in the previous chapter. The bifurcation diagram with respect to the delay elucidated the tolerance of the start control with the inaccurate delay time for maintaining the periodic rotation. In particular, the control method can establish the periodic rotation at large mistuned difference of the delay time in the direction of short delay. The reason was interpreted as the effect of frequency entrainment through analyzing the parametric pendulum driven by a constant torque. Synchronization phenomenon governs the tolerance of the start control with the mistuned delay time. Finally, we demonstrated the experimental energy scavenging by a periodic rotation of the mechanical pendulum from the vibration of the shaker.

Chapter 7

Conclusions and Future Prospects

The thesis investigated the energy aspect of synchronization in a pendulum to understand and apply the conversion of energy. As an application, we introduced energy scavenging by the resonant or synchronized motions of the parametrically excited pendulum and proposed a control method for starting a periodic rotation of the pendulum based on synchronization. The conclusions of this study are presented and the future work is summarized below.

7.1 Conclusions

Chapter 2 described the theory of synchronization in a pendulum. First, the notion of phase was reviewed which plays a central role in the theory of synchronization. Then, we introduced the notion of energy conversion in synchronization. A value of energy stored in a pendulum can be assigned with a closed orbit in the state space. In this sense, energy possibly becomes more general notion than amplitude. In addition, we gave the self-sustained oscillator and rotator defined in the state space of a pendulum analyzed in the thesis. The steady oscillations are interpreted as the limit cycles which are distinguishable according to the topological property. Finally, the parametric pendulum was explained as a energy conversion device for the energy scavenging.

Chapter 3 was devoted to the analysis of energy conversion in frequency entrainment of libration. We employed the van der Pol oscillator as a model system in which the entrainment phenomenon occurs. Response curves were obtained to understand the relationship between the supplied energy and the characteristics of entrained librations. The averaging and calculation revealed that the maximum energy is converted with the resonance phenomenon occurring in the entrainment region. Energy conversion can be estimated by the magnitude of amplitude of the libration. Then, the energy conversion was tried to associate with the transient phenomenon of the entrainment of libration. Energy exchanged between the system and the external does not develop the frequency entrainment in terms of the theory based on the phase dynamics. Therefore, the phase regulation which governs the frequency entrainment of libration is not essentially affected by any energy supply from the external. The energy conversion determines

amplitude of the libration.

In Chapter 4, we analyzed energy conversion in frequency entrainment of rotation by using the same approach as the previous chapter. The phase-locked system was considered as a dynamical system with a stable rotational limit cycle. At the entrained states, response curves were obtained numerically and theoretically for the supplied energy and the characteristics of entrained rotations. The phase for the synchronization and the excitation frequency governs the energy conversion. In the transient regime, we associated the development of the entrainment phenomenon with the energy conversion. By identifying the phase through response characteristics and the expression of the limit cycle, the phase equation was derived to represent the dynamics of phase for the frequency entrainment of rotation. The entrainment phenomenon develops according to the change of the stored energy. The relationship implies the possibility to induce the frequency entrainment of rotation or regulate the phase of rotation by exchanging energy.

In addition, we discussed the difference between the frequency entrainment phenomena of libration and rotation. The obtained result indicated advantages of periodic rotations over periodic librations for the energy scavenging in terms of energy conversion by synchronization. Energy conversion is associated with amplitude for libration and with phase for rotation. Thus, the entrainment phenomena with the common mechanism of phase regulation can be characterized in terms of energy conversion.

In chapter 5, we proposed a control method for starting a periodic rotation of the parametric pendulum. We began with investigation into the properties of the periodic rotations. The onset of the periodic rotations depends on the initial state of the pendulum and requires energy supply because the periodic rotations are motions with high energy. The possibility to regulate the phase of rotation in Chapter 4 gave the strategy to construct the control method. That is, the energy supply and extraction regulate the phase or the frequency of rotation. In the control scheme, energy exchange is realized by applying the constant torque, and the temporal change of phase is identified by using at every moment the difference between states at a distance of the excitation period. Furthermore, the proposed control method was numerically studied. The control behaviors showed that the expected control is achieved. The remaining of the chapter numerically confirmed the performance of the start control with respect to the domain of attraction and the bifurcation diagram. Here, we found the range of the control gain in which the target periodic rotation is established from any initial state of the pendulum.

Chapter 6 provided experiments on the controlled states of the mechanical pendulum under the delayed feedback. First, the vertically excited mechanical pendulum was introduced as an experimental system for the parametric pendulum. The mechanical pendulum connected with the DC motor exhibited periodic rotations. For the experimental setup, we installed the control system for starting the periodic rotation. The experiments verified the feasibility of the proposed method. Next, the performance of the control method is discussed. The observed bifurcation with respect to the control gain showed the same structure as the numerical result in the Chapter 5. The bifur-

cation diagram with respect to the delay time elucidated the window of the periodic rotation. This results indicates the tolerance of the start control with the mistuned delay time. The window was explained by synchronization region with respect to torque. Thus synchronization governs the tolerance of the control toward the inaccurate delay. We confirmed that the mechanism of the start control is closely related to synchronization. Finally we demonstrated energy scavenging by the mechanical pendulum from the vertical vibration generated by the electromagnetic shaker.

In the thesis, we began with the basic research for the energy conversion in synchronization of a pendulum. The analysis of energy conversion gave us the perspective to the applications such as energy scavenging. In addition, the obtained results contribute to the applied research as the proposition of a control based on synchronization. The proposed method with time delay operates as a control to cross over a separatrix which forms a boundary between basins of steady states. The control generates a pass to the target by adding dimensions to the inherent state space.

7.2 Future prospects

Energy conversion by synchronization has still rich possibilities of engineering applications. The effective example we can mention is energy scavenging from external vibration in nature through the synchronized motions.

Vibration in nature exhibits power spectrum extended from a main frequency component [88]. We first have to know the feasibility of synchronization and the synchronized frequency. Irregularity of the vibration possibly breaks the periodic structure required for synchronization. By regarding the irregularity as noise, stochastic resonance is expected [89]. The resonance phenomenon enhances the main frequency component. Synchronization extracts energy at a frequency component related to the synchronized cycle except for chaos synchronization, but the maximum energy conversion is realized by the stochastic resonance. The combination use of multiple synchronized frequency can cover the extended power spectrum.

In the thesis, we dealt with forced synchronization of a pendulum. If a pendulum is coupled with another pendulum, mutual synchronization may be observed. It is obvious that energy is converted between the pendulums through the mutual synchronization. The mutual synchronization possibly enhances energy supplied by the external. In this sense, energy conversion in coupled pendulums becomes an issue we have to solve.

In application of energy scavenging, conversion to electricity is needed for a variety of energy use. The performance of electric generators governs the efficiency and the realization of energy scavenging. In the thesis, we proposed a torque control for the onset of a periodic rotation of the parametric pendulum. This control scheme requires two parallel electric systems for the generator and the motor in the practical system. If the generator is designed for usage as an electric motor, the two electric systems are integrated into one. The development of generators is one of the most important work for the practical realization.

Bibliography

[1] I. I. Blekhman, *Synchronization in Science and Technology*, ASME Press, New York, 1988.

[2] A. Pikovsky, M. Rosenblum, and J. Kurths, *Synchronization: A universal concept in nonlinear sciences*, Cambridge University Press, Cambridge, 2001.

[3] R. Adler, A study of locking phenomena in oscillators, Proc. IRE **34**(6), 351–357 (1946).

[4] A. T. Winfree, Biological rhythms and the behavior of populations of coupled oscillators, J. Theor. Biol. **16**(1), 15–42 (1967).

[5] A. T. Winfree, *The Geometry of Biological Time*, Springer-Verlag, Berlin, 1990.

[6] J. Guckenheimer, Isochrons and phaseless sets, J. Math. Biol. **1**(3), 259–273 (1975).

[7] Y. Kuramoto, Self-entrainment of a population of coupled nonlinear oscillators, in Intern. Symp. on Math. Prob. in Theor. Phys., *Lecture Notes in Physics* (H. Araki, ed.) **39**, Springer-Verlag, New York, 1975, pp. 420–422.

[8] Y. Kuramoto, *Chemical Oscillations, Waves, and Turbulence*, Springer-Verlag, Berlin, 1984; Dover Publications, New York, 2003.

[9] I. I. Blekhman, *Vibrational Mechanics: Nonlinear dynamics effects, general approach, applications*, World Scientific, Singapore, 2000.

[10] S. H. Strogatz, From Kuramoto to crawford: exploring the onset of synchronization in populations of coupled oscillators, Physica D **143**(1–4), 1–20 (2000).

[11] J. A. Acebrón, L. L. Bonilla, C. J. Pérez, F. Ritort, and R. Spigler, The Kuramoto model: A simple paradigm for synchronization phenomena, Rev. Mod. Phys. **77**(1), 137–185 (2005).

[12] J. Takagi, History and future tasks in research on synchronization phenomena, in *1974 Joint Convention Record of Four Institutes of Electrical Engineers, Japan***6**, IECE, Tokyo, 1974, pp. 97–100, 1974 (in Japanese).

[13] Y. Ueda and M. Hirano, On synchronization phenomena between electric power systems, IEICE Tech. Rep., NLP98-65, 1998 (in Japanese).

[14] Y. Ueda and M. Hirano, On synchronization phenomena between electric power systems (2), IEICE Tech. Rep. NLP98-82, 1998 (in Japanese).

[15] Y. Ueda and M. Hirano, On synchronization phenomena between electric power systems (3), IEICE Tech. Rep. NLP98-99, 1999 (in Japanese).

[16] S. H. Strogatz, Exploring complex networks, Nature **410**(6825), 268–276 (2001).

[17] M. L. Cartwright, Forced oscillations in nearly sinusoidal systems, J. Inst. Electr. Eng. **95**(34), 88–96 (1948).

[18] R. K. Brayton and J. K. Moser, A theory of nonlinear networks–i, Quart. Appl. Math. **22**(1), 1–33 (1964).

[19] M. Kuramitsu and F. Takase, An analytical method for multimode oscillators using the averaged potential, IECE Trans. **J66-A**(4), 336–343 (1983) (in Japanese).

[20] M. Kuramitsu and F. Takase, Analytical method for multimode oscillators using the averaged potential, Electron. Commun. Jpn. **66-A**(4), 10–19 (1983).

[21] M. Kuramitsu, F. Takase, and H. Nitta, A new method for the analysis of forced self-oscillatory systems using the averaged potential, in *Proc. ISCAS 85*, pp. 863–866, 1985.

[22] C. Sarasola, F. J. Torrealdea, A. d'Anjou, A. Moujahid, and M. Graña, Nonzero error synchronization of chaotic systems via dynamic coupling, Physica D **177**(1–4), 39–49 (2003).

[23] C. Sarasola, F. J. Torrealdea, A. d'Anjou, A. Moujahid, and M. Graña, Energy balance in feedback synchronization of chaotic systems, Phys. Rev. E **69**(1), 011606 (2004).

[24] C. Sarasola, A. d'Anjou, F. J. Torrealdea, and M. Graña, Minimization of the energy flow in the synchronization of nonidentical chaotic systems, Phys. Rev. E **72**(2), 026223 (2005).

[25] D. A. Paley, N. E. Leonard, R. Sepulchre, D. Grünbaum, and J. L. Parrish, Oscillator models and collective motion, IEEE Contr. Syst. Mag. **27**(4), 89–105 (2007).

[26] S. H. Strogatz, *Nonlinear Dynamics and Chaos: With applications to physics biology, chemistry, and engineering*, MA: Addison-Wesley, Reading, MA, 1994.

[27] J. B. McLaughlin, Period-doubling bifurcations and chaotic motion for a parametrically forced pendulum, J. Stat. Phys. **24**(2), 375–388 (1981).

[28] R. W. Leven and B. P. Koch, Chaotic behaviour of a parametrically excited damped pendulum, Phys. Lett. A **86**(2), 71–74 (1981).

[29] B. P. Koch, R. W. Leven, B. Pompe, and C. Wilke, Experimental evidence for chaotic behaviour of a parametrically forced pendulum, Phys. Lett. A **96**(5), 219–224 (1983).

[30] R. W. Leven, B. Pompe, C. Wilke, and B. P. Koch, Experiments on periodic and chaotic motions of a parametrically forced pendulum, Physica D **16**(3), 371–384 (1995).

[31] M. J. Clifford and S. R. Bishop, Approximating the escape zone for the parametrically excited pendulum, J. Sound Vib. **172**(4), 572–576 (1994).

[32] M. J. Clifford and S. R. Bishop, Rotating periodic orbits of the parametrically excited pendulum, Phys. Lett. A **201**(2–3), 191–196 (1995).

[33] S. R. Bishop and M. J. Clifford, Zones of chaotic behaviour in the parametrically excited pendulum, J. Sound Vib. **189**(1), 142–147 (1996).

[34] W. Garira and S. R. Bishop, Rotating solutions of the parametrically excited pendulum, J. Sound Vib. **263**(1), 233–239 (2003).

[35] X. Xu, M. Wiercigroch, and M. P. Cartmell, Rotating orbits of a parametrically-excited pendulum, Chaos Soliton. Fract. **23**(5), 1537–1548 (2005).

[36] S. R. Bishop, A. Sofroniou, and P. Shi, Symmetry-breaking in the response of the parametrically excited pendulum model, Chaos Soliton. Fract. **25**(2), 257–264 (2005).

[37] A. Sofroniou and S. R. Bishop, Breaking the symmetry of the parametrically excited pendulum model, Chaos Soliton. Fract. **28**(3), 673–681 (2005).

[38] X. Xu and M. Wiercigroch, Approximate analytical solutions for oscillatory and rotational motion of a parametric pendulum, Nonlinear Dyn. **47**(1–3), 311–320 (2007).

[39] S. Lenci, E. Pavlovskaia, G. Rega, and M. Wiercigroch, Rotating solutions and stability of parametric pendulum by perturbation method, J. Sound Vib. **310**(1–2), 243–259 (2008).

[40] B. Horton, M. Wiercigroch, and X. Xu, Transient tumbling chaos and damping identification for parametric pendulum, Phil. Trans. R. Soc. A **366**(1866), 767–784 (2008).

[41] M. Wiercigroch, private communication (2008).

[42] H. Kanki, Recent trend of ocean energy, IEEJ J. **129**(8), 548–551 (2009) (in Japanese).

[43] A. Clément, P. McCullen, A. Falcão, A. Fiorentino, F. Gardner, K. Hammarlund, G. Lemonis, T. Lewis, K. Nielsen, S. Petroncini, M. Pontes, P. Schild, B. Sjöström, H. C. Sørensen, and T. Thorpe, Wave energy in europe: current status and perspectives, Renew. & Sust. Energ. Rev. **6**(5), 405–431 (2002).

[44] Ocean energy conversion in europe: Recent advancements and prospects, 2006, at http://www.wave-energy.net/index files/documents/.

[45] J. Falnes, A review of wave-energy extraction, Mar. Struct. **20**(4), 185–201 (2007).

[46] J. Scruggs and P. Jacob, Harvesting ocean wave energy, Science **323**(5918), 1176–1178 (2009).

[47] R. Vautard, J. Cattiaux, P. Yiou, J. Thépaut, and P. Ciais, Northern hemisphere atmospheric stilling partly attributed to an increase in surface roughness, Nat. Geosci. **3**(11), 756–761 (2010).

[48] L. M. Pecora and T. L. Carroll, Synchronization in chaotic systems, Phys. Rev. Lett. **64**(8), 821–824 (1990).

[49] L. M. Pecora and T. L. Carroll, Driving systems with chaotic signals, Phys. Rev. A **44**(4), 2374–2383 (1991).

[50] E. Ott, C. Grebogi, and J. A. Yorke, Controlling chaos, Phys. Rev. Lett. **64**(11), 1196–1199 (1990).

[51] K. Pyragas, Continuous control of chaos by self-controlling feedback, Phys. Lett. A **170**(6), 421–428 (1992).

[52] K. Pyragas and A. Tamaševičius, Experimental control of chaos by delayed self-controlling feedback, Phys. Lett. A **180**(1–2), 99–102 (1993).

[53] D. J. Gauthier, D. W. Sukow, H. M. Concannon, and J. E. S. Socolar, Stabilizing unstable periodic orbits in a fast diode resonator using continuous time-delay antosynchronization, Phy. Rev. E **50**(3), 2343–2346 (1994).

[54] S. Bielawski, D. Derozier, and P. Glorieux, Controlling unstable periodic orbits by a delayed continuous feedback, Phys. Rev. E **49**(2), R971–R974 (1994).

[55] T. Hikihara and T. Kawagoshi, An experimental study on stabilization of unstable periodic motion in magneto-elastic chaos, Phys. Lett. A **211**(1), 29–36 (1996).

[56] K. Pyragas, Delayed feedback control of chaos, Phil. Trans. R. Soc. A **364**(1846), 2309–2334 (2006).

[57] H. G. Schuster, ed., *Handbook of chaos control*, WILEY-VCH, Weinheim, 1999.

[58] E. Schöll and H. G. Schuster, eds., *Handbook of chaos control* (2nd ed.), WILEY-VCH, Weinheim:, 2008.

[59] C. C. de Wit, H. Olsson, K. J. Åström, and P. Lischinsky, A new model for control of systems with friction, IEEE T. Automat. Contr. **40**(3), 419–425 (1995).

[60] M. Urbakh, J. Klafter, D. Gourdon, and J. Israelachvill, The nonlinear nature of friction, Nature **430**(6999), 525–528 (2004).

[61] H. Mori and Y. Kuramoto, *Dissipative Structure and Chaos*, Springer-Verlag, Berlin, 1998.

[62] J. K. Hale, *Ordinary Differential Equations*, John Wiley & Sons, New York, 1969.

[63] N. Minorsky, *Introduction of Non-Linear Mechanics*, Edwards Brothers, Ann Arbor, MI, 1947.

[64] C. Hayashi, *Nonlinear Oscillations in Physical Systems*, McGraw-Hill, New York, 1964.

[65] J. Guckenheimer and P. Holmes, *Nonlinear Oscillations, Dynamical Systems, and Bifurcations of Vector Fields*, Springer-Verlag, New York, 1983.

[66] B. van der Pol, Forced oscillations in a circuit with non-linear resistance (reception with reactive triode), Philos. Mag. **3**, 65–80 (1927).

[67] D. D'Humieres, M. R. Beasley, B. A. Huberman, and A. Libchaber, Chaotic states and routes to chaos in the forced pendulum, Phys. Rev. A **26**(6), 3483–3496 (1982).

[68] G. L. Baker and J. A. Blackburn, *The pendulum: a case study in physics*, Oxford University Press, New York, 2005.

[69] D. E. McCumber, Effect of ac impedance on dc voltage-current characteristics of superconductor weak-link junctions, J. Appl. Phys. **39**(7), 3113–3118 (1968).

[70] R. L. Kautz, The ac Josephson effect in hysteretic junctions: Range and stability of phase lock, J. Appl. Phys. **52**(5), 3528–3541 (1981).

[71] F. Salam and S. Sastry, Dynamics of the forced Josephson junction circuit: The regions of chaos, IEEE T. Circuit. Syst. **32**(8), 784–796 (1985).

[72] G. Filatrella, B. A. Malomed, and R. D. Parmentier, Threshold analysis for the inverse ac josephson effect, Phys. Lett. A **180**(4–5), 346–349 (1993).

[73] T. Endo and L. O. Chua, Chaos from phase-locked loops, IEEE T. Circuit. Syst. **35**(8), 987–1003 (1988).

[74] Y. Susuki and Y. Ueda, Amplitude response curves of frequency-locked rotations, IEICE Trans. Fundamentals **E90-A**(10), 2250–2252 (2007).

[75] Y. Susuki and T. Hikihara, Transient dynamics in electric power system with dc transmission: fractal growth in stability boundary, IEE Proc.-Circ. Dev. Syst. **152**(2), 159–164 (2005).

[76] H. Tanaka, A. J. Lichtenberg, and S. Oishi, First order phase transition resulting from finite inertia in coupled oscillator systems, Phys. Rev. Lett. **78**(11), 2104–2107 (1997).

[77] H. Tanaka, A. J. Lichtenberg, and S. Oishi, Self-synchronization of coupled oscillators with hysteretic responses, Physica D **100**(3–4), 279–300 (1998).

[78] N. Levinson, Transformation theory of non-linear differential equations of the second order, Ann. Math. **45**(4), 723–737 (1944).

[79] I. I. Blekhman, P. S. Landa, and M. G. Rosenblum, Synchronization and chaotization in interacting dynamical systems, Appl. Mech. Rev. **48**(11), 733–752 (1995).

[80] T. S. Parker and L. O. Chua, *Practical Numerical Algorithms for Chaotic Systems*, Springer-Verlag, New York, 1989.

[81] N. Grønbech-Jensen and M. R. Samuelsen, Phase-locking of an overdamped pendulum, Phys. Lett. A **191**(1–2), 57–60 (1994).

[82] S. Shapiro, Josephson currents in superconducting tunneling: The effect of microwaves and other observations, Phys. Rev. Lett. **11**(2), 80–82 (1963).

[83] J. Miles, On resonant rotation of a weakly damped pendulum, J. Sound Vib. **280**(1–2), 401–406 (2005).

[84] T. Ushio, Limitation of delayed feedback control in nonlinear discrete-time systems, IEEE T. Circuit. Syst. **43**(9), 815–816 (1996).

[85] H. Nakajima, On analytical properties of delayed feedback control of chaos, Phys. Lett. A **232**(3–4), 207–210 (1997).

[86] K. Pyragas,Control of chaos via extended delay feedback, Phys. Lett. A **206**(5–6), 323–330 (1995).

[87] X. Xu, E. Pavlovskaia, M. Wiercigroch, F. Romeo, and S. Lenci, Dynamic interactions between parametric pendulum and electro-dynamical shaker, Z. Angew. Math. Mech. **87**(2), 172–186 (2007).

[88] W. J. Pierson and L. Moskowitz, A proposed spectral form for fully developed wind seas based on the similarity theory of S. A. Kitaigorodskii, J. Geophys. Res. **69**(24), 5181–5190 (1964).

[89] S. Fauve and F. Heslot, Stochastic resonance in a bistable system, Phys. Lett. A **97**(1–2), 5–7 (1983).

List of Publications

Journal articles

- Y. Susuki, Y. Yokoi, and T. Hikihara, Energy-based analysis of frequency entrainment described by van der Pol and phase-locked loop equations, Chaos **17**(2), 023108 (2007).

- Y. Yokoi and T. Hikihara, Start control of parametric pendulum into periodic rotation, Trans. ISCIE (accepted for publication) (in Japanese).

- Y. Yokoi and T. Hikihara, Tolerance of start-up control of rotation in parametric pendulum by delayed feedback, Phys. Lett. A (accepted for publication).

- Y. Yokoi, Y. Susuki, and T. Hikihara, Energy conversion in transient regime of frequency entrainment (in revision).

International conference proceedings

- Y. Yokoi, Y. Susuki, and T. Hikihara, A dissipated power-based analysis of frequency entrainment described by van der Pol and PLL equations, 2007 International Symposium on Nonlinear Theory and its Applications, Vancouver, Canada, September 16–19, 2007.

- Y. Yokoi, Y. Susuki, and T. Hikihara, Energy-based analysis of mutual entrainment in vibro-exciters on oscillatory base, 8th World Congress on Computational Mechanics, 5th European Congress on Computational Methods in Applied Sciences and Engineering, Venice, Italy, June 30–July 5, 2008.

- Y. Yokoi, Y. Susuki, and T. Hikihara, A power-based study on frequency entrainment in phase-locked loop equation system, Dynamics Days Asia Pacific 5, The 5th International Conference on Nonlinear Science, Nara, Japan, September 9–12, 2008.

- Y. Yokoi, R. Morrison, M. Wiercigroch, and T. Hikihara, Modelling synchronisation of parametrically excited pendulums, Recent Advances in Nonlinear Mechanics, Kuala Lumpur, Malaysia, August 24–27, 2009.

- Y. Yokoi and T. Hikihara, A study on frequency entrainment in externally excited phase oscillator –Operation of excitation based on energy–, 2009 International Symposium on Nonlinear Theory and its Applications, Sapporo, Japan, October 18–21, 2009.

- Y. Yokoi and T. Hikihara, A study on swing up control for rotation of parametric pendulum, IUTAM Symposium on Nonlinear Dynamics for Advanced Technologies and Engineering Design, Aberdeen, UK, July 27–30, 2010.

Domestic conference proceedings and technical reports

- Y. Susuki, Y. Yokoi, and T. Hikihara, A study on response curves of phase-locked system via energy balance relation, IEICE Society Conference, A-2-10, Kanazawa University, September 19–22, 2006.

- Y. Yokoi, Y. Susuki, and T. Hikihara, An energy-based study of mutual entrainment in vibro-exciters on oscillatory base, IEICE Technical Report, NLP2007-38, Shizuoka University, August 6–7, 2007.

- Y. Yokoi, Y. Susuki, and T. Hikihara, Response curves for dissipated power in frequency entrainment: A study on van der Pol and PLL equations, IEICE Society Conference, A-2-9, Tottori University, September 10–14, 2007.

- Y. Yokoi, Y. Susuki, and T. Hikihara, Phase difference equation and energy exchange for frequency entrainment –A study on PLL equation–, IEICE General Conference, A-2-10, Kitakyushu Science and Research Park, March 18–21, 2008 (in Japanese).

- Y. Yokoi and T. Hikihara, A study on frequency entrainment of externally excited phase oscillator –based on energy formed by elliptic function–, IEICE Technical Report, NLP2008-171, The Consortium of Universities in Kyoto, March 10–11, 2009.

- Y. Yokoi and T. Hikihara, Entrainment of rotating pendulum based on energy –Theoretical approach by elliptic functions–, The 58th National Congress of Theoretical and Applied Mechanics, 2C06, Science Council of Japan, August 9–11, 2009 (in Japanese).

- Y. Yokoi and T. Hikihara, Oscillation characteristics of parametric pendulum and its application to wave energy extraction, Kansai-section Joint Convention of Institute of Electrical Engineering, G4-11, Osaka University, November 7–8, 2009 (in Japanese).

- Y. Yokoi and T. Hikihara, Entrainment to periodic rotation of parametric pendulum by external force control, The 54th Annual Conference of ISCIE, W16-7, Kyoto Research Park, May 19–21, 2010.

- Y. Yokoi and T. Hikihara, Externally forced onset control of rotation in parametric pendulum with time delay, IEICE Technical Report, NLP2010-86, Osaka University, October 28–29, 2010.